



HAL
open science

Non-smooth model of the grand piano action

Anders Thorin

► **To cite this version:**

Anders Thorin. Non-smooth model of the grand piano action. Solid mechanics [physics.class-ph]. Ecole Polytechnique X, 2013. English. NNT: . pastel-00939493

HAL Id: pastel-00939493

<https://pastel.hal.science/pastel-00939493v1>

Submitted on 30 Jan 2014

HAL is a multi-disciplinary open access archive for the deposit and dissemination of scientific research documents, whether they are published or not. The documents may come from teaching and research institutions in France or abroad, or from public or private research centers.

L'archive ouverte pluridisciplinaire **HAL**, est destinée au dépôt et à la diffusion de documents scientifiques de niveau recherche, publiés ou non, émanant des établissements d'enseignement et de recherche français ou étrangers, des laboratoires publics ou privés.

“

Imagine, maintenant : un piano. Les touches ont un début. Et les touches ont une fin. Toi, tu sais qu'il y en a quatre-vingt-huit, là-dessus personne peut te rouler. Elles ne sont pas infinies, elles. Mais toi, tu es infini, et sur ces touches, la musique que tu peux jouer est infinie. Elles, elles sont quatre-vingt-huit. Toi, tu es infini. Voilà ce qui me plaît. C'est quelque chose qu'on peut vivre. Mais si tu /

Mais si je monte sur cette passerelle, et que devant moi /

Mais si je monte sur cette passerelle, et que devant moi se déroule un clavier de millions de touches, des millions et des milliards /

Des millions et des milliards de touches, qui ne finissent jamais, c'est la vérité vraie qu'elles ne finissent jamais, et ce clavier-là, il est infini /

Et si ce clavier-là, il est infini, alors /

Sur ce clavier-là, il n'y a aucune musique que tu puisses jouer. Tu n'es pas assis sur le bon tabouret : ce piano-là, c'est Dieu qui y joue /

Nom d'un chien, mais tu les as seulement vues, ces rues?

Rien qu'en rues, il y en avait des milliers, comment vous faites là-bas pour en choisir une /

Pour choisir une femme /

Une maison, une terre qui soit la vôtre, un paysage à regarder, une manière de mourir /

Tout ce monde, là /

Ce monde collé à toi, et tu ne sais même pas où il finit /

Jusqu'où il y en a /

Vous n'avez pas peur, vous, d'exploser, rien que d'y penser, à toute cette énormité, rien que d'y penser? D'y vivre... /

Moi, j'y suis né, sur ce bateau. Et le monde y passait, mais par deux mille personnes à la fois. Et des désirs, il y en avait aussi, mais pas plus que ce qui pouvait tenir entre la proue et la poupe. Tu jouais ton bonheur, sur un clavier qui n'était pas infini.

C'est ça que j'ai appris, moi. La terre, c'est un bateau trop grand pour moi. C'est un trop long voyage. Une femme trop belle. Un parfum trop fort. Une musique que je ne sais pas jouer. Pardonnez-moi. Mais je ne descendrai pas.

”

Alessandro Baricco – Novecento : pianiste

À Daniel Yvon

Remerciements

Encore indécis à m'engager sur un doctorat à l'époque, je me souviens lire le descriptif de la thèse proposée par le LMS et le CEA LIST sur internet. Mes hésitations se sont instantanément levées : il s'agissait d'une conciliation entre ma passion pour la musique et celle des sciences. Je suis très reconnaissant envers le LMS et le CEA LIST ainsi que des membres qui les composent, d'avoir rendu possible la réalisation de la thèse dans un environnement si favorable et fructueux.

Mes premiers remerciements s'adressent à Xavier Boutillon, avec qui j'ai pris plaisir à collaborer de façon symbiotique tout au long de la thèse et grâce à qui j'ai beaucoup appris. Je lui suis d'autant plus reconnaissant qu'il s'est toujours montré attentif quand il le fallait, compréhensif et humain. Merci également à José Lozada et Xavier Merlhiot pour leurs nombreux conseils avisés et leur initiation aux domaines de la mécanique analytique, de la géométrie différentielle ou de la mécatronique.

Merci à Jean-Christophe Eytard, Vincent de Greef, Hakim Gharbi, Erik Guimbretière, Ali Bozetine et William Gilbert pour leur aide sur la partie expérimentale.

Je souhaite également remercier Bernard Brogliato et René Caussé d'avoir accepté la charge de rapporteur, Paul Fiset celle d'examinateur et de président, et Stephen Paulello de s'être joint au jury.

Puis, il m'est très important de remercier ceux qui contribuent à ce qui me semble être l'un des plus précieux attributs de la recherche : le partage inconditionnel de savoir. Je tiens en effet à souligner la générosité de ceux qui donnent de leur temps pour transmettre leurs connaissances, même à des inconnus, aussi je prends le risque d'offusquer ceux que j'omets en ne citant que certains altruistes m'ayant aidé directement pour ma thèse. Merci donc à Patrick Ballard (accumulations d'impact), Alain Ehrlacher (énumérer les objets serait trop long !), Tony Lelièvre (mesures de Stieljes), Antonin Chambolle (décomposition des mesures), Vincent Acary (dynamique non-régulière) et particulièrement Mathieu Gautier et Jean Sreng (C++ et Python pour XDE). Que les autres sachent qu'ils ne sont pas pour autant oubliés !

Enfin, je remercie les acteurs du LMS, du CEA LIST et du LadHyx pour leur contribution à la si bonne ambiance qui y règne. Cela inclut en particulier Benoît Theckes et Loïc Tadrast avec chacun desquels j'ai passé deux tiers de thèse très riches en discussions fructueuses, mais aussi des collègues qui auront plus marqués le bureau 65 20 08 par leur caractère que par la durée de leur passage, tels Thomas Barois et ses sacs, Pascal Khalife (alias 110Ch210) et son tornado976 ou encore Eddy Malou – ça, c'est clair !

Résumé

Le mécanisme de la touche de piano à queue sert à propulser le marteau vers les cordes. Ce mécanisme permet au pianiste de contrôler avec précision la vitesse et l'instant d'impact du marteau sur la corde. Il est raisonnable de penser que c'est le comportement dynamique de la touche qui permet cette contrôlabilité. Avec pour perspective l'amélioration du rendu haptique des claviers numériques, cette thèse propose une méthode de simulation d'un modèle complet du mécanisme. Le son généré par la vibration qui suit l'impact du marteau sur les cordes n'entre pas dans le cadre de l'analyse. Des modèles du mécanisme comportant plusieurs degrés de liberté, des frottements et des contacts intermittents, ont été proposés depuis une quinzaine d'années. Notre approche se distingue de celles suivies jusqu'ici par un changement du point de vue adopté pour valider et pour simuler le modèle. En se fondant sur l'étude approfondie d'un modèle à un degré de liberté, il est en effet montré que la simulation d'un modèle dynamique complet doit se faire à l'aide d'un pilotage en déplacement, tandis que les travaux récents et anciens présentent des simulations pilotées en force.

Une analyse des problèmes numériques liés aux discontinuités de vitesses survenant au sein du mécanisme durant l'enfoncement de la touche est présentée. Ils sont résolus par des méthodes de dynamique non-régulière implémentées dans le logiciel XDE. Les résultats sont présentés sous forme de comparaison avec les mesures expérimentales. La plupart des irrégularités des forces mesurées se retrouvent dans les forces simulées, en jeu *piano* comme en jeu *forte*. Les simulations rendent également bien compte de la cinématique de chaque élément du mécanisme. Une analyse de sensibilité du comportement dynamique aux paramètres du modèle est enfin exposée.

Mots-clefs : *piano, dynamique multi-corps, dynamique non régulière, modélisation, simulation, haptique.*

Abstract

The grand piano action aims at propelling the hammer up to the strings. This mechanism provides the pianist with a high-controllability of the time of impact of the hammer with the strings and the hammer's velocity at the impact. This controllability is believed to be due to the dynamic behaviour of the piano action. The present thesis proposes a simulation method of a complete model of the mechanism, which opens doors to improvements of the haptic rendering of digital keyboards. The sound following the impact of the hammer on the strings is not analysed. In the last fifteen years, various models of the piano action including several degrees of freedom, friction and intermittent contacts, have been proposed. Our approach differs from existing work in that it is based on a new viewpoint for model validation and simulation. Indeed, using an in-depth study of a model with a single degree of freedom, it is shown that the simulation of a complete dynamic model must be driven with a displacement whilst, until now, only force driven simulations have been presented.

Velocity discontinuities, occurring during the descent of the key, raise numerical issues which are analysed. They are overcome by non-smooth numerical methods that have been implemented in the computer program XDE. The results of the simulation are presented and compared to experimental measurements. For both *piano* and *forte* keystrokes, most of the irregularities in the measured force are reflected in the simulated force. The kinematics of the bodies is also correctly predicted. Eventually, a sensitivity analysis of the dynamic behaviour to the model's parameters is proposed.

Keywords : *piano, multibody dynamics, non-smooth dynamics, modelling, simulation, haptic.*

Contents

General introduction	1
1. Introduction	3
1.1. Presentation of the grand piano	4
1.2. Description of the grand piano's action	4
1.3. History	7
1.4. Motivations and objectives	8
1.5. Literature review	12
1.6. Studied action	15
2. Modelling the dynamics of the piano action: is apparent success real?	17
2.1. Introduction	18
2.2. Experiments	20
2.3. Simple models	22
2.4. Simulations	25
2.5. Discussion	27
2.6. Conclusion	30
3. Experimental set-up	33
3.1. Kinematics	35
3.2. Force	39
3.3. Actuation of the key	41
3.4. Trigger and acquisition	45
3.5. Summary of measurement errors and uncertainties	45
4. Model	47
4.1. Characteristics of the piano action	48
4.2. Generalities	49
4.3. Physical elements	52
4.4. Classification of parameters	56
4.5. Dynamics: description and values	57
4.6. Matrix formulation of the dynamics	68
5. Simulation methods	75
5.1. Limitations of the regularising approach	76
5.2. Formulation of the piano action as a non-smooth dynamical multibody system	85
5.3. eXtended Dynamic Engine (XDE)	90
5.4. Adjustments of the model for its implementation	91
5.5. Adjustments of XDE for the simulation	93
5.6. Simulating in practice	95

6. Results and discussions	97
6.1. Regulation of the virtual piano action	98
6.2. Position-driven simulations	98
6.3. Force-driven simulations	106
6.4. Discussion	107
6.5. A sensitivity analysis	113
Conclusion	123
A. Adjustment procedure of the grand piano action	I
B. Application of the Lagrangian to a double pendulum	V
C. Example of the calculation of $\partial_{\mathbf{x}}\delta_{KH}$	IX

List of Figures

1.1. Modern grand piano [Blackham, 1965]	4
1.2. Side view of the grand piano	5
1.3. Terminology of the grand piano action	6
1.4. Piano action at successive stages	6
1.5. Action of the clavichord	7
1.6. Cristofori's pianoforte, 1726	7
1.7. Today's state-of-art actions for digital keyboards	11
1.8. Lozada's haptic device (2007)	11
2.1. Experimental set-up	20
2.2. Measured position y , measured acceleration \ddot{y} , measured force F in a <i>mezzo forte</i> keystroke	21
2.3. Grand piano action (without damper)	22
2.4. Simplified scheme of the grand piano action	22
2.5. Simple model of the piano action: the simplistic key	23
2.6. Position y of the end of the key during various strokes	26
2.7. Force F applied on the end of the key during various strokes	27
3.1. Complete experimental set-up	34
3.2. Scheme of the measurements	34
3.3. Set-up for actuating the key	35
3.4. Comparison of the integration of the acceleration and the differentiation of the position, <i>piano</i> keystroke	36
3.5. Tested patterns for KLT tracking	38
3.6. Illustration of KLT tracking with the selected patterns	38
3.7. Angles of the bodies tracked by KLT algorithm	39
3.8. Correction of the 50 Hz signal captured in the force measurement	40
3.9. Typical measurements, <i>piano</i>	40
3.10. Typical measurements, <i>forte</i>	41
3.11. Scheme of the piston used to press on the silicone	42
3.12. Typical fit of the linear viscoelastic behaviour of the piston	43
3.13. Ten identifications of the linear viscoelastic parameters of the piston	44
3.14. Comparison of the force measurement and its estimation using the viscoelastic piston	44
3.15. Scheme of the set-up	45
3.16. Photography of the piano action equipped for measurements	45
4.1. Approximation of each rigid body as a clamped beam	50
4.2. Location of the felts of the grand piano action	52
4.3. Photograph of the felt bushing on the jack	53
4.4. Zones where Coulomb friction is considered	54

4.5. Location of the coupling springs	55
4.6. Adjustable geometrical parameters, on a real grand piano action	56
4.7. Examples of non-measurable parameters	57
4.8. Parameters for the description of the geometry for the contact zone centred in P	58
4.9. Key frame, measurements	60
4.10. Contacts description, key	60
4.11. Whippen frame, measurements	61
4.12. Contacts description, whippen	61
4.13. Jack frame, measurements	62
4.14. Contacts description, jack	62
4.15. Lever frame, measurements	63
4.16. Contacts description, lever	63
4.17. Hammer frame, measurements	64
4.18. Contacts description, hammer	64
4.19. Damper frame, measurements	65
4.20. Contacts description, damper	65
4.21. Ground frame, measurements	66
4.22. Contacts description, ground	66
4.23. Initial positions of the frames	67
5.1. Plots of multi-valued sign and single-valued $\widetilde{\text{sign}}$ functions	77
5.2. Scheme of the hammer studied as a freely oscillating pendulum	79
5.3. Example of instability of the explicit scheme	83
5.4. Example of non-physical convergence due to regularisation	84
5.5. Example of non-convergence due to too small Θ	84
5.6. Chattering of regularised schemes	84
5.7. Convergence of the implicit scheme	85
5.8. Convergence of the non-smooth scheme	89
5.9. Comparison of the regularised and non-smooth approaches	89
5.10. Convergence of the regularised scheme and the non-smooth scheme for several Υ	90
5.11. Scheme of the Kelvin-Voigt model added for the simulation	91
5.12. Description of the contact with prismatic joint and felt law, illustrated with the hammer-string contact	93
5.13. Illustration of the implementation of the felt law as a linear model with adjustable parameters	94
5.14. Synchronized connexions of Orocos agents	95
5.15. Simulations principle	95
6.1. Scheme of the measured and simulated physical quantities (position-driven)	99
6.2. Simulation results for a <i>piano</i> keystroke (input: displacement)	100
6.3. Simulation results for a <i>forte</i> keystroke (input: displacement)	101
6.4. Comparison of the position of the bodies (tracking vs simulation) for a <i>piano</i> keystroke	103
6.5. Film and simulation screenshots comparison for notable events (see Fig- ure 6.9)	105
6.6. Scheme of the measured and simulated physical quantities (force-driven)	106

6.7. Simulation results for a <i>piano</i> keystroke (input: force)	106
6.8. Simulation results for a <i>forte</i> keystroke (input: force)	106
6.9. Notable events during a <i>piano</i> keystroke	107
6.10. Computed force F_{simu} for different time steps	111
6.11. Simulation results for a <i>piano</i> keystroke without felts (input: force)	111
6.12. Simulation results for a <i>piano</i> keystroke without felts (input: displacement)	112
6.13. Sensitivity of \mathcal{J} with respect to S_{K+y}	114
6.14. Sensitivity of \mathcal{J} with respect to K_{Wx}	114
6.15. Sensitivity of \mathcal{J} with respect to K_{Wy}	114
6.16. Sensitivity of \mathcal{J} with respect to S_{Jy}	115
6.17. Sensitivity of \mathcal{J} with respect to J_{Wx}	115
6.18. Sensitivity of \mathcal{J} with respect to S_{Ly}	115
6.19. Sensitivity of \mathcal{J} with respect to L_{Wy}	115
6.20. Sensitivity of \mathcal{J} with respect to K_{Hx}	116
6.21. Comparison of simulation results with measured and optimised values of L_{Wy} for a <i>piano</i> keystroke (input: displacement)	116
6.22. Comparison of simulation results with measured and optimised values of L_{Wy} for a <i>forte</i> keystroke (input: displacement)	116
6.23. Comparison of the position of the bodies (tracking vs simulation) for a <i>piano</i> keystroke with the optimised value of L_{Wy}	121
A.1. Terminology of the grand piano action	I
A.2. Location of the regulation settings	II
A.3. Appropriate adjustment of the jack regulating screw	II
B.1. Non-inertial frame of the lever and the jack connected to the whippen with hinges joints	V
B.2. Scheme and parametrisation of the double pendulum	V
C.1. Scheme of the key compressing the front rail punching	IX

List of Tables

2.1. Parameter values of the grand piano action used in experiments according to Lozada [2007] or measured by us	24
2.2. Parameters of the SK and BH models, according to Eqs. (2.1), (2.2) and (2.4)	25
2.3. Sensitivity of the results of the simulation	28
3.1. Summary of measurements	43
3.2. Summary of all measurement's errors	46
3.3. Details of kinematic errors	46
4.1. Order of magnitude of the influence of flexibility in statics and dynamics . .	50
4.2. Description of the contact geometries	51
4.3. The three cases of dry friction (M : external moment, D : dry friction)	54
4.4. The three cases of Coulomb friction (F : external force, T : tangential friction force)	55
4.5. Conventions for the notations of the parameters	58
4.6. Elements involved in the key's dynamics	60
4.7. Elements involved in the whippen's dynamics	61
4.8. Elements involved in the jack's dynamics	62
4.9. Elements involved in the lever's dynamics	63
4.10. Elements involved in the hammer's dynamics	64
4.11. Elements involved in the damper's dynamics	65
4.12. Parameters of the linear elastic law of the coupling springs	68
5.1. Summary of the three dimensionless parameters	81
5.2. Value of Υ for each body	81
6.1. Escapement velocities, measured and simulated	110
6.2. Sensitivity of the cost function with respect to parameters of Category II . . .	118
6.3. Sensitivity of the cost function with respect to parameters of Category III . .	119

General introduction

The grand piano allows a tremendous variety of musical expressions, which is a reason for its success. This instrument is made of two uncoupled systems: the action, which transfers the energy given by the pianist to the hammer, and the vibrating ensemble, which produces the sound after the hammer has hit the strings.

The action of the pianist, during a keystroke, results in a precise instant and a precise velocity of escapement of the hammer. The expressive potential of the piano results from the fact that the action allows pianists to control these two physical quantities with precision. This property is believed to originate in the tactile feedback of the key, hence in its dynamical behaviour. The piano action is therefore a haptic system which differs from many other ones by the highly accurate control that it offers. This concept is referred to as human-controllability.

The grand action is a planar mechanism composed of several wooden pieces, joined by hinges with felt bushings around their axes. The possible contacts between pieces are ensured by felts. The mechanism also includes springs, screws and some metallic parts. Its overall dynamics is complex and highly non-linear. Moreover, it is very sensitive to small geometrical adjustments.

Because touch is so important, manufacturers of digital pianos try to design keyboards that are haptically realistic. Old or cheap keyboards fail to reproduce the behaviour of the grand piano action. Nowadays, the best keyboards tend to imitate the original action by using some of its elements, if not all. However, these passive systems are still not fully satisfactory.

This thesis is part of a research project led at LMS and CEA List, which aims at reproducing the dynamic behaviour of the grand piano action by means of an active or semi-active system controlled in real time. This approach is expected to provide cheaper, lighter, realistic and haptically-adjustable keyboards, and also an interface which allows to carry out series of experiments in view of improving the understanding of human-controllability in haptics. The reproduction of the dynamical behaviour of the grand piano action, by means of an active or semi-active solution, requires a valid model of the action and its real-time simulation.

The literature reports many models, more and more complex. Complete models, where all the pieces of the grand piano action are considered, started to appear around 2000. All dynamical models, even the simple ones, were claimed to be good models in that their simulation exhibited a high degree of similarity with recorded positions of the key or the hammer, in response to an applied force. However, the fact remains that no satisfactory haptic device has been proposed yet.

This thesis has two main purposes. The first one is to examine why simple models look as good as complex ones. The second one is to propose a complete model and efficient numerical methods to simulate it, with the requirement of real time applicability.

The dissertation is divided into six chapters.

In Chapter 1, the piano and its action are presented and described. The motivations of our research project are detailed. Then, the literature on piano action models and simulations is reviewed, with an insight on the haptic aspects.

A single degree-of-freedom model, similar to the models proposed until approximately 2000, is studied in Chapter 2 in view of understanding why its predictions look so realistic. The conclusion is that a model of the dynamics of the piano action should be validated by a comparison of measured and calculated forces, in response to a displacement instead of a force.

The experimental set-up is described in Chapter 3. It includes dynamic measurements of the key and kinematic measurements of the whole. Typical measurements are presented for *piano* and *forte* keystrokes.

A complete model, widely inspired of [Lozada, 2007], is given in Chapter 4. It consists in a multibody system made of six rigid bodies. All its parameters have a physical interpretation and are measurable. They are categorised in view of a sensitivity analysis. All their values are given in this chapter.

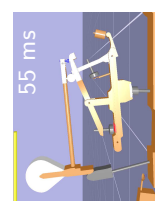
Simulating this model raises difficulties because of its non-smooth laws. In Chapter 5, we discuss their different possible treatments. We chose to apply a non-smooth method, implemented in the computer program XDE. A pendulum with dry friction is used to illustrate a numerical method for non-smooth systems and quantify its efficiency compared with a method based on a regularised model.

Eventually, results are presented as a comparison with measurements in Chapter 6 with a displacement input, for both *piano* and *forte* dynamics. Results are also presented for the same model, using a force as an input. A sensitivity analysis of the reaction force of the key on the finger to the model's parameters is carried out.

1 Introduction

Contents

1.1. Presentation of the grand piano	4
1.2. Description of the grand piano's action	4
1.3. History	7
1.4. Motivations and objectives	8
1.4.1. Haptical point of view	9
1.4.2. Digital keyboards	9
1.5. Literature review	12
1.5.1. Description of the piano action	12
1.5.2. Simple models	12
1.5.3. Complete models	13
1.5.4. Haptical devices	14
1.6. Studied action	15



1.1. Presentation of the grand piano

A grand piano is a musical instrument played by means of a keyboard, see Figure 1.1. The modern keyboard is typically made of 88 keys. Each key is part of an action which transfers the energy given by the pianist to its hammer. The hammer strikes the strings which then vibrate. The strings transmit their vibrations to a bridge, and to a large wooden plate called soundboard. Eventually, the vibrations of the soundboard produces acoustic waves in the air: the sound of the piano.

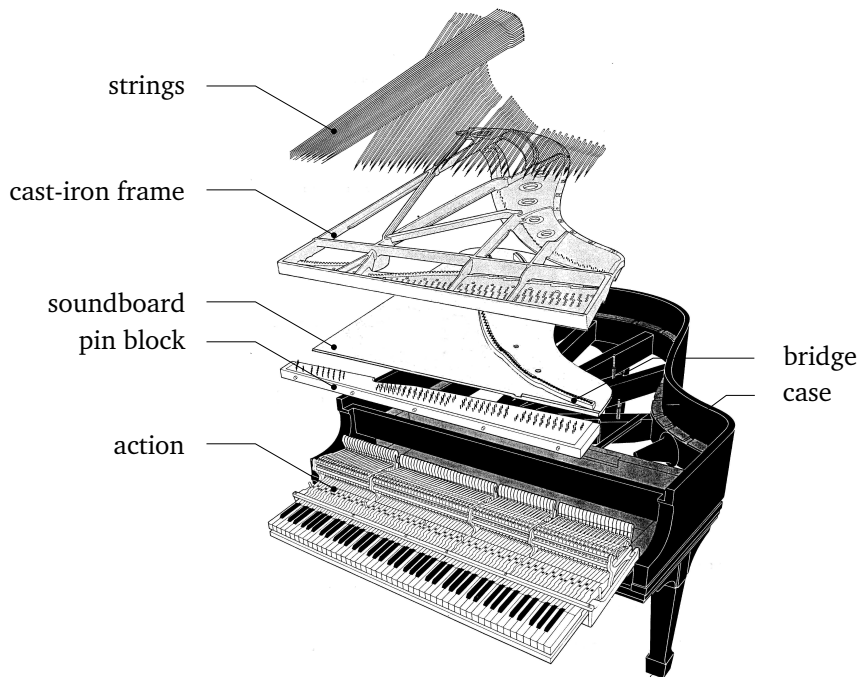


Figure 1.1 – Modern grand piano [Blackham, 1965].

Once the hammer has escaped from the action, it moves freely until it strikes the strings: the pianist has no more control on its motion. Therefore, the keyboard and the strings of the grand piano are uncoupled. The instrument can therefore be described as two separate mechanisms: one which propels the hammers, and one (strings, bridge, soundboard, frame) which produces the sound. For this reason, it is possible to study these two elements independently. Here, we focus on the study of the grand piano action.

It is shown in [Repp, 1999] that once a piece of music has been learnt, the playing of the musician is not coupled to the sound feedback of the piano. This justifies why the piano action can be studied from of mechanical point of view, independently of the sound it produces.

1.2. Description of the grand piano's action

The location of the action is shown in Figure 1.2.

The purpose of the piano action is to propel the hammer up towards the string and to catch it back after its escapement. The terminology of the mechanism is given in Figure 1.3 and the way it works is explained in the following sequence of events, the main stages of which are displayed in Figure 1.4.

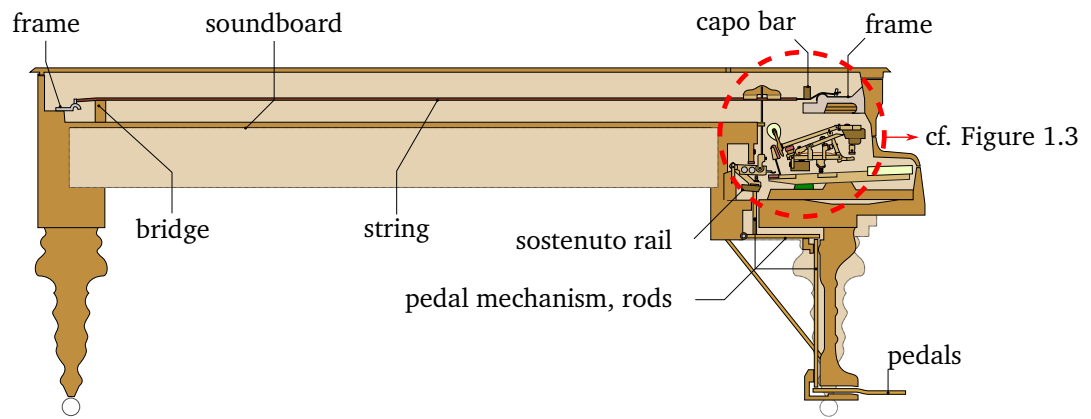


Figure 1.2 – Side view of the grand piano [after Olek Remesz / Wikimedia Commons].

Before the hammer hits the string

1. The key starts to rotate, lifting the whippen-lever-jack assembly.
2. Half-way through, the key also begins to lift the damper.
3. The jack stops at the let-off button and at the same time¹ the repetition lever stops at the drop screw (Figure 1.4(b)).
4. The key continues to lift the whippen-lever-jack assembly and the jack and the repetition lever rotate relatively to the whippen. The hammer is now being pushed only by the jack.
5. Propelled by the jack, the hammer escapes from the action at a given speed (Figure 1.4(c)).
6. The key compresses the front rail punching and stops.
7. If its velocity is high enough, the hammer hits the string.

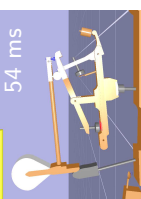
This phase lasts between 20 ms and 200 ms [Askenfelt and Jansson, 1990] depending on the dynamics of the keystroke.

After the hammer has hit the string Depending on the position of the key and the speed of the hammer, the latter is either checked, or blocked at the hammer knuckle.

When it is checked, it is blocked by the backcheck fixed on the key (Figure 1.4(d)). The hammer knuckle pushes the repetition lever downwards and compresses its spring. As soon as the key begins to go up, the backcheck releases the hammer. The spring lifts the hammer and the jack returns to its resting position, ready to send the hammer up to the string even if the key has not been completely released. The piano action is then back to the state 4. If the player presses the key again, the piano action continues with the following stages. If he releases the key, all the mechanism returns to its resting position, because of gravity.

The numerous felts play a major role in the touch but are humidity-sensitive. Moreover, the whole mechanism moves with time so that the action, which is very sensitive, has to be periodically regulated. A classical regulation procedure is given in Appendix A.

¹If the action is properly adjusted.



Cristofori's death in 1731. Frederick the Great of Prussia ordered seven pianofortes at once. Silbermann had also exchanges with Bach who first criticised the instrument, but then gave his approval two years later of the improved pianoforte.

The real success of the fortepiano began in the second half of the 18th century, mainly in Germany, France and England. Bach's son Johann Christian played the pianoforte publicly and taught it to Queen Charlotte, while Mozart was composing specifically for the pianoforte.

Meantime the square piano, smaller and cheaper, had an increasing success especially in England.

In 1777, a skilled craftsman by the name of Sébastien Érard built his first pianoforte. He managed to get along with Louis XVI, and had to flee to London during the French revolution, in 1789. He came back to Paris from 1796 to 1808, then to London again until 1815. During this period he made many inventions, especially one for which he is still famous: in 1823, he invented the double escapement, allowing to propel the hammer up to the string several times in a row. Pleyel made some criticism about its fragility and preferred to use the simple escapement, but eventually had to face the success of the double escapement and lined up with the other piano makers.

Many small changes were added to the piano and its action in the 19th century. The upright piano is an example of an instrument which originates from the piano. Henri Pape joined the Pleyel factory in Paris in 1811 and then continued on his own. He applied for 137 patents, most of which were not used, but including some inventions which have become today's standards such as the addition of felts on the hammers (1826) or the crossing of the strings (1839). Pleyel also innovated, with for instance the addition of a cast iron frame in 1826. His factory prospered and he became an important rival of Érard.

Many French factories were created in the 19th century but the small ones disappeared. Germany and England also produced large quantities of pianos. At the end of the century, Pleyel and Érard had both build their hundred-thousandth piano [Closson and Ames, 1977].

The pianos also spread to America in the 19th century, especially as many Germans emigrated over there. A famous example is that of Steinweg and his sons who fled from Europe to avoid the revolutions of 1848 and settled in New York in 1850, where they created Steinway & Sons in 1853. It became a major factory within a few years. Square pianos had a large success although they had developed from reconditioned clavichords and had been surpassed by grand and upright pianos from a technical point of view. In 1904, the American piano makers and dealers bought two hundreds of them, and burnt them in a giant bonfire at Atlantic City [Times, 1904] in order to inform the populace about the obsolescence of square pianos, and revive grand and upright pianos.

1.4. Motivations and objectives

The present thesis is part of a larger double-faceted research project. The first facet concerns the research on the mechanical properties of haptic devices which allow them to perform highly accurate dynamical tasks. The other one is to develop digital keyboards with realistic touch, using active or semi-active systems.

"For even more realism, this new keyboard also uses a new hammer action that lets you actually feel the hammers and cushions as you play. [...] The result is the same feel and response as a grand piano's keyboard when playing fast, delicate passages."

This last quote underlines that low dynamics, such as for *piano* keystrokes, are harder to be haptically rendered.

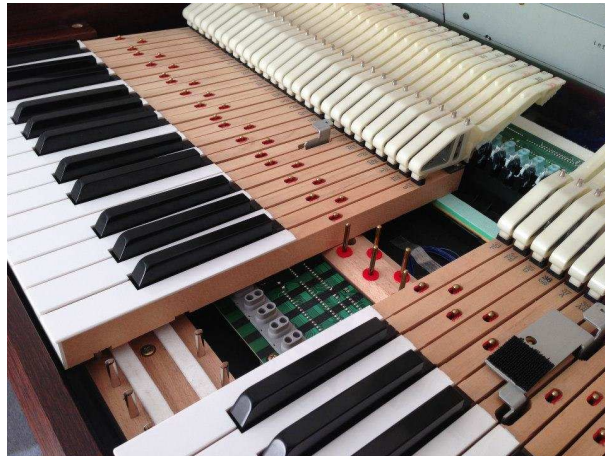
The peak of this tendency is reached with the Yamaha AvantGrand, which includes a complete grand action (except hammer felts).

Instead of reproducing the piano action's dynamic behaviour by copying its complexity, the present research aims at doing so with cheap electronic active or semi-active³ components. They would be controlled in order to reproduce a faithful force feedback, computed by real-time simulations. Such a solution is likely to be much cheaper, lighter, smaller, but also to enable adjustable touch.

A haptic device was proposed in 2007 by Lozada, see Figure 1.8. When a controlled magnetic field \underline{B} is generated from the solenoid, the ferromagnetic particles inside the magnetorheological fluid react by creating aggregates, so that the apparent viscosity of the fluid is raised. Adjusting \underline{B} results in adjusting the reaction force of the key, so that it matches the dynamical behaviour of the key. For numerical reasons related to the complexity of the piano action, Lozada did not succeed to simulate the model.

The realisation of a haptic device which reproduces the dynamical behaviour of the grand piano action requires a valid model of mechanism, as well as efficient simulation techniques. Both are presented in the present thesis.

³Such as magnetorheological fluids which have a short time response.



(a) "Natural Keyboard", Yamaha ©pianoworld



(b) PHA III, Roland (2009) ©Roland



(c) RM3, Kawai (2010) ©musicpromusic

Figure 1.7 – Today's state-of-art actions for digital keyboards.

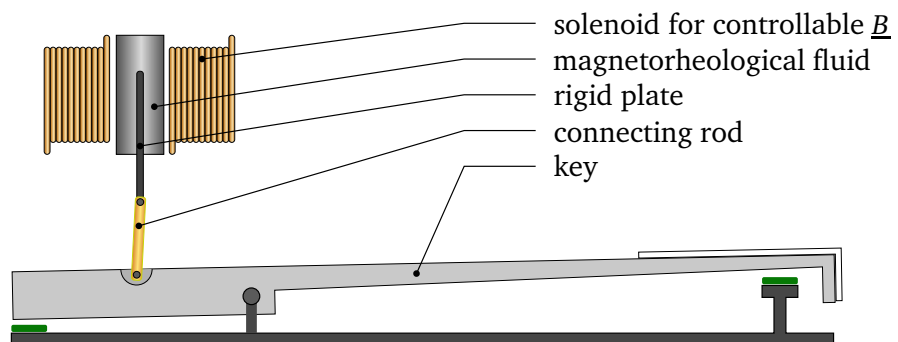
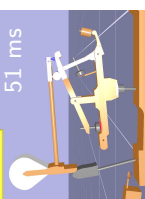


Figure 1.8 – Lozada's haptic device (2007) aiming at reproducing the dynamical behaviour of the key.



1.5. Literature review

1.5.1. Description of the piano action

The piano action, from Cristofori's action (e.g. [Pollens, 2002]) to modern actions, has been extensively described, from several point of views. Some are focused on its history, some are intended to piano technicians, others are haptically-oriented.

In [Pfeiffer, 1962], most of the actions developed in history are presented. Pfeiffer made elementary models of the hammer and basic experimental testing by means of calibration weights. He mentioned the friction force occurring at escapement⁴.

The intermittent contacts occurring within the grand piano action, often referred to as changing kinematic constraints, have been studied in [Askenfelt and Jansson, 1990] where their timing is experimentally quantified. The touch, the motion of the mechanism and the hammer-string contact were characterised experimentally in [Askenfelt and Jansson, 1991]. The vibrations of the hammer shank were already discussed (first mode frequency: 50 Hz).

Many studies starting in the 90s aimed at contributing to the domain of haptics. [Gillespie, 1996] noted that contrary to pianos', synthesisers' actions are not subject to changing kinematic constraints, even though keyboardists rely upon them to develop and exert fine control. [Hayashi et al., 1999] explained that producing a stable soft tone (*piano* keystroke) is difficult, even for experienced pianists.

[Goebel et al., 2005] investigated the temporal behaviour of grand piano actions from different manufacturers under different touch conditions and dynamic levels.

1.5.2. Simple models

After World War I, the piano manufacturer Pfeiffer applied scientific methods to the piano action [Pfeiffer, 1950, 1962; Pfeiffer et al., 1967]⁵.

Several elementary models of the action were proposed. They became more and more complex. A unidimensional model was given in [Rimski-Korsakov and Maveev, 1938]⁶. It inspired some improvements [Oledzki, 1973] where two masses (one for the hammer and one for all the other parts) were connected by a spring representing the internal flexibility of the action. In order to improve the results, the mass of the hammer were then made time-varying. A frictionless model was also proposed in [Dijksterhuis, 1965] where the key, the whippen-jack assembly and the hammer were superimposed masses. The last two models used forces as inputs.

Later, [Gillespie and Cutkosky, 1992] presented a model made of four bodies (key, whippen, jack and hammer), for the motion from the beginning until the hammer-string contact. It included inertia and weight but neglected damping, compliance and friction. Gillespie mentioned that friction did matter at let-off. In order to simplify the simulation for real-time, a 2-DOF model, not good for escapement but allowing the solving, was

⁴He concluded that because the upright action has less friction, it is better than the grand piano action. This is questionable from the haptical point of view, and does not correspond to the common preference of pianists.

⁵Wolfgang Pfeiffer passed away in 1960; the posthumous dates actually corresponds to the translations.

⁶A. Rimski-Korsakov, relative to the composer Nikolai Rimski-Korsakov, studied string instruments (for example [Rimski-Korsakov, 1937] and [Rimski-Korsakov and Samoilenko, 1937]).

A micromechanical model of piano felts based on interactions between fibres is proposed in [Masoudi, 2012]. The model was implemented in an upright piano action model, based on Hirschhorn's [Masoudi and McPhee, 2012]. The simulations were driven with a force and the kinematics were observed. The reported running time for one simulation was 87 min.

Another a complete model with measured parameters is proposed in [Lozada, 2007]. Friction laws were regularised but still, numerical difficulties were encountered when simulating the multibody system with input positions, in order to calculate the reaction forces of the key on the pianist's finger.

[Mamou-Mani and Maniguet, 2009] claimed to have characterised differences in the mechanical behaviour of Érard and Broadwood's pianos. No details on the model were given.

In [Gillespie et al., 2011], the piano action is modified using rubber, in order to "linearise" its behaviour. The authors call the model a hybrid dynamical model because it combines continuous variables, and discrete variables to describe the state of the kinematic constraints. The input is still a force, and the discussion is focused on the position of the key.

Another model where Coulomb friction is smoothed is proposed in [Links, 2011]. The position of the key is correctly simulated, except at the beginning of the motion. The correlations between the measured and simulated hammer positions is good.

A study, aimed at understanding the historical evolution of the piano action, is given in [Bokiau et al., 2012]. The kinematics are simulated from an input idealised smooth force profile.

To sum up, many different complete models have been proposed. In all of them, friction has been regularised to make the simulation easier. Also, none of them calculated the reaction force of the key: nearly all of them used it as an input and made kinematic observations.

1.5.4. Haptical devices

We give here a brief insight of a few haptically-oriented studies. Details on the musculoskeletal system of the finger are given in [Dennerlein et al., 1998].

In 1990, Cadoz et al. created a keyboard with tactile feedback [Cadoz et al., 1990]. It was also a modular device: the feedback could be changed.

[Gillespie and Cutkosky, 1992] relate the importance of touch and the idea of replacing the piano action by actuators or programmable passive devices coupled with a control system. Voice-coil motors are employed in an electro-mechanical apparatus in [Gillespie and Cutkosky, 1993] and [Gillespie, 1994]. In [Gillespie, 1996], the author explains that real-time feedback is possible during events which last longer than 200 ms. Otherwise, the control requires learning and practise.

[Chu, 1996] exposes the project of building a force-feedback based MIDI controller. Another haptic device aimed at reproducing the piano action behaviour using voice-coil motors is proposed in [Oboe and Poli, 2002] and [Oboe, 2006]. The model used for the real time simulations is made of two bodies (key and hammer) without friction, damping or escapement.

Indications on the design of haptic keyboards are given in [Horváth and Töröcsik, 2013].

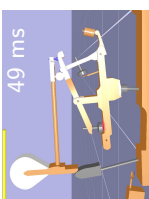
Goebel states that "[his findings] suggest that sensory information available at finger-key contact enhances the timing accuracy of finger movements in piano performance" [Goebel and Palmer, 2008].

[Links, 2011] reports some interesting orders of magnitude: the smallest observable change in tactile sensing is around 0.25 N for a static force and 0.5 N for a dynamic force. The spinal reflex is at least 40 ms and a conscious reflex is longer than 150 ms.

1.6. Studied action

The experiments are performed on a single piano key mechanism manufactured by the Renner factory for demonstration purposes but similar to the mechanisms in use in grand pianos, particularly with respect to its regulation possibilities. The action has been carefully adjusted by a professional piano technician in line with the standards observed in a piano keyboard. We stabilized the provided sample action by screwing it to a thick metal plate and fixing it solidly to a heavy support. The action is that of a white key, covered by a white plastic coating. The coating may have some influence on the feeling, but not on the kinesthetic sense of haptics, which is studied here. The key is not weighted with key leads.

This action is presumed to be representative enough of the grand piano action in general. A general model is presented in the thesis. The validation of the model is done on this particular piano action.



2 Modelling the dynamics of the piano action: is apparent success real?

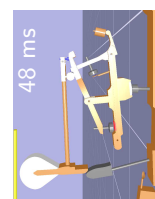
The present chapter is an article under submission to Acta Acustica. The original article includes its own references, which are here gathered with the other references.

Note that this version of the article is not the latest.

Overview The goal of this chapter is to determine which input should be used for the simulation of the model presented in Chapter 4. The main result of this chapter is the demonstration that comparisons of simulated forces calculated from position-driven simulations with measured forces are not sufficient to validate a dynamical model of the piano action.

Contents

2.1. Introduction	18
2.2. Experiments	20
2.3. Simple models	22
2.4. Simulations	25
2.5. Discussion	27
2.6. Conclusion	30



Abstract The kinematics and the dynamics of the piano action mechanism have been much studied in the last 50 years and fairly sophisticated models have been proposed in the last decade. Surprisingly, simple as well as sophisticated models seem to yield very valuable simulations, when compared to measurements. We propose here a too simple model, with only 1-degree of freedom, and compare its outcome with force and motion measurements obtained by playing a real piano mechanism. The model appears either as very good or as very bad, depending on which physical quantities are used as the input and output. We discuss the sensitivity of the simulation results to the initial conditions and to noise and the sensitivity of the experimental/simulation comparisons to the chosen dynamical model. It is shown that only motion-driven simulations should be used for validating a dynamical model of the piano action, contrary to what has been proposed in the literature.

2.1. Introduction

The mechanical function of the piano action is to throw the hammer towards the strings. As a human-machine interface, its role is to provide the pianist with a means to perform the following musical task: obtain a given impact velocity of the hammer on the strings at a given instant, with as much as precision as possible. We focus here on the grand piano action but all what is proposed here would apply to the upright piano mechanism.

Piano actions are complex systems mostly resulting from engineering during the 18th and 19th centuries, mostly by trial-and-error. The assembly of dozens of pieces is the fruit of a few major inventions (particularly by Cristofori and Érard, for the mechanisms that remained in the 20th century) and many minor refinements. In the resulting sophisticated design, it is not any more obvious to distinguish what are the features due to engineering – economy, ease of manufacturing in given historical conditions, necessity of a silent motion, ease of repair and adjustment, *etc.* – and those imposed by piano playing requirements: ease and precision of control, compliance with the playing tradition. Actions that are built for digital pianos (sound synthesisers) can be seen as tentatively complying with the latter group of requirements by means of markedly different engineering solutions. Although constantly improving over years, it is interesting to notice that the results are not yet judged as entirely convincing.

We focus here on the dynamics of the piano action – the force-motion relationship – as seen from (or felt at) the finger-end of the key. In this paper, the piano action is considered either subject to a given force or to a given motion, which would be imposed by an operator. As of today, the physical quantity controlled by the pianist during the keystroke (or before) in order to perform the musical task has not been identified. In reality, the dynamics of the piano action is coupled to that of the finger/hand/arm/... musculoskeletal system which is coupled itself to a neurological system of efferent and afferent nerves. A vast literature is available on various questions pertaining to the pianist control, involving sensory-motor questions as well as the dynamics of the pianist limbs and fingers. This complex question is not analysed here.

Since the 60's, many dynamical or mechanical models of the piano action have been proposed, each of their authors more or less claiming that it emulates successfully the kinematics (usually the angular positions of the key and hammer) or the dynamics of the mechanism as seen at the end of the key. These claims are usually supported by

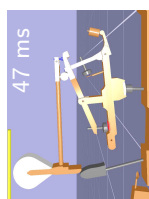
comparisons between experimental measurements and numerical results issued by the model. The experimental results are generally obtained by imposing a force (constant or varying in time) on the key, by measuring this force, the resulting motion of the key, that of the hammer and, sometimes, of other pieces. Since it is not known whether the control by the pianist is more of a force- or a motion-nature, the choice of given force-profiles or motion-profiles for controlling the dynamics in experiments and simulations may appear as more or less arbitrary, and irrelevant for validating a given model. This paper aims at demonstrating that this is not so. To this end, we analyse the predictions of very simple models of the mechanism, with only one degree-of-freedom.

A few elementary models of the piano action or of some of its parts have been proposed in the first half of the 20th century. In 1965, a frictionless model with superimposed masses is proposed by Dijksterhuis Dijksterhuis [1965]. Oledzki Oledzki [1973] studied a model where two masses (one for the hammer and one for all the other parts) were connected by a spring, representing the internal flexibility of the action. Gillespie and Cutkosky Gillespie and Cutkosky [1992] presented a model with four bodies (key, whippen, jack and hammer) where damping, compliances and friction were neglected. In Gillespie [1994], one model is considered for each set of kinematic constraints. A unidimensional model was exposed by Mori Mori [1997], who applied forces to the key with calibrated weights. Another model was proposed by Hayashi *et al.* Hayashi *et al.* [1999], consisting in a 2-DOF model with a free mass representing the hammer. Contrary to all the other simulations in the literature which are driven by forces, Hayashi's are driven either by a constant velocity, or by a constant acceleration. However, forces are not considered in this paper. A 2-DOF model is also proposed by Oboe Oboe [2006]. The key and the hammer are modelled, neglecting friction, but the escapement is not considered. In 1995, Van den Berghe *et al.* Van den Berghe *et al.* [1995] considered a 3-DOF model where the whippen-lever-jack assembly is rigid. The escapement is therefore not modelled either. The kinematics in response to a force input is discussed.

More complex models appear in the late 90s. The repetition lever is taken into account in Gillespie [1996]. A complete model (5-DOF, the damper is ignored), with measured parameters, is proposed by Hirschhorn Hirschhorn [2004]. Links presents a similar model Links [2011]. Lozada Lozada [2007] gives a different model with all the values of its parameters. It also includes the first attempt of driving the simulations with a position, without success. Recently, Bokiau *et al.* Bokiau *et al.* [2012] have also proposed a rather sophisticated model. Force-driven simulations yield the motion of various pieces.

Except those of Hayashi *et al.* [1999] and Lozada [2007], all the simulations were driven with a force input (sometimes, the applied force is constant or idealised), and the resulting kinematics was observed.

In this paper, the experiments consist in playing a real key mechanism almost like a pianist, at three different dynamical levels, and in recording the motion of the key and the force acting on it (Section 2.2). We then consider very simple models, so simple that they can hardly be considered as valid (Section 2.3). Their parameters are derived from static measurements on the real mechanism and from measurements on separate pieces that have been taken apart. The models predict the resulting motion for a given force exerted at the end of the key. When driven by an imposed motion, they can predict the reacting force as well. Comparisons are made between the measured and the predicted motions in the first case, and between the measured force and the predicted force in the other one



The minimum force initiating down-motion and the maximum force preventing up-motion have been estimated with the standard procedure (adding and removing small masses at the end of the key). They are respectively $F_{\text{down}} \approx 0.70$ N and $F_{\text{up}} \approx 0.38$ N, both exceeding by about 0.15 N the values normally adjusted by technicians.

The key acceleration is measured by a light (0.4 g) accelerometer (Endevco 2250A-10, with B&K Nexus measurement amplifier) glued approximately mid-way between the end and the rotation centre of the key. The force exerted on the end of the key is measured with a light-weight (1.2 g) piezoelectric sensor (Kistler 9211, with charge amplifier 5015). The data are sampled at 50 kHz (ADC USB-6211 by National Instruments).

In what follows, the motion of the key is reported at the end of the key (with measured signals multiplied by the appropriate factor) and shifted so that the zero-values correspond to the rest position. The force signal is also shifted so that its value is zero as long as the user has not touched the key.

Since the models include viscosity, the key velocity must be estimated. The velocity is obtained numerically by two independent algorithms: integration of the acceleration signal (after removal of the average value of the signal at rest) and differentiation of the position signal, using a total-variation regularisation Chartrand [2011] (here: 30 iterations, 200 subiterations, a regularisation parameter of $5 \cdot 10^{-5}$ and $\varepsilon = 10^{-9}$). In practice, choosing one or the other estimation of the velocity has very small influence on the simulation results.

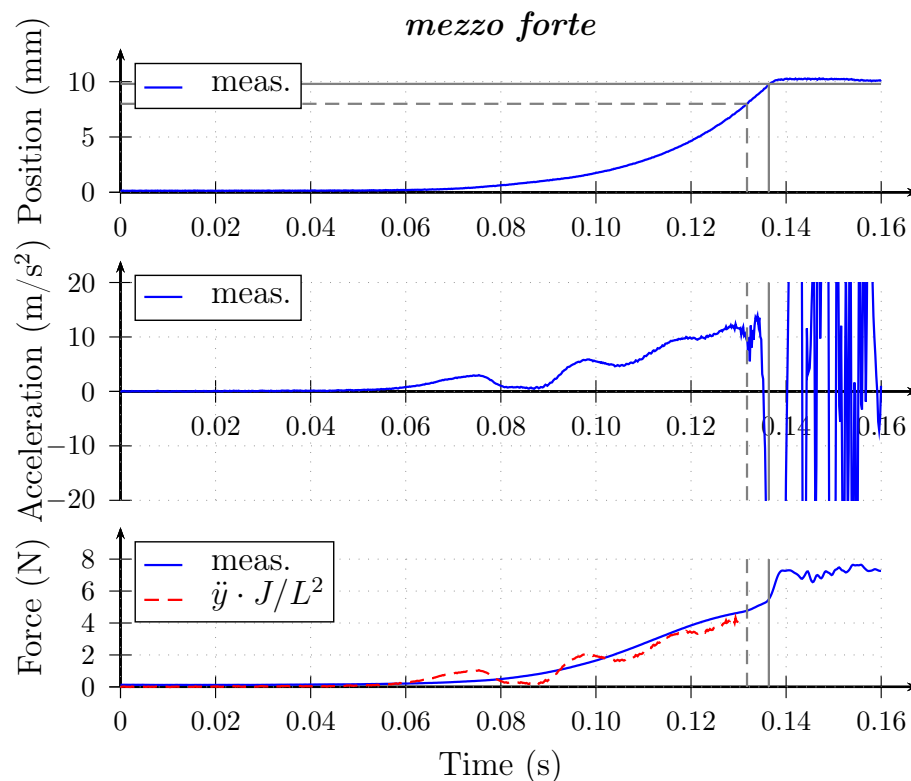
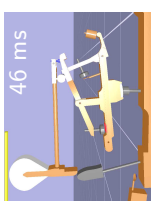


Figure 2.2 – Measured position y (top), measured acceleration \ddot{y} (middle), measured force F (bottom) in a mezzo forte keystroke. An estimation of the inertial part $(J/L^2)\ddot{y}$ of the force F is represented as a dashed line in the bottom frame. The gray dashed-lines and gray continuous lines correspond to $t = t_e$ (escapement of the hammer, see text for additional precisions) and to $\theta = \theta_p$ (the key meets the front rail punching) respectively.



the mutual dependencies between the θ_i are approximated by geometrical relationships:

$$\begin{cases} \theta_2 = -\frac{l_{12}}{l_{21}}\theta_1 = -\alpha_{21}\theta_1 \\ \theta_3 = -\frac{l_{23}}{l_{32}}\theta_2 = -\alpha_{32}\theta_2 = \alpha_{31}\theta_1 \end{cases} \quad (2.1)$$

with $\alpha_{31} = \alpha_{32} \alpha_{21}$.

A more drastically simplified model (Figure 2.5) consists in a single-degree-of-freedom rotating object with angular position $\theta = \theta_1$, referred to as "the simplistic key" (SK) in what follows.

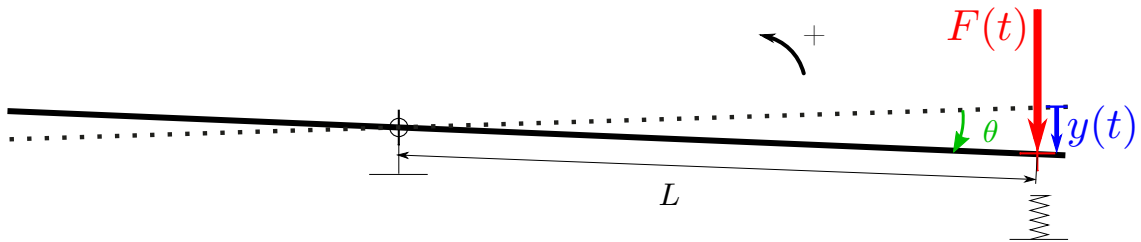


Figure 2.5 – Simple model of the piano action: the simplistic key.

Within the frame of the above approximations, the moment of inertia J of the simplistic key is equivalent to the one of the whole mechanism if:

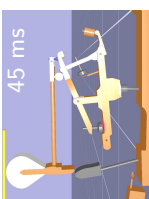
$$J = J_1 + \alpha_{21}^2 J_2 + \alpha_{31}^2 J_3 \quad (2.2)$$

with the parameters given in Table 2.1.

For very small key displacements from its rest position, dry friction in the hammer's and the whippen's axes prevents their motion. Experimentally, we also observed that the compression of the small felt below the centre of rotation of the key (in Figure 2.1 see the small red felt between the middle of the key and the piece of wood supporting it) cannot be neglected any more. This lasts at least as long as the force applied to the key is less than F_{down} . By various inspections of the motions of the different pieces (position tracking, not reported here), it was found that the dynamics was distinctively different whether θL was less or more than ≈ 0.8 mm. Before the force reaches that threshold, a different model must be used, which is proposed further.

The momentum of the hammer is several times that of the rest of the mechanism. It follows that the inertia of the whole mechanism differs strongly from that of the simplistic key model when the hammer is dissociated from the rest of the mechanism (a few milliseconds between the escapement and the check of the hammer). Continuation of the model is discussed further in Section 2.4.

The actions of the torques exerted on the real mechanism are transposed on the simplistic key as follows. Non-permanent torques imposed by the stops limiting the motion of the key are considered and denoted by C_s . This torque includes the reaction of the rest support which disappears as soon as $\theta(t) > 0$ and the reaction of the front rail punching LF which appears when $\theta(t) > \theta_p$. The compression law $F(L\theta)$ of the front rail punching is that of a felt. Besides the various felt models which have been proposed, we use a phenomenological model that has been experimentally validated on that class of felt and



geometry Brenon [2002]:

$$F(\delta) = k\delta^r + b\delta^2\dot{\delta} \quad (2.3)$$

where δ is the compression of the felt.

After the hammer check, an additional source of dissipation is located in the back-check: the key (with the whippen block resting on it) becomes also coupled to the support *through the hammer and the back-check felt*. Hypothetically, the corresponding friction dissipates significantly more than the internal compression of the felt of the front rail punching. Therefore, the value of b has been arbitrarily taken 100 times more than that measured by Brenon. The values of k , b and r are given in Table 2.2.

i	J_i (kg.m ²)	C_{wi} (N.m)	C_{di} (N.m)	c_{vi} (N.m.s)	Spring	Geometry (m)	α
1	3.36×10^{-3}	-0.0155	0.012	0.022		$l_{12} = 0.129$ $L = 0.245$	
2	3.97×10^{-4}	-0.0103		4.93×10^{-5}	$\kappa_2 = 0.087$ N.m, $\theta_2^0 = 0.42$ rad	$l_{21} = 0.060$ $l_{23} = 0.080$	$\alpha_{21} = 2.15$
3	1.65×10^{-4}	0.0133		4.93×10^{-5}		$l_{32} = 0.017$	$\alpha_{31} = 10.1$

Table 2.1 – Parameter values of the grand piano action used in experiments according to Lozada [2007] or measured by us.

Permanent torques independent of the key motion include the action of the pianist $C(t)$ (kept as is) and the torques C_{wi} due to the weights of the different parts of the mechanism. Their effects amount to C_w given by Eq. (2.4). Permanent and motion-dependent torques due to strains at pivots are modelled by viscous and dry friction: $c_{vi} \dot{\theta}_i$ and $C_{di} \text{sign}(\dot{\theta}_i)$ respectively. As before, their effect is written as $c_v \dot{\theta}$ and $C_d \text{sign}(\dot{\theta})$. In some mechanisms, including ours, a pre-stressed spring is inserted between the support and the whippen. Its effect is modelled by a torque $\kappa(\theta - \theta_0)$. Within the approximation of small angles, the moments of the coupling forces R_{ij} are given by $R_{ij} l_{ij}$ with the fixed lengths l_{ij} represented in Figure 2.4. It comes:

$$\Rightarrow \begin{cases} C_w = C_{w1} - \alpha_{21} C_{w2} + \alpha_{31} C_{w3} \\ c_v = c_{v1} + \alpha_{21}^2 c_{v2} + \alpha_{31}^2 c_{v3} \\ \kappa = \alpha_{21}^2 \kappa_2 \end{cases} \quad (2.4)$$

At the very beginning of the key motion, when $F < F_{\text{down}}$, the force exerted by the key on the whippen is too low to completely overcome the dry friction in the axes of the whippen-lever-jack and of the hammer blocks. In consequence, there is a phase where the key moves while the hammer does not: $L C_{d1} < F(t) < F_{\text{down}}$. The hammer behaves as if it was fixed to the support and the motion of the key is limited by the compression of coupling felts and springs (in the whippen cushion, etc.). For the sake of simplicity, we model them as one linear equivalent spring. Its stiffness K is estimated as the average ratio between F_{meas} and x_{meas} for the three different dynamics considered here. This model is denoted below as "the blocked hammer" (BH) model.

The dynamical equations of the two successive models finally read as:

$$J_1 \ddot{\theta} + c_{v1} \dot{\theta} + C_{d1} \text{sign}(\dot{\theta}) + K\theta - C_{w1} = C(t) \quad (2.5)$$

for $F_{\text{down}}L \geq C(t) \geq 0$

$$J\ddot{\theta} + c_v\dot{\theta} + C_d \text{sign}(\dot{\theta}) + \kappa(\theta - \theta_0) - C_w + C_s(\theta, \dot{\theta}) = C(t) \quad (2.6)$$

for $F_{\text{down}}L \leq C(t)$

The parameters of the model can be estimated by means of a few experiments and measurements. The parameters of the right-hand sides of Eq. (2.2) and Eq. (2.4) have been estimated by measurements on the separate elements, as described in Lozada [2007]. Their values are given in Table 2.1. The other values of the parameters of Eqs. (2.5) and (2.6) are given in Table 2.2. A second estimation of C_w and the estimation of C_d are given by the static test described in Section 2.2:

$$C_w = L \frac{F_{\text{down}} + F_{\text{up}}}{2} \quad (2.7)$$

$$C_d = L \frac{F_{\text{down}} - F_{\text{up}}}{2} \quad (2.8)$$

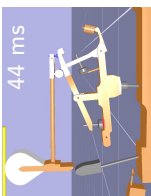
Parameter	Numerical value
J	0.0221 kg.m ²
C_w	0.138 N.m (Eq. (2.7) yields $C_w = 0.132$ N.m)
C_d	0.039 N.m
c_v	0.0273 N.m.s ⁻¹
κ	0.4 N.m
θ_0	0.1947 rad
θ_e	0.0343 rad
θ_p	0.0397 rad
k	1.6×10^{10} SI unit
b	2×10^9 N.s.m ⁻³
r	2.7
K	60 N.m

Table 2.2 – Parameters of the SK and BH models, according to Eqs. (2.1), (2.2) and (2.4).

2.4. Simulations

This part presents simulations of the position of the key in response to given forces (force-driven simulations) and conversely, the reaction of the key to a prescribed motion at its end (motion-driven simulations).

As mentioned in Section 2.3, the inertial aspect of the model is invalid between the escapement and the check of the hammer. However, we chose to continue the simulation all along.



For a given force profile (here: $F_{\text{meas}}(t)$), the angular position of the key $\theta_{\text{simul}}(t)$ (and the displacement $y_{\text{simul}} = L\theta$ of the end) has been obtained by solving numerically Eq. (2.5) followed by Eq. (2.6) with $C(t) = F(t)_{\text{meas}}/L$. The link between the two models was done by linear interpolation of the momentum of inertia $\tilde{J}(\theta)$ and the momentum of weights $\tilde{C}_w(\theta)$ from their values in the first phase to their values in the second phase. The numerical integration has been done by the NDSolve function of Mathematica[®], using an Adams method with a maximum step limit of 30000. The results of these force-driven simulations are presented in Figure 2.6 for three different strengths of the keystroke: *piano*, *mezzo forte* and *forte*.

We also present the result of the simulation of Eq. (2.6) alone, with initial conditions given by the observation of θ and $\dot{\theta}$ at t corresponding to $F(t) = F_{\text{down}}$. The drift that can be observed in these simulations is discussed in Section 2.5.

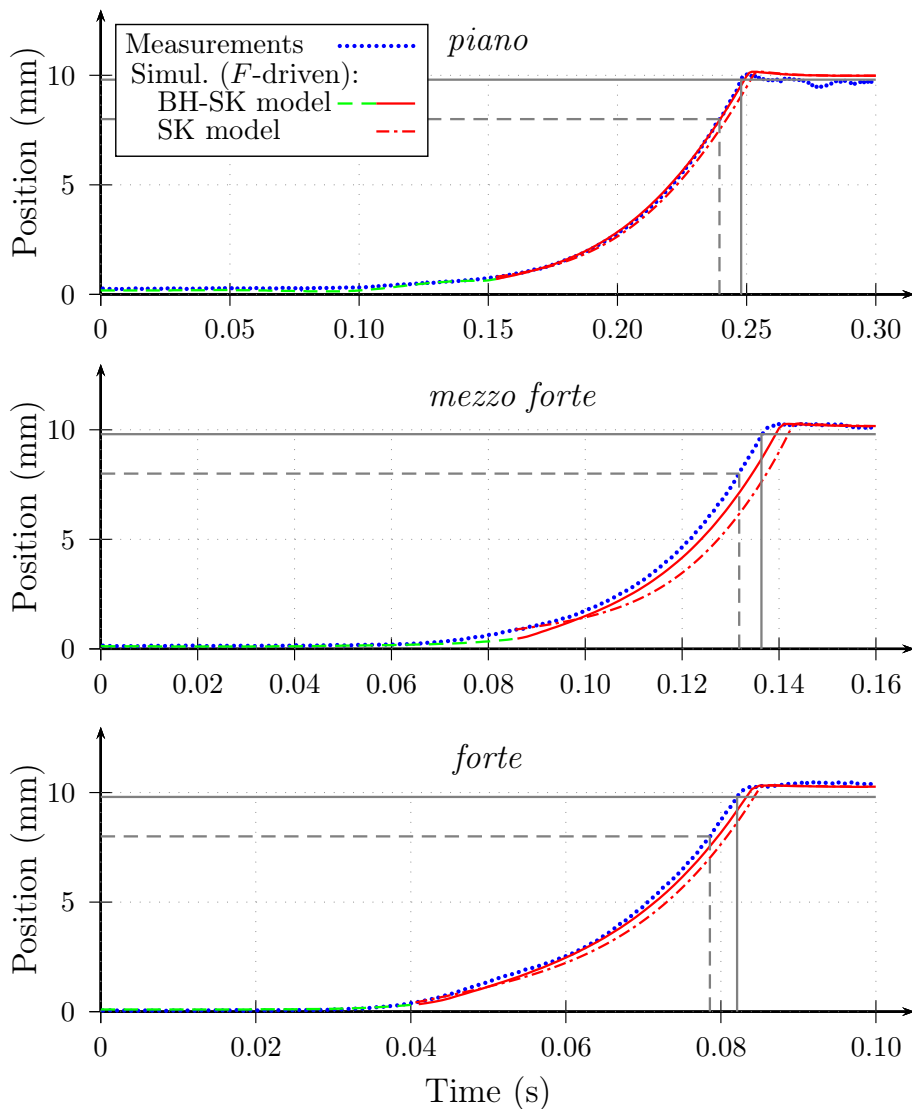


Figure 2.6 – Position y of the end of the key during various strokes. Dotted (blue) line: measured position. Dashed (green) line: simulated position according to Eq. (2.5) (BH model). Plain (red) line: simulated position according to Eq. (2.6) (SK model). Dash-dotted (red) line: simulated position according to the SK model starting with initial conditions taken in experimental data (see text). Gray vertical and horizontal lines: see caption of Figure 2.2.

Conversely, motion-driven simulations yield $F_{\text{simul}}(t) = C(t)/L$, the opposite of the reaction force exerted by the key for a prescribed motion $\theta(t)$ (here, $\theta(t) = x_{\text{meas}}/L$). According to Eq. (2.5) and Eq. (2.6), such simulations are straightforward, once the position and the acceleration of the key have been measured and the velocity has been estimated (see Section 2.2). The results are presented in Figure 2.7 for the same keystrokes as in Figure 2.6.

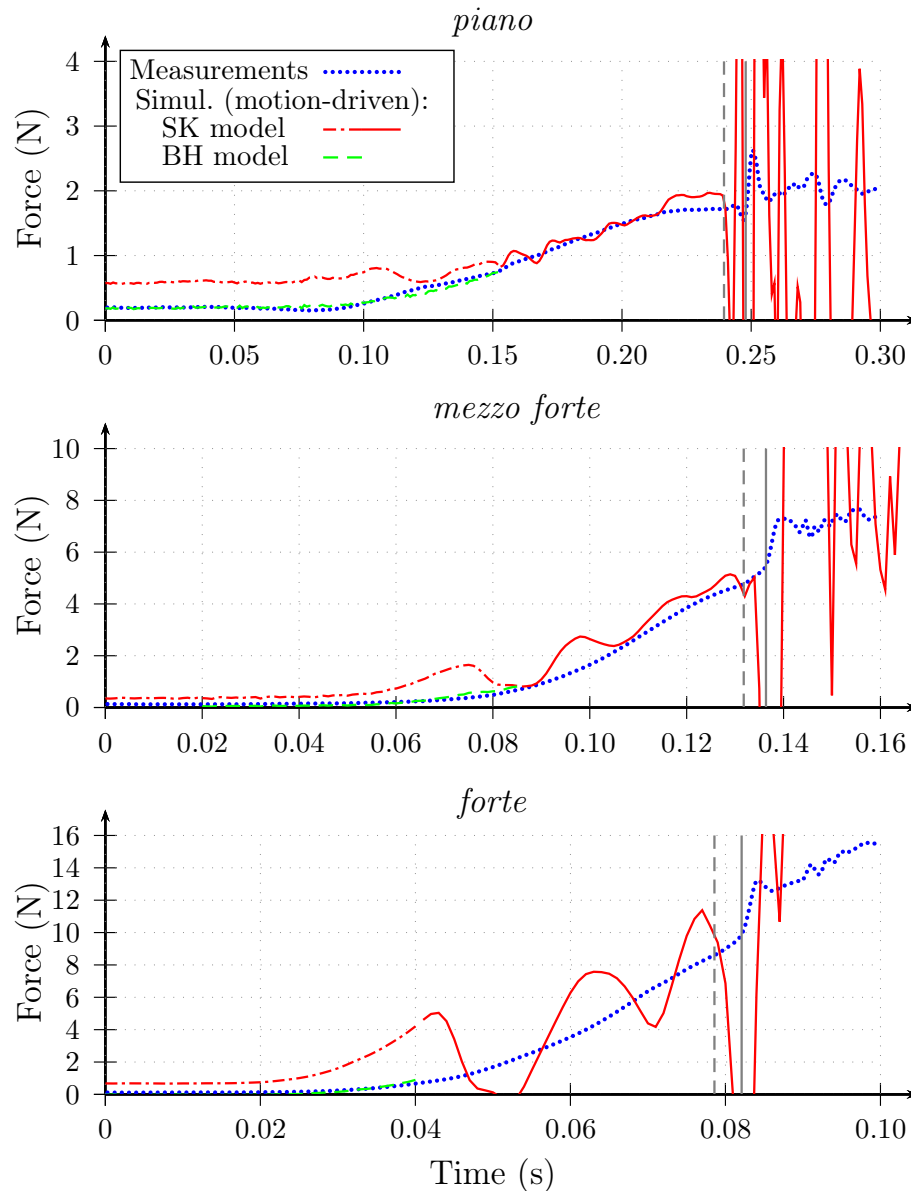
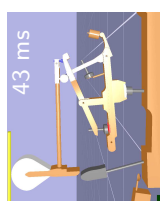


Figure 2.7 – Force F applied on the end of the key during various strokes. Dotted (blue) line: measured force. Dashed (green) line: simulated force according to Eq. (2.5) (BH model). Dash-dotted and plain (red) line: simulated position according to Eq. (2.6) (SK model). Before the split between the dash-dotted and the plain lines, corresponding to $y = \theta L \approx 0.8\text{mm}$, it is clear that the BH model must be used instead of the SK model. Gray vertical lines: see caption of Figure 2.2.



2.5. Discussion

After the escapement, the key hits the front rail punching. This piece does not differ between traditional keyboards and numerical keyboards. Since the latter are not judged as of equivalent quality by pianists, one should infer from this observation as well as from how pianists test and feel a keyboard, that the haptic feedback before escapement is of prime interest for them. Therefore, the discussion is primarily focused on this phase of the motion.

A first and basic finding can be deduced from the experimental observations reported in Figure 2.2. As can be seen in the bottom frame of this figure, the dynamics of the mechanism is dominated before escapement by the inertia of its pieces, taken as a whole. The other-than-inertial dynamical effects due the internal degrees of freedom, the various stops that are met or left by the pieces, etc. appear as time variations of the difference $F(t) - \ddot{y}(t)J/L^2$. The corresponding wiggles can easily be distinguished in the bottom frame of Figure 2.2, even though the motion (top frame) is quite smooth. Although not surprising, this elementary observation has important implications with regard to the main point raised in the introduction: in order to validate a dynamical model, should the dynamics be examined as producing a force in response to an imposed displacement or vice-versa?

From a purely experimental point of view, it is generally difficult to drive a mechanism with a rapidly changing force or acceleration. In this particular case, it would not be advisable either, since it would generate vibrations in the key that would mask the time-variation of the key displacement that are expected to be characteristic of the dynamics mechanism, considered as an assembly of rigid bodies. Altogether, realistic experimentations would consist in pushing this mechanism with a smooth force-profile, or with a smooth motion-profile similar to the ones reported here. Since the dynamics of this particular mechanism is dominated by inertia until escapement, it follows that the acceleration is generally smooth, possibly displaying some wiggles. When looking at the angular position of the key or *displacement* of the end of the key (imposed force), these potential wiggles in the acceleration are heavily filtered by the double time-integration: the differences between inertia and the complete dynamics of the system becomes hard, if not impossible, to distinguish. In other words, *any* model, provided that it is inertia-dominated, is likely to appear as very good when checking its validity by means of comparisons of motion-results obtained in force-driven simulations and tests, before escapement. This lack of sensitivity of the results to the model is represented by a "0" in upper left cell in Table 2.3.

Input	F	\dot{y} and y	y	\ddot{y}
Output	y	F	F	F
Model	0	+	+	+
Initial cond.	+	0	0	+
Noise	0	0	+	0

Table 2.3 – Sensitivity of the results of the simulation, driven as indicated in the first line, to the elements indicated in the first column. "+" means "sensitive". "0" means not or little sensitive.

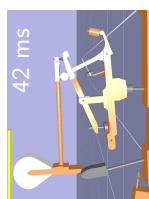
Bearing that in mind, we analyse now the diagrams in Figure 2.6, where the "blocked hammer" (BH) and "simplistic key" (SK) models are ruled by a given force and yield a certain motion (plain red line). Our first remark pertains to the sensitivity of the SK model to initial conditions. Simulations based on the SK model alone are represented by a dashed line. They are run with initial conditions that are taken from the experimental data: position and velocity for a force slightly exceeding F_{down} . The corresponding curves display a drift compared to those issued of the succession of BH-SK models. This denotes a high-sensitivity of the SK-model to the initial conditions, more precisely, the initial velocity, consistent with the fact that the dynamics is dominated by inertia. This sensitivity is represented by a "+" in the second cell of the left-most column in Table 2.3. The experiment/simulation comparisons that can be done in Figure 2.6 seem to fully validate the succession of the "blocked key" and the "simplistic key" models, including after escapement and the check of the hammer. Although this is obviously a very crude model, this is consistent with the above remark that any model seems correct under the circumstances and restrictions described above (upper left "0" in Table 2.3).

Simulations with the same experimental tests, using the same model but driven by the motion data (instead of the force data) yield force results that look, by contrast, very different from their experimental counterparts. The experimental/simulation comparisons presented in Figure 2.7 cannot be considered as a validation of the "simplistic key" model. Only a more elaborate model could yield simulation results that would better match the observations. This sensitivity to the model is summarised by the "+" in the second column of the first line in Table 2.3. Although not of essential interest, it is worth noticing that at the very beginning of the motion, the BH model seems to predict kinematics (force-driven simulations) as well as dynamics (motion-driven simulations).

The results reported here have been obtained by using both position and acceleration experimental data. If one uses only position data, the velocity and the acceleration must be calculated by successive time-derivations, before escapement. The result is known to be very sensitive to noise in the initial data. Conversely, using acceleration-data only requires successive time-integrations, generating drifts and corresponding to a high-sensitivity to the determination of initial conditions. For a synthesis of these remarks, see the corresponding cells in Table 2.3.

In the literature, many authors chose to report their results in terms of the kinematics of the hammer. We did not represent the motion of the hammer but it derives directly from that of the key. Since the SK model relies on geometrical relationships between the angular positions of the pieces, the motion of the hammer is zero in the "blocked hammer" phase and becomes proportional to the shifted angular position of the key, the shift corresponding to the angular position of the key when the hammer begins to move.

The first set of comparisons presented by [Oboe, 2006] (Figure 18) is purely kinematical. His second set (Figure 19) presents key and hammer motions in response to a force applied to a 2-DOF model. Van den Berghe presents a 3-DOF model. Again, the resulting key's and hammer's motions in response to a force look very similar to measurements. Using different 2-DOF models for different kinematic constraints, Gillespie [Gillespie et al., 2011] also compares the calculated and measured key's displacements (Figure 9). Rubber has been added between the bodies in order to regularise the behaviour of the system. Hirschorn & al. use a 5-DOF model to compute the hammer's and key's positions for a given force input, in *piano* (Figure 12 and 14) and in *forte* (Figure 13 and 15). The authors



deduce from the similarities with measurements that the model predicts the behaviour of the piano action with reasonable accuracy. Again, the kinematics of the bodies are calculated by Links with a 5-DOF model for a force input (Figure 5.3 to 5.6) and match well the measurements.

All these authors (a) compare simulated kinematics in response to a force-profile and (b) find a good agreement with measurements. According to the previous remarks, (b) is quite understandable. It would also be surprising that significantly different models could be valid to the same precision. Our first and main conclusion is that looking at the resulting motion of force-driven simulations cannot discriminate between good and bad models (provided they are inertia-dominated before escapement) and thus is not appropriate as a validation method. Moreover, the sensitivity of the simulated position of the key (or of the hammer) to initial conditions is an other reason for ruling out this choice of simulating the dynamics of a piano action by means of a force input. We recall here that this sensitivity is due to the dominance of inertia in the dynamics, not to the model itself.

Some events are very important for the pianist such as the jack/let-off button contact (dashed vertical gray lines in the diagrams) or the escapement of the hammer. The model presented here and other models with 1 or 2 DOF do not take them into account, which probably makes them haptically irrelevant. What matters is that this irrelevance does not appear in the force-driven simulations. On the reverse, the measured force becomes very different from the force calculated by motion-driven simulations with the SK model, starting from the let-off.

Almost immediately after escapement, the key meets the front rail punching (plain vertical gray lines in the diagrams), the dynamics of the mechanism is dominated by the corresponding nonlinear and lossy spring (Eq. (2.3)). This can be seen in the right part of the top and bottom frames of Figure 2.2: the position is almost constant and the force on the key has a main constant component with, again, some wiggles. Following the same analysis as above, any model which includes a stop with the appropriate stiffness is likely to appear as very good if one looks at the motion, considered as the output of a dynamical system subject to a smooth force profile. As explained before, the rapidly changing forces represented in the bottom frame of Figure 2.2, or the forces measured in Figure 2.7, are not good candidates for a profile to be used either as a driving experimental force. For the reasons explained previously, they are not good inputs for a dynamical model either.

After escapement, the SK model is evidently worse than before escapement: the change in momentum of the hammer is ignored, as is the blocking due to the catch. However, driving the SK model with the measured forces yields an excellent agreement with the measured displacement at the end of the key (Figure 2.6). Conversely, tests where (smooth) position profiles are used as inputs yield simulated forces which differ strongly from the measurements (Figure 2.7). The previous reasoning on the apparent validity of inertia-dominated models can be transposed to stiffness-dominated models, after escapement. The conclusion is the same: matching measured motion and results of force-driven simulations cannot prove that a model is valid.

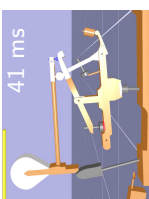
2.6. Conclusion

Observations of the dynamics of the piano action show that it is dominated by inertia before escapement and by stiffness after the key has met the front rail punching. By

means of simulations of too simple models, we have shown that the comparison between measured positions (of the key or the hammer) and positions given by force-driven simulations cannot validate a dynamical model of the piano action. Although they may be subject to noise, position-driven simulations must be used instead and the forces be compared. A minor conclusion of this paper is that the blocked-hammer model seems to be valid during the very first stage of the key motion. However, the main parameter (stiffness) of this model was adjusted here.

Driving the mechanism (whether experimentally or virtually) with a force profile yields kinematic information. A 1-DOF model is sufficient to account for the kinematics of the key all along. Only one parameter (damping after hammer check) of the 1-DOF model had to be somewhat arbitrarily chosen. Although the bibliography of the late fifteen years presents 2- or more DOF models, a 1-DOF model may also well be sufficient for rendering the hammer kinematics before escapement.

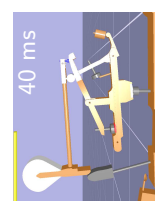
Driving the mechanism with a motion profile and looking at the reaction force reveals the dynamics. The complexity of the internal dynamics is reflected in the rapid wiggles of the measured forces. Only a sophisticated model may render the dynamics of the action, possibly one of those which have been published, if it meets the force-comparison test.



Overview In this chapter, the experimental set-up of the piano action is described. It includes kinematical measurements of all the bodies and dynamical measurements of the key. These experimental results are compared to simulation results in Chapter 6 and used to validate the model presented in Chapter 4.

Contents

3.1. Kinematics	35
3.1.1. Laser sensors	35
3.1.2. Accelerometer	36
3.1.3. Estimation of the velocity	36
3.1.4. Tracking of the position of each body	37
3.2. Force	39
3.3. Actuation of the key	41
3.4. Trigger and acquisition	45
3.5. Summary of measurement errors and uncertainties	45



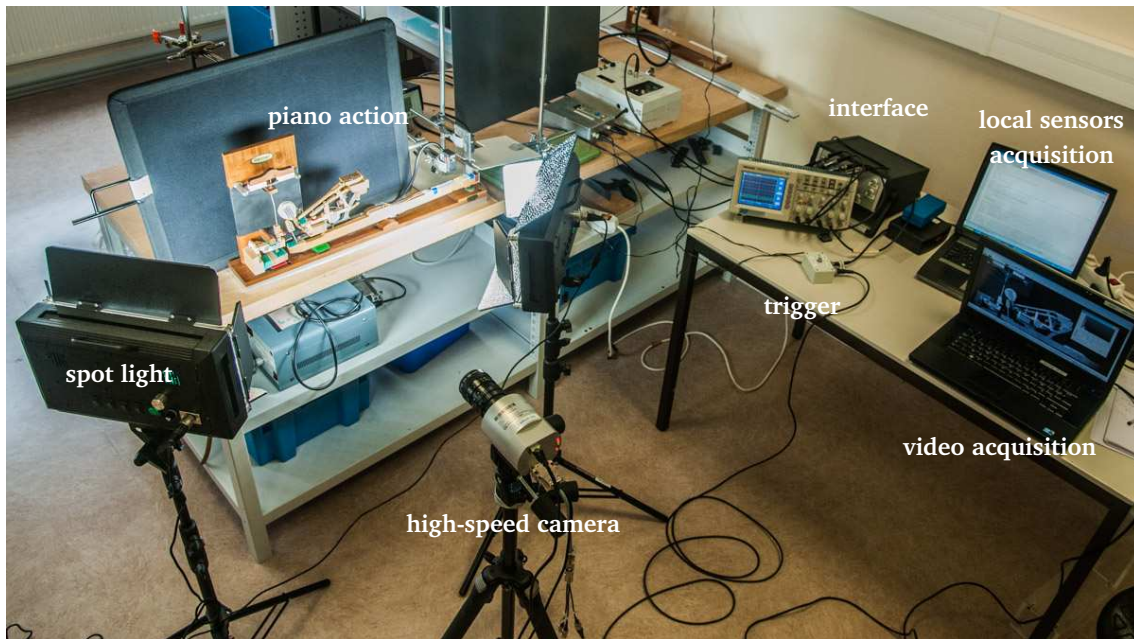


Figure 3.1 – Complete experimental set-up.

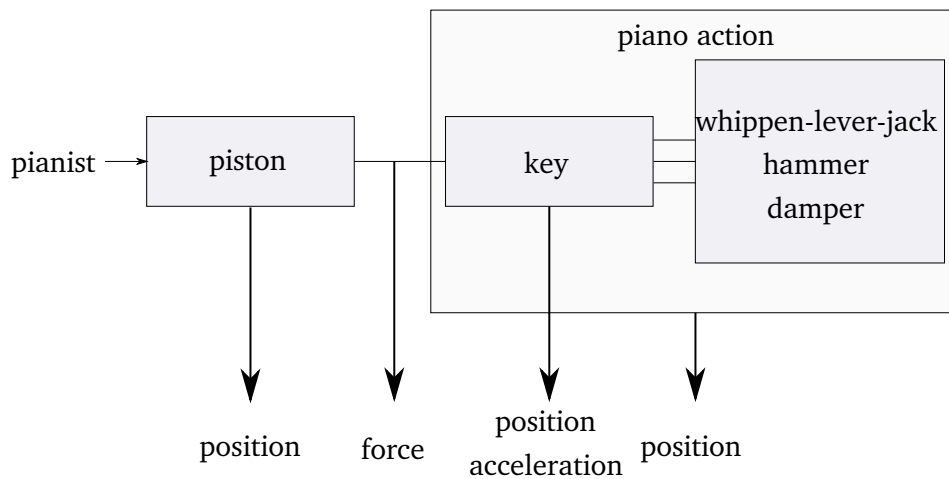


Figure 3.2 – Scheme of the measurements.

The motion of the piano action had to be measured in order to be compared with the numerical results of the simulations. We essentially focused on the measurements of the key because that is where the pianist interacts with the action. Complementary measurements on each rigid body were done for a better comparison.

Because it was not possible to use directly the displacement of the key as an input for the simulation, a piston was inserted between the finger and the key. The upper face of the piston had to be measured. More details on the necessity of the piston are given in 5.4.1 page 91.

A photograph of the complete set-up is shown in Figure 3.1 and the various measurements are presented in Figure 3.2. The kinematic ones included:

- the position of the key (3.1.1);
- the position of the upper face of the actuation device (3.1.1);

- the acceleration of the key (3.1.2);
- an estimation of the velocity of the key (3.1.3);
- the position of each body using a high-speed camera and video tracking (3.1.4).

As we are interested in the dynamics of the piano action, the reaction force of the key on the pianist's finger was also measured (3.2).

The actuation of the key is described in 3.3. Data acquisition and synchronisation are presented in 3.4. All the measurements errors and uncertainties are summarised in 3.5.

3.1. Kinematics

3.1.1. Laser sensors

To measure the position of the upper face of the piston and that of the key, laser sensors (Keyence LB12 with LB72 amplifier units) were used, since they do not change the dynamics of the piano action. Their response was set to 0.15 ms, which corresponds to a resolution of $50\ \mu\text{m}$. Their sensitivities were measured using a graduated marking gauge and were estimated at 0.398 V/mm and 0.449 V/mm. The lasers were positioned as shown in Figure 3.3.

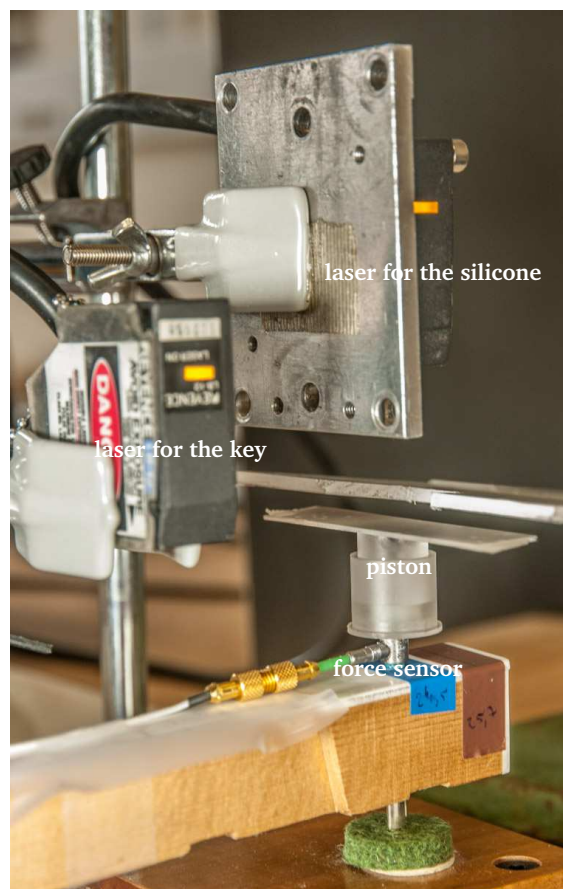
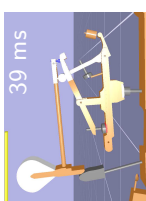


Figure 3.3 – Set-up for actuating the key.



3.1.2. Accelerometer

An Endevco[®] 2250A piezoelectric sensor was used to measure the acceleration of the key (sensitivity: $0.316 \text{ V}/(\text{m} \cdot \text{s}^{-2})$). The accelerometer was placed in the middle of the key, between its the centre of rotation and the piston. This signal was amplified with a Brüel & Kjær Nexus conditioning amplifier and filtered by a band-pass filter (lower and upper cut-off frequencies: 0.1 Hz and 3 kHz, respectively). The mass of this accelerometer is 0.4 g.

3.1.3. Estimation of the velocity

Trials with a Polytec PDV-100 laser vibrometer failed to measure the velocity, as the motion of the key was too slow. Two alternatives were studied. The first one uses the Matlab script corresponding to [Chartrand, 2011] and proposed by its author. It consists in minimising the functional

$$\mathcal{F}(u) = \alpha \int_{[0,T]} |u'| + \frac{1}{2} \int_{[0,T]} |Au - y|^2 \quad (3.1)$$

where y is the position signal, T its temporal length and A is the operator of anti-differentiation ($Au(t) = \int_{[0,t]} u$). The first integral controls the regularity of the solution without penalising jumps. The second integral ensures that u is the differentiation of y . This solution gave acceptable results, see Figure 3.4. The parameters¹ were empirically chosen as $\alpha = 5 \times 10^{-5}$, 20 iterations and $\varepsilon = 10^{-9}$.

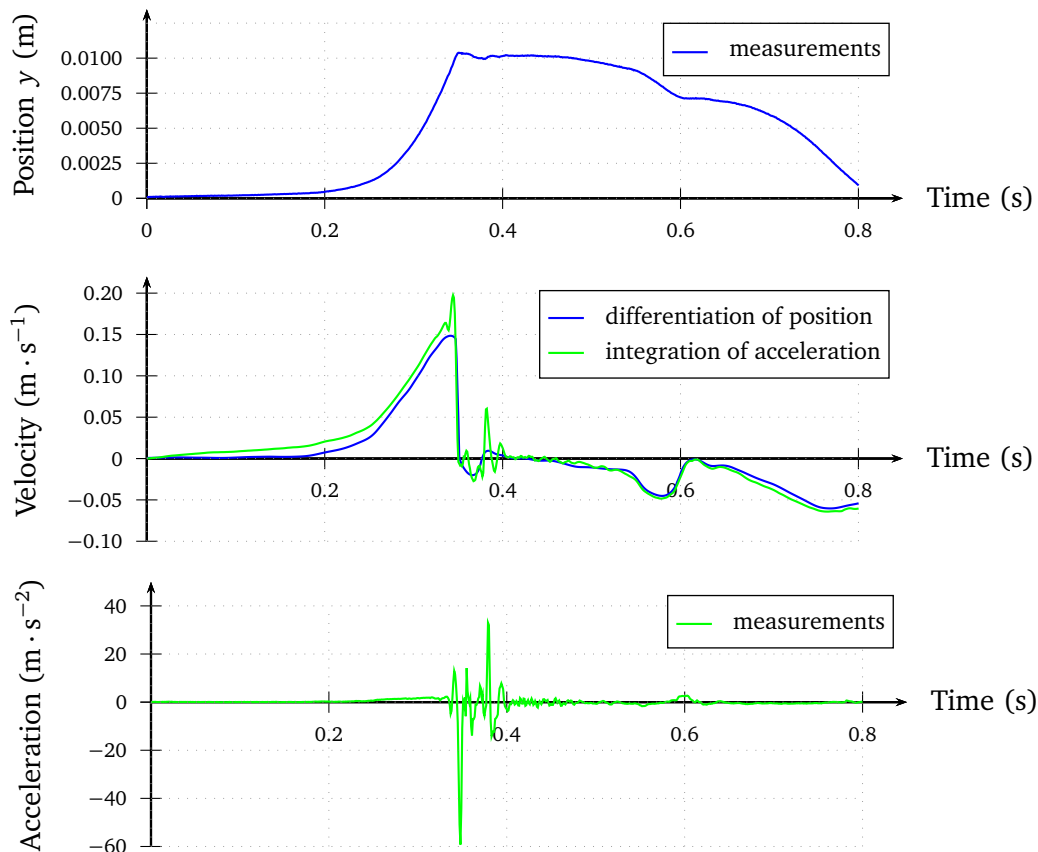


Figure 3.4 – Comparison of the integration of the acceleration and the differentiation of the position, piano keystroke.

¹ ε is a numerical parameter to avoid division by zero and α is a weighting factor, see [Chartrand, 2011].

The second estimation was done by integrating of the acceleration after making sure that it actually corresponded to zero when the key was at rest. Integrated data showed good agreement with the derivative of the position for *piano* keystrokes, see Figure 3.4. For *forte* keystrokes, the acceleration was either saturated (too large accelerations), or inaccurate (large resolution to avoid saturating).

Total-variation differentiation was used because it worked straightforwardly for all keystrokes. Also, no noticeable differences appeared in the results between the two estimations of the velocity, because the actuation device was only slightly dissipative.

3.1.4. Tracking of the position of each body

The kinematics of all the bodies provided information on the dynamics, and allowed additional comparisons of simulation results. The purpose of measuring the position of each body was to estimate the shape of their curves and especially the instant of significant variations, which indicates a change in the contacts. The qualitative behaviour was compared to the simulated position (see Chapter 6). The positions were measured using a high-speed camera, which does not disturb the dynamics of the piano action.

We used a Simi HCC-1000 high-speed high-resolution camera, composed of four CMOS sensors. The highest available acquisition frequency with a resolution of $1024\text{px} \times 512\text{px}$ was 923 fps which corresponds to one image every 1.083 ms.

The camera acquisition was triggered by a hardware trigger sending an +5 V rising edge, which allowed synchronisation with other measurement devices (see section 3.4).

The videos were treated using the KLT tracking algorithm.

KLT tracking

KLT stands for Kanade-Lucas-Tomasi who developed so-called KLT feature trackers. The recorded video is decomposed in N images (frames) of size $1024\text{px} \times 512\text{px}$ and coded in RGB colour space². Let us call F_n the n -th frame. F_n assigns to any pixel its associated RGB colour, therefore $\forall i \in \llbracket 1, N \rrbracket, F_i : \llbracket 1, 1024 \rrbracket \times \llbracket 1, 512 \rrbracket \rightarrow \llbracket 1, 256 \rrbracket^3$. Let us denote by \mathcal{Z} the zone which has to be tracked. The KLT algorithm consists in finding $h \in \mathbb{R}^2$ which minimises a distance between $F_n(x)$ and $F_{n+1}(x+h)$, $\forall x \in \mathcal{Z}$. Kanade and Lucas proposed to measure the distance using the L_2 norm which leads to a classical minimisation problem. More details are given in [Lucas et al., 1981; Tomasi and Kanade, 1991].

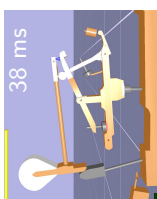
An implementation of the KLT algorithm was proposed in the Matlab CRTtoolbox [Barbacci et al., 2013].

To make the tracking easier, high-contrast patterns were stuck to every rigid body.

Pattern choice

Different patterns have been tested: single signs such as squares, triangles, stars and dots gave acceptable results but were either too small to be spotted or too large to be accurate. In order to reduce the measurements uncertainties, more complex patterns were tested: grids, draughtboards, parallel lines, dot grids and irregular draughtboards, see Figure 3.5. All the regular patterns failed to give acceptable results for the hammer: its velocity was

²In our case, the videos were made in 8 levels of grey, but this does not matter for the understanding of the KLT algorithm.



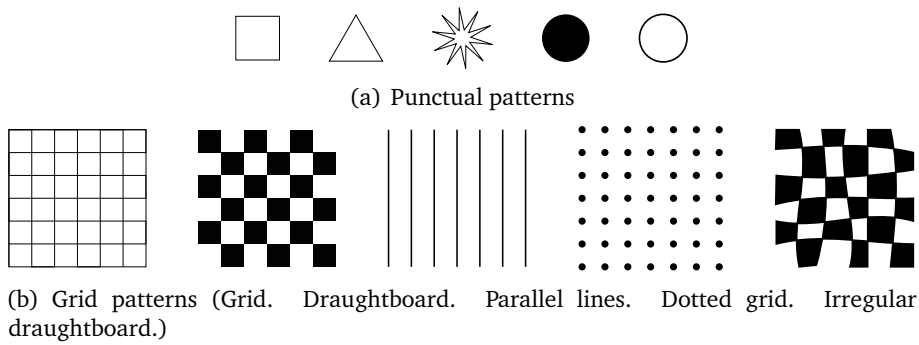


Figure 3.5 – Tested patterns for KLT tracking.

high so that its displacement observed in two consecutive frames could be equal to several periods of the pattern. This made the determination of its correct position impossible: the algorithm could detect minima of the cost function³ in the neighbourhood of the tracked points which were not the right one. This phenomenon could be seen as the tracked points of the hammer shifted from their initial positions and all ended in the same area. On the contrary, this was not observed using irregular draughtboards which probably increase the convexity of the cost function.

An overview of the tracking is shown in Figure 3.6 and typical results from the final treatment are plotted in Figure 3.7. The comparison of the estimated position of the key using the laser sensor and the high-speed camera shows that the latter gives a relative error of 5%, which was considered acceptable for the qualitative analysis of Chapter 6.

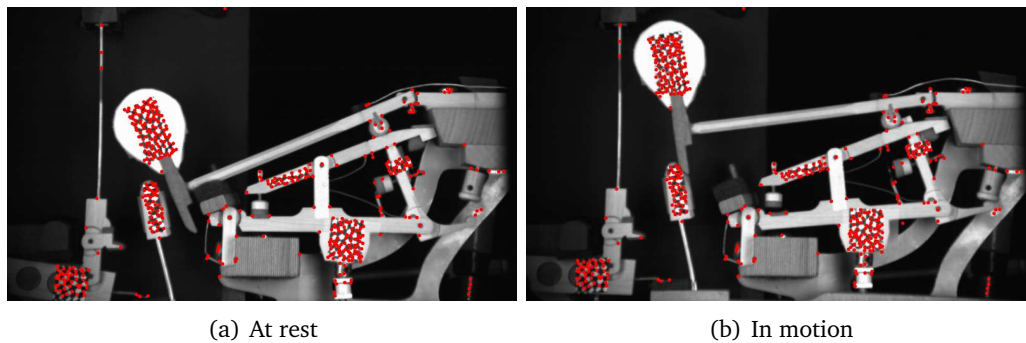
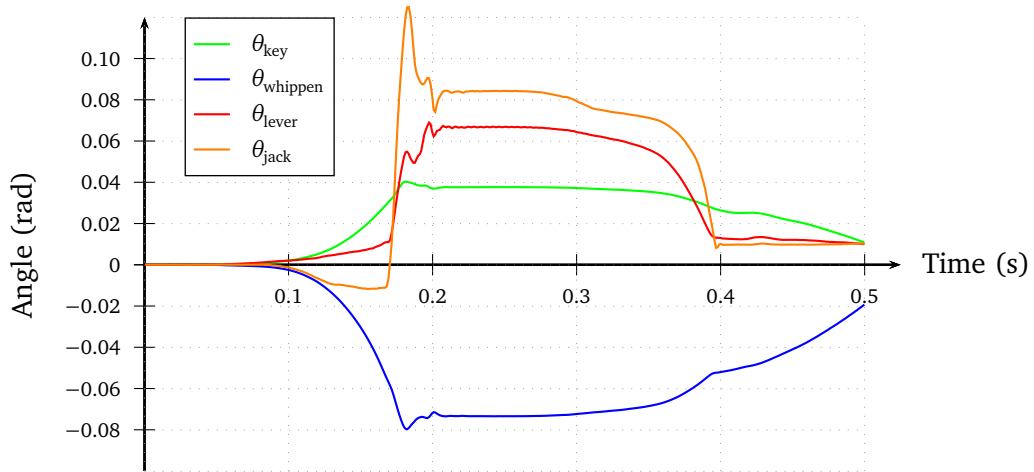


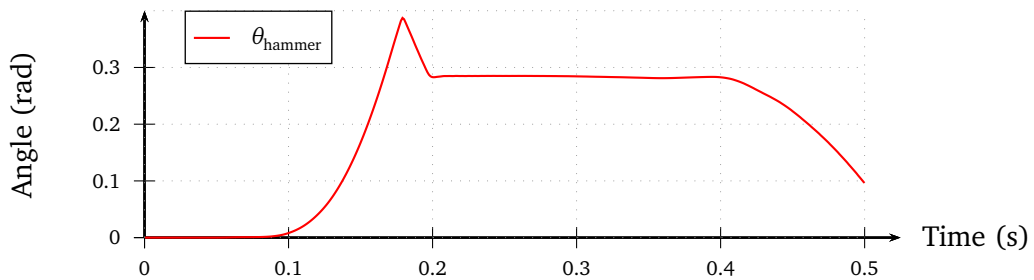
Figure 3.6 – Illustration of KLT tracking with the selected patterns.

³The cost function is defined by

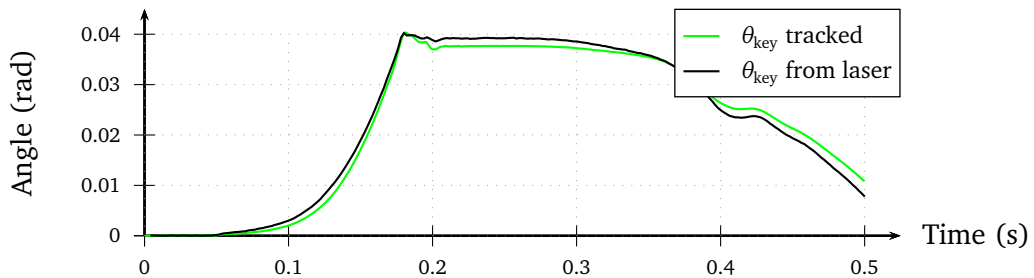
$$\mathcal{J}(h) = \sum_{x \in \mathcal{Z}} \|F_n(x) - F_{n+1}(x+h)\|^2 \quad (3.2)$$



(a) Tracking of the key, whippen, lever and jack positions



(b) Tracking of the hammer position



(c) Comparison of the key's position measurements

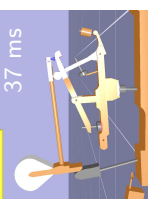
Figure 3.7 – Angles of the bodies tracked by KLT algorithm.

3.2. Force

We also measured the force exerted on the key to capture the dynamics of the action. The force sensor was a Kistler Model 9211 of 1.2 g. When compressed, this piezoelectric sensor (quartz) generates a charge signal proportional to the load acting on the sensor (sensitivity: 4.403 pC/N). The signal was amplified using a Kistler 5015 Charge Meter with a high-pass filter (cut-off frequency $\ll 1$ Hz) and a second order low-pass filter (cut-off frequency: 3 kHz). Probably due to insufficient insulation, a very regular 50 Hz sinusoidal signal was detected in the force signal. The oscillatory nuisance was subtracted by a fitting of the form

$$\alpha \sin(100 \pi t + \phi) \quad (3.3)$$

with a least squares method, on a few periods just before the keystroke. It perfectly corrected the disturbance, see Figure 3.8.



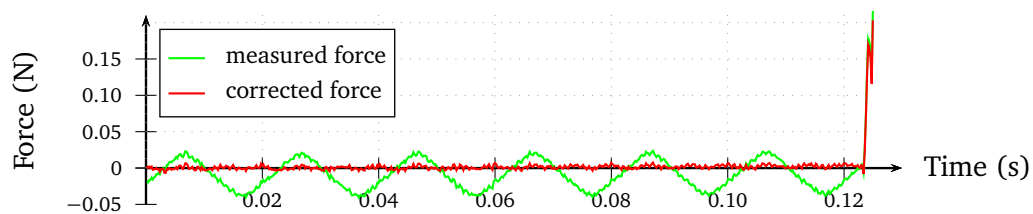


Figure 3.8 – Correction of the 50 Hz signal captured in the force measurement.

Typical measurements are shown in Figures 3.9 and 3.10 for *piano* and *forte* keystrokes, respectively. The position curves are much smoother than the force curves, as observed in Chapter 2.

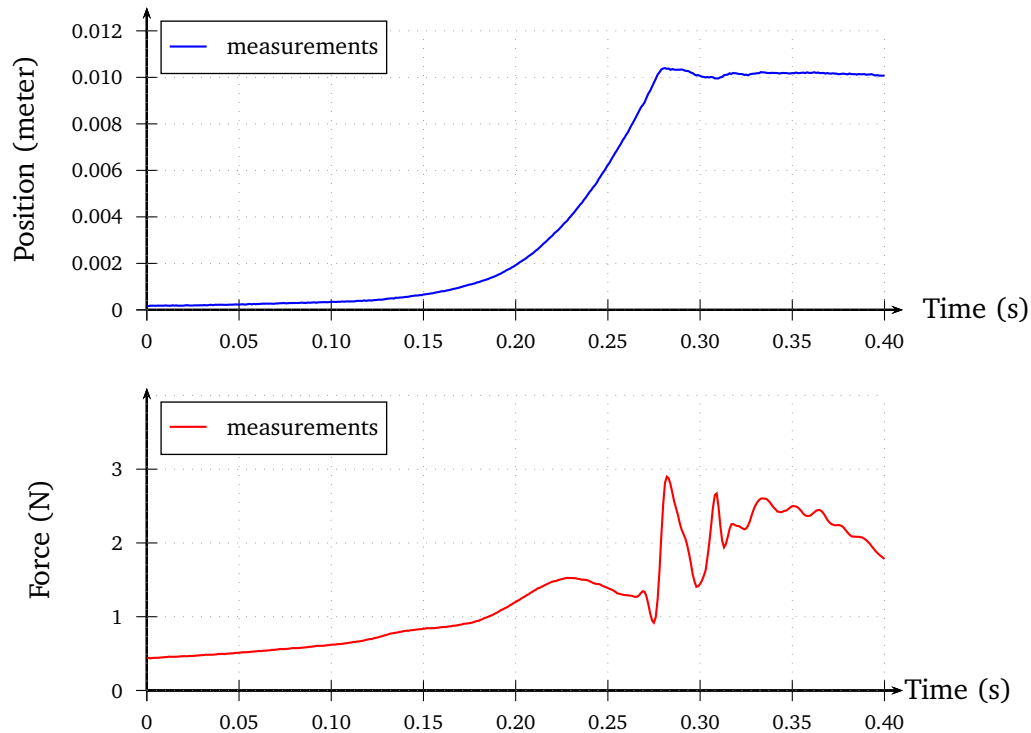


Figure 3.9 – Typical measurements of the force exerted on the key and its position, piano keystroke.

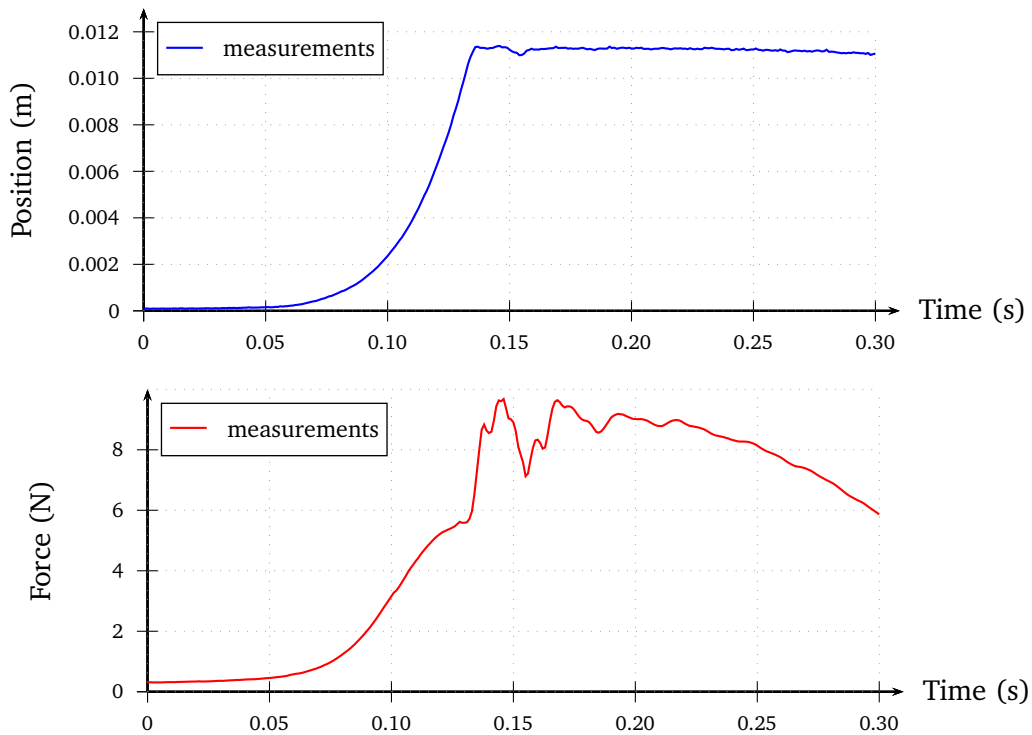


Figure 3.10 – Typical measurements of the force exerted on the key and its position, forte keystroke.

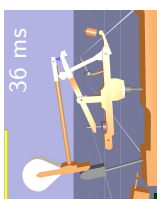
3.3. Actuation of the key

As the piano action is a highly non-linear mechanism, it must be studied for keystrokes that are representative of the players' ones. In particular, using a mass to apply a constant load does not ensure that the proper dynamics is being studied. It has been observed that the use of a pendulum does not lead to the same depressing of the key as that of a human player [Askenfelt and Jansson, 1990].

For the same reasons, results of this thesis are usually presented for different keystrokes, reaching respectively about 2 N and 10 N. For simplicity, they are referred to as *piano* and *forte* keystrokes. A standard *forte* corresponds to a maximum of 30 N according to [Hirschhorn et al., 2006].

Some attempts were done to actuate the key with a step-by-step motor, but the latter could not deal with the velocities and the accelerations needed. Satisfactory results were obtained when actuating the key by applying the force directly on the force sensor. Reproducibility of the motion, which depends on the skills of the player, was indeed not required.

The main conclusion from Chapter 2 was that the simulations should be driven by a position. The simulation methods we used did not offer such a possibility. This was worked around by coupling the key, in the model, to a PD corrector, the free end of which would be driven by a position – this solution had been implemented in the computer program used for the simulation. In the experiments, we added a device which aimed at corresponding to the PD corrector. The device included a piece of silicone, the behaviour of which was correctly modelled with a viscoelastic law. More details of the PD corrector are given in Chapter 5 (5.4.1).



The viscoelastic material was chosen so that it had a behaviour close to that of a finger, in order to filter the force in a similar way. The Ecoflex®Shore 00-30 hardness A silicone was finally selected. The identification of its viscoelastic properties is set forth in paragraph 3.3.

Addition of a piston between the finger and the force sensor The silicone was placed inside a piston, the upper position of which was measured by a laser, see Figure 3.11. A photograph of the piston has been shown in Figure 3.3. We denote by y_{silicone} the upper position of the piston, and by y_{key} the position of the key.

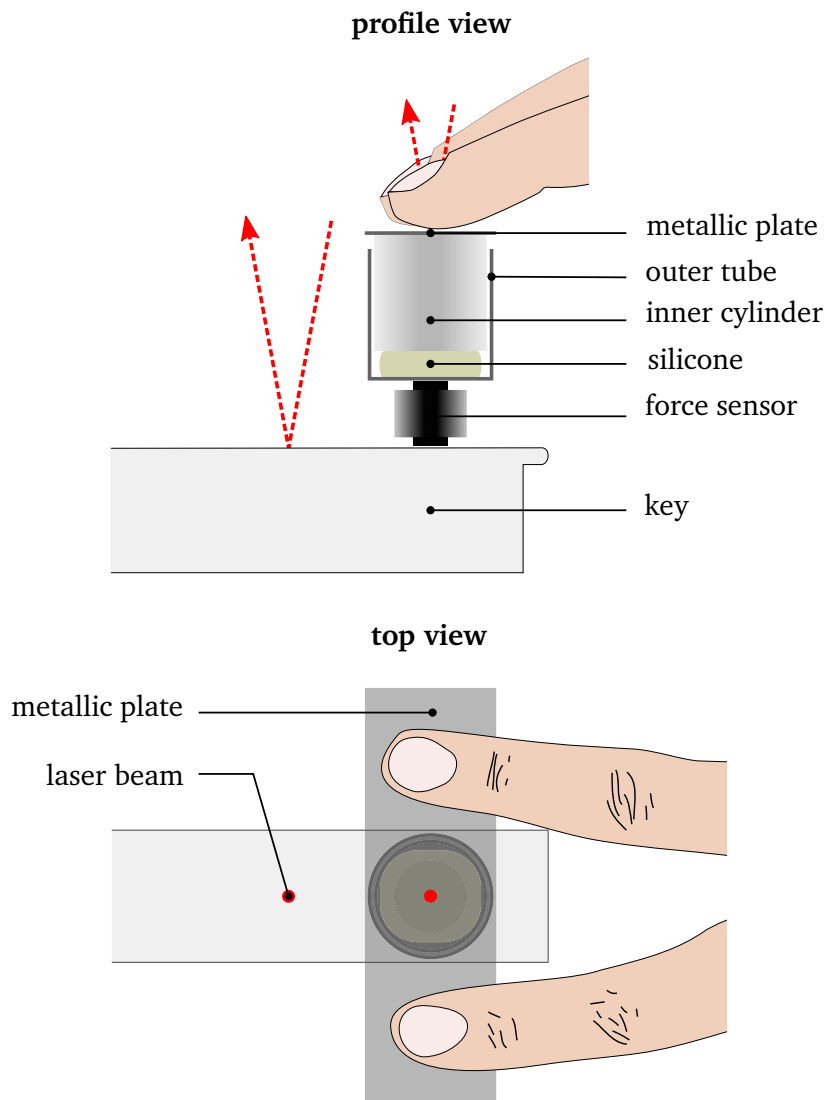


Figure 3.11 – Scheme of the piston used to press on the silicone.

Chapter 6 shows that this solution led to good results. Yet, it has some drawbacks:

- the force exerted by the pianist had to be symmetrical enough so that the device would not topple over, which in practise also limited the maximum applied force;
- a gap between the outer tube and the inner cylinder was required so that they could slide; this gap introduced a bias in the measurement of the upper face's position of the silicone.

Identification of the viscoelastic properties of the silicone The silicone was assumed to be viscoelastic. The parameters of the law (elastic coefficient a and viscous coefficient b) were determined using the above-mentioned piston on the clamped key, in order to remain as close as possible to the measurements of the piano action.

The position of the upper face of the piston y_{silicone} as well as the reaction force F of the key were measured. The values of a and b were then identified using a least square method. Setting the initial position to 0 mm and as the initial velocity was $0 \text{ m} \cdot \text{s}^{-1}$, the least square optimisation problem consisted in finding (a, b) which minimised the function

$$J(a, b) = \sum_{i=0}^{i=N} [F(t_i) - (a y(t_i) + b \dot{y}(t_i))]^2 \quad (3.4)$$

where t_i is the i -th measurement time and t_N the final time. The velocity \dot{y} was calculated as described in 3.1.3.

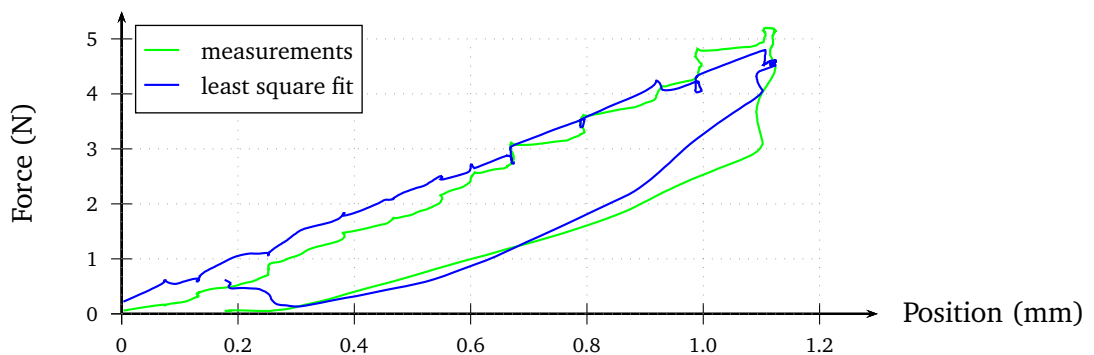


Figure 3.12 – Typical fit of the linear viscoelastic behaviour of the piston.

A typical result of such an optimisation is given in Figure 3.12. In total, ten measurements were completed for varying maximum forces. Identifications results are plotted in Figure 3.13. The arithmetic mean and standard deviation of the values of a and b are set forth in Table 3.1.

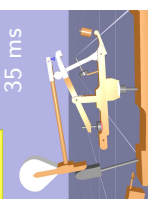
	mean value	standard deviation
elastic coef. a	$\bar{a} = 6.5 \times 10^3 \text{ N} \cdot \text{m}^{-1}$	$\sigma(a) = 702 \text{ N} \cdot \text{m}^{-1}$
viscous coef. b	$\bar{b} = 134 \text{ N} \cdot \text{s} \cdot \text{m}^{-1}$	$\sigma(b) = 92 \text{ N} \cdot \text{s} \cdot \text{m}^{-1}$

Table 3.1 – Summary of measurements.

Even if the correlation between the measured and identified viscoelastic forces shows some discrepancies, the linear viscoelastic law is deemed acceptable for the silicon as the error⁴ is about 15%.

The value of the linear elastic stiffness of $6.5 \times 10^3 \text{ N} \cdot \text{m}^{-1}$ is in a reasonable accordance with the results of [Serina et al., 1998] for the behaviour of the finger tip. Therefore, we considered that what is felt by the pianist is not significantly changed by the addition

⁴The error is defined by the ratio of the integral of the difference of the absolute value of the two forces, and the integral of the measured forces



of the silicon since the finger and the silicone filter the force in a similar way, which is necessary for the simulations of the piano action to be relevant.

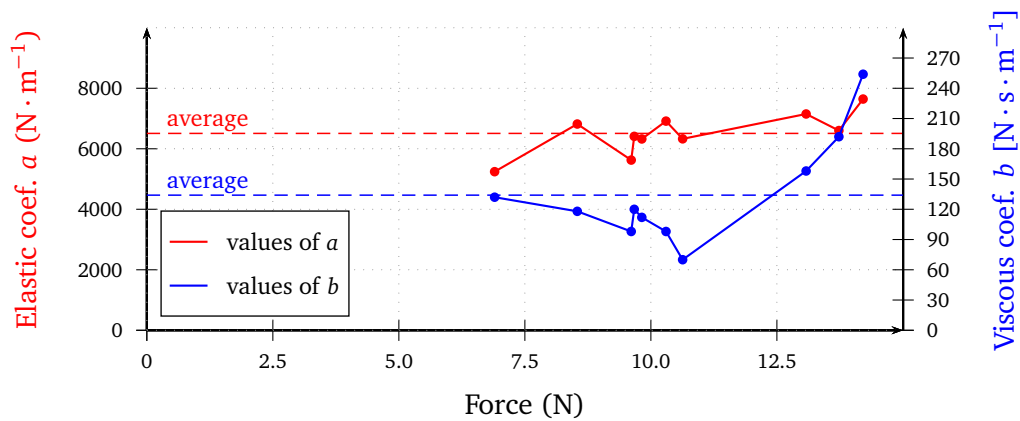


Figure 3.13 – Ten identifications of the linear viscoelastic parameters of the piston.

Examples of measurements Figure 3.14 shows a comparison between the measured force F_{meas} and the estimated normal compression force of the silicone, which should be equal. The discrepancies were mainly due to:

- the friction in the piston which invalidates the model;
- the bias of the measurement of y_{silicone} (see table 3.2);
- the differences between the position sensors and the force sensors (and their amplifier).

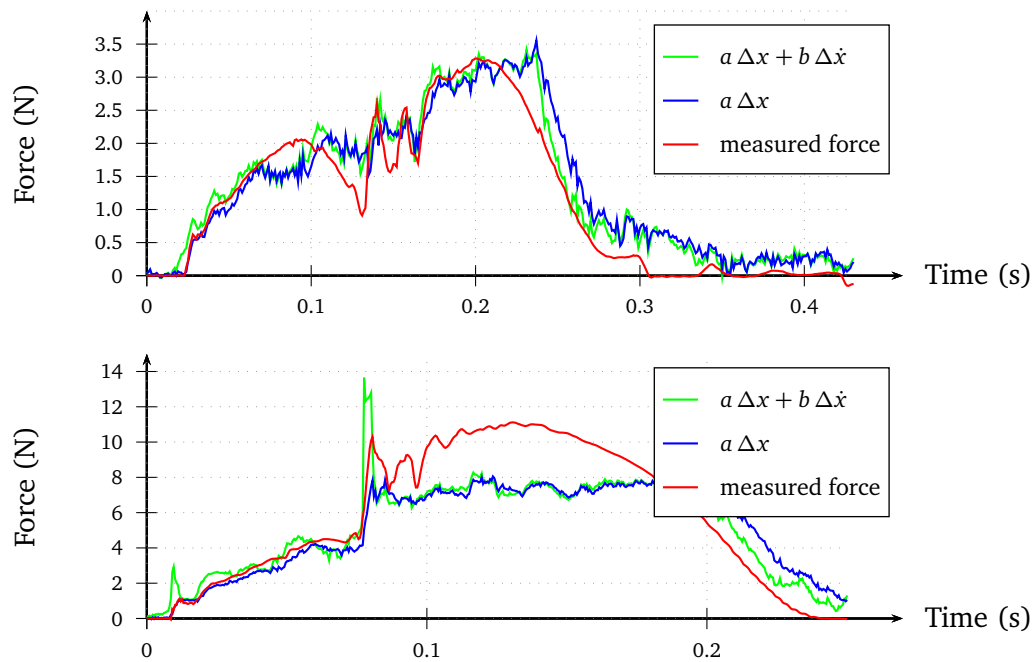


Figure 3.14 – Comparison of the force measurement and its estimation using the viscoelastic piston. Top: piano keystroke. Bottom: forte keystroke.

	geometry (m)	laser key (m)	laser silicone (m)	velocity (m/s)	force (N)	kinematics (rad)
resolution	10^{-4}	5×10^{-5}	5×10^{-5}	–	5×10^{-4}	≤ 0.02
systematic error	0	2×10^{-4}	1×10^{-4}	–	0	0
+ linearity	0	10^{-4}	10^{-4}	–	≤ 0.1	0
+ hysteresis				–	≤ 0.1	0
uncertainties	10^{-3}	$\leq 10^{-4}$	$\leq 5 \times 10^{-4}$	–	0.1	≤ 0.05

Table 3.2 – Summary of all measurement’s errors.

key and of the silicone respectively, and k the stiffness of the silicone,

$$a(1.2 y_{\text{silicone}} - y_{\text{key}}) - a(y_{\text{silicone}} - y_{\text{key}}) = 0.2 a y_{\text{silicone}} \quad (3.5)$$

which is of the order of magnitude of 1 N. Such an amplification of the errors can be seen in Figure 3.14, where the difference between the estimated and the measured forces reaches up to 1 N for the *piano* keystroke and three times more for the *forte* keystroke. This is believed to be responsible for a significant part of the discrepancies between the measured and simulated forces presented in Chapter 6.

Estimating the errors and uncertainties separately for each body allows to refine them, see Table 3.3. This is because even if the accuracies are about the same for the tracking of each pattern, the corresponding accuracies in angles differ, as the lever arms changes from one body to another.

	key (rad)	whippen (rad)	jack (rad)	lever (rad)	hammer (rad)	damper (rad)
resolution	10^{-3}	5×10^{-3}	10^{-2}	2×10^{-2}	2×10^{-3}	10^{-2}
uncertainty	5×10^{-3}	10^{-2}	3×10^{-2}	4×10^{-2}	10^{-2}	2×10^{-2}

Table 3.3 – Details of kinematic errors.

4.5.9. Initial positions of the frames	67
4.5.10. Viscoelastic and elastic behaviours	67
4.6. Matrix formulation of the dynamics	68
4.6.1. Equation	68
4.6.2. Details of the terms	68
4.6.3. Example for the key	72

A model of the grand piano action is qualified as complete when each body of the mechanism is modelled, except the ones for which the actions are neglected. Such models stem from a non-phenomenological approach consisting in writing the dynamical equations for every body and coupling them with the reaction forces.

Several complete models of the grand piano action have been proposed [Gillespie and Cutkosky, 1992; Hirschhorn et al., 2006; Lozada, 2007]. In [Gillespie and Cutkosky, 1992], no viscous nor dry friction is taken into account. Nevertheless, it is mentioned that friction contributes significantly to what is felt by a player. The models proposed in [Hirschhorn et al., 2006] and [Lozada, 2007] are quite similar. They differ mostly by slightly different felt laws, the damper which is considered by Lozada, and by the regularisation of dry friction in [Hirschhorn et al., 2006].

The model described in the present chapter is based on Lozada's. It is completed by a description of the contact geometries, including that of the backcheck. After introducing the model, all the physical elements involved in the model are presented and detailed for each body. The corresponding values are also given. Most of them were taken from [Lozada, 2007] as described in Chapter 3. All the equations are then written in a synthetic matrix form.

4.1. Characteristics of the piano action

The parameters of the piano action model are classified into:

- the geometry (positions and lengths);
- the inertial properties of the bodies (masses, moments of inertia, centres of inertia);
- the material properties of felts and hinges (dry and viscous friction coefficients).

All the geometrical quantities (positions and angles) were estimated from two photographs of the action: one of the entire mechanism and the second zoomed on the whippen-jack-lever assembly and the hammer. The photographs were taken at 3 m from the action to reduce the parallax, and the lens distortion was corrected using DxO Optics Pro. Because of the time-worn felts of the used action (see Figure 4.7(b) page 57) and as a double-check, complementary measurements were completed with a dial calliper.

The values of the measurements are given in Section 4.5. Some geometrical measurements differed significantly from Lozada's. In [Lozada, 2007],

- the let-off button is 1 mm lower;
- the drop screw was also 2.5 mm lower;
- the whippen spoon was 2 mm closer to the whippen pivot;

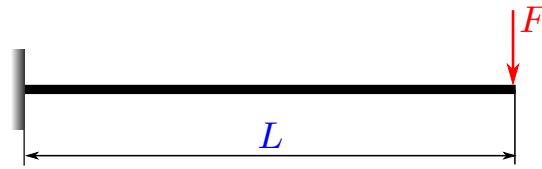


Figure 4.1 – Approximation of each rigid body as a clamped beam.

Dynamic criterion

The modal frequencies are again roughly estimated from a clamped position. The mode of longest period is the first mode, of frequency

$$f_1 = \frac{1.875^2}{2\pi} \frac{1}{L^2} \sqrt{\frac{EI}{\rho S}} \quad (4.2)$$

where $S = bh$ is the area of the section.

Results

Table 4.1 gathers the results of Equations (4.1) and (4.2) for a typical force of 10 N on the key. The characteristic force varies from one body to another because of the different lever arms. τ is the characteristic time during a stroke, estimated at $\tau = 5 \times 10^{-2}$ s. The Young modulus of the wood was taken as $E = 10^{10}$ Pa, its density as $\rho = 1000$ kg/m³.

body	L (m)	b (m)	h (m)	F (N)	$\frac{\delta}{L}$ (-)	$\frac{1}{f_1 \tau}$ (-)
key	0.380	0.015	0.025	10	0.002	0.230
whippen	0.060	0.010	0.008	20	0.005	0.020
jack	0.025	0.005	0.005	30	0.012	0.004
lever	0.030	0.005	0.005	10	0.008	0.007
hammer	0.130	0.005	0.005	30	0.300	0.130
damper	0.070	0.010	0.02	10	0.0002	0.010

Table 4.1 – Order of magnitude of the influence of flexibility in statics and dynamics.

It appears that most of the bodies can be considered as rigid. The vibration of the key might have an influence when in transitory motion. It is assumed that this influence is sufficiently low in our study. Also, the hammer shank has a low stiffness and its first mode has a long period. This period is even greater when estimated from a punctual mass model, which is likely to model the hammer better, as it consists in reality of an elongated shank and a mass made of felt. This flexibility has been studied in [Askenfelt and Jansson, 1991] and taken into account in [Izadbakhsh et al., 2008] where Izadbakhsh concludes from force-driven simulations that the only observed significant influence of the flexibility of the hammer shank occurs during the contact with the string. As the most interesting phase for haptics ends at the escapement and because the hammer has already escaped from the mechanism when it hits the string, the flexibility of the hammer is not taken into account here.

The conclusion of this paragraph is that for the above reasons, all the bodies are modelled by rigid bodies.

4.2.4. Contacts description

The complete model has to take into account the collisions between different bodies of the action. This requires to estimate distances between rigid bodies, in the neighbourhood of a possible contact zone¹. The geometry of contact surfaces therefore has to be described. For computational reasons (see Chapter 5), this description was kept as simple as possible, ideally using one segment and one circle, possibly of very large radius relatively to the characteristic length of the contact. The key-hammer contact (more precisely the backcheck-hammer contact) differs because it involves Coulomb friction, so that the description in the tangential direction of the contact surface matters. Also, the geometry of the top part of the jack, which lifts the hammer knuckle, is slightly more complex. Table 4.2 lists the different geometries for each contact. A similar description of the geometry was done in [Hirschhorn et al., 2006].

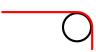
contact name	body A	body B	contact geometry of body A	contact geometry of body B
KS ⁺	key	ground at key front	○	
KW	key	whippen		○
KS ⁻	key	ground at key rest	○	
KH	key	hammer	○	○
KD	key	damper		○
KJ	whippen	jack		○
KL	whippen	lever		○
JG	jack	ground at button	○	
JL	jack	lever	○	
JH	jack	hammer		○
LG	lever	ground at stop		○
LH	lever	hammer		○
HG	hammer	ground at string	○	
DG	damper	ground at rest	○	

Table 4.2 – Description of the contact geometries.

The parametrisation of the contact geometries is described in 4.5.1.

¹The contact zone is larger than a point because of the multiple degrees of freedom.

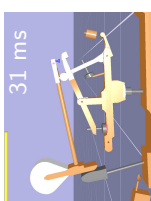




Figure 4.3 – Photograph of the felt bushing on the jack.

4.3.4. Viscous and dry friction in hinges

The hinges of the different piano action elements have felt bushings (see Figure 4.3) which enable them to be smooth, silent and working properly for a long time. As it can be easily observed on any dismantled hammer, the free oscillations of a body of the piano action is highly damped, and the final equilibrium does not correspond to the minimum of the potential energy. This phenomenon is even used by piano technicians who add some lubricant to the hammer hinge if the hammer stops before three pseudo-periods (see Appendix A). Denoting by θ the angle made by the considered rigid body, this energy dissipation is modelled by:

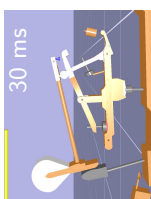
- a rotational linear viscous friction which creates a moment of the form $c_v \dot{\theta}$, where c_v is a positive constant term called viscous friction coefficient;
- a rotational dry friction of the form $c_d \text{sign}(\dot{\theta})$, where c_d is a positive constant term called dry friction coefficient.

In [Lozada, 2007], this model gave a relative error of the hammer displacement of 0.27% for the optimal values of c_v and c_d found by minimising the Euclidean distance on the displacements. It is worth noting that this 1-DOF problem required a special treatment of the sign function (page 59).

Quite similarly to the Coulomb friction described in the following paragraph, dry friction in hinges presents singularities when the velocity converges to 0. These singularities are concealed in the sign function defined by:

$$\text{sign}(\dot{\theta}) = \begin{cases} 1 & \text{if } \dot{\theta} > 0 \\ [-1, 1] & \text{if } \dot{\theta} = 0 \\ -1 & \text{if } \dot{\theta} < 0 \end{cases} \quad (4.5)$$

which is set-valued in 0. This is consistent with the infinity of possible equilibriums (in the mechanical sense) for $\dot{\theta} = 0$. Table 4.3 enumerates the three different cases of dry friction



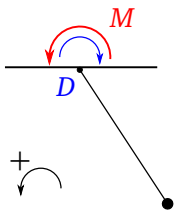
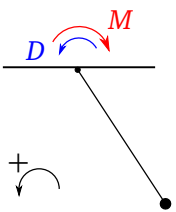
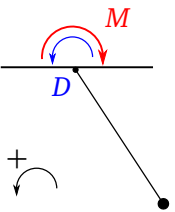
	slip	stick	slip
external moment M	$M > c_d$	$M \in [-c_d, c_d]$	$M < -c_d$
scheme			
moment of dry friction D	$D = -c_d$	$D = -M$	$D = c_d$
sign of $\dot{\theta}$	$\dot{\theta} > 0$	$\dot{\theta} = 0$	$\dot{\theta} < 0$

Table 4.3 – The three cases of dry friction (M : external moment, D : dry friction).

in hinges summed up as:

$$\mathbf{D}(\dot{\theta}) = D(\dot{\theta})\mathbf{e}_z = -c_d \mathbf{e}_z \begin{cases} 1 & \text{if } \dot{\theta} > 0 \\ [-1, 1] & \text{if } \dot{\theta} = 0 \\ -1 & \text{if } \dot{\theta} < 0 \end{cases} \quad (4.6)$$

The notation $=$ is a misuse (\in is more appropriate), justified further.

4.3.5. Coulomb friction

Coulomb friction is a contact model very similar to the above-described dry friction in hinges. In the Coulomb model (1781), the stick-slip threshold of tangential contact force varies linearly with the normal contact force, contrary to dry friction in hinges where the threshold c_d is constant. Coulomb friction is considered in the model of the piano key in three zones corresponding to the jack - let-off button contact, the jack - hammer knuckle contact and the hammer - backcheck contact. These three zones are represented in Figure 4.4.

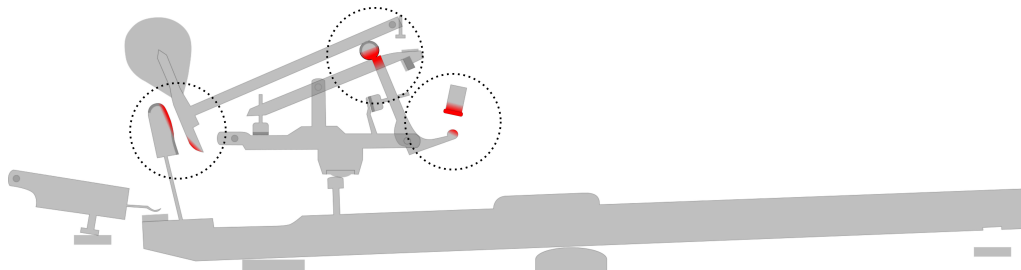


Figure 4.4 – Zones where Coulomb friction is considered.

For instance, the geometry of the end of the jack which gets in contact with the escapement button is approximated by a disk, but the diameter of this disk is not measurable as the shape of the end of the actual jack is not a disk. Another example is induced by the irregularities of felts surfaces, see Figure 4.7. These irregularities implies large inaccuracies in the estimated positions of the simplified contact descriptions. This was also observed in [Hirschhorn et al., 2006].

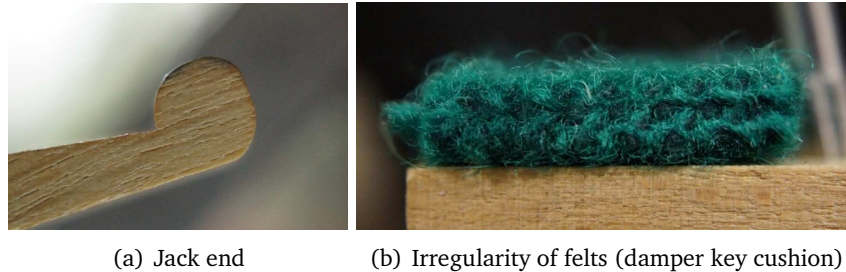


Figure 4.7 – *Examples of non-measurable parameters.*

Fixed parameters not to be studied: category IV

The category IV includes all the parameters which are assumed, for some reason, not to have any significant influence of the simulation results.

For example, the position of the centre of gravity of the key is supposed to have very little influence on the overall behaviour of the key mechanism, because the moment of the weight of the key is small compared to the moment exerted by the player's finger.

4.5. Dynamics: description and values

All the values presented here have been identified as described in Chapter 3.

4.5.1. Conventions

The conventions chosen in this paper are presented below.

Conventions for the frames

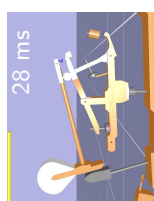
A reference frame is attached to each rigid body, using the following conventions:

- the centre of each frame is the centre of rotation of the rigid body the frame is attached to;
- the horizontal axis is defined along a main direction of the rigid body close to horizontal.

The angles of the frame are denoted by θ_B , where B stands for the first name of the body.

Conventions for the name of the parameters

Bodies were named after their first letter. B is given below as an example: replace it by the appropriate letter. All the conventions for the parameters of the piano action are summarised in Table 4.5.



generic term	meaning
B_G	centre of gravity of body B
B_O	centre of rotation of body B
$B_{\Pi x}$	x -coordinate of point B_{Π} in the frame of body B
$B_{\Pi y}$	y -coordinate of point B_{Π} in the frame of body B
B_C	centre of the contact zone of body B and body C in the frame of body B
$I_{B, B_{\Pi}}$	moment of inertia of the body B around the point B_{Π}
c_{dB}, c_{vB}	dry and viscous coefficient of the hinge joint of body B
m_B	mass of body B
$B_{C\rho}, B_{C\lambda}, B_{C\theta}$	description of the geometry of body B which collides with body C in the frame of body B, see Figure 4.8
ν_{BC}	coefficient of Coulomb friction between bodies B and C
κ_{BC}	stiffness of coupling spring between bodies B and C
θ_0^{BC}	resting angle of coupling spring between bodies B and C

Table 4.5 – Conventions for the notations of the parameters.

For convenience, each contact geometry is defined with respect to the centre of the contact zone P , defined by its coordinates (P_x, P_y) in the body B frame. The associated parameters are represented in Figure 4.8.

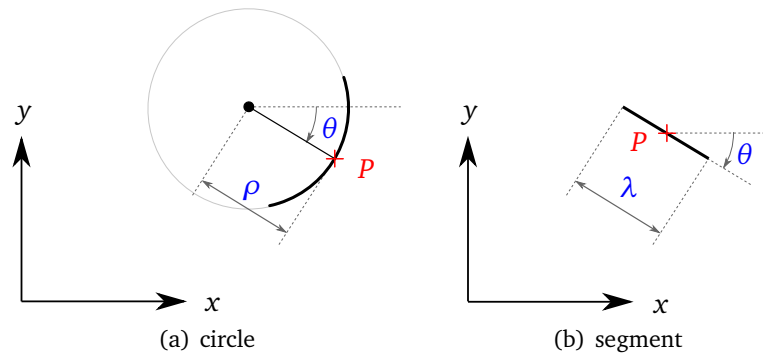
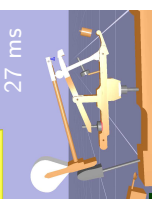


Figure 4.8 – Parameters for the description of the geometry for the contact zone centred in P .

- If the geometry of the body in the neighbourhood of the contact point P is described by a circle (case 4.8(a)), then the circle is defined by its radius ρ and its centre, which is itself defined by the set of polar coordinates (ρ, θ) .
- If it is described by a segment (case 4.8(b)), then the segment is defined by its angle θ in the body frame and its length λ .

The measured geometry and the values of the parameters which were used for the simulations (Chapter 6) are presented for each body from Figure 4.5.2 to 4.5.8.



4.5.2. Key

external forces	inertia	felt reactions	hinge frictions	Coulomb friction	coupling springs
gravity	yes	front rail	yes	hammer	no
player		whippen			
		back rail			
		hammer			
		damper			

Table 4.6 – Elements involved in the key's dynamics.

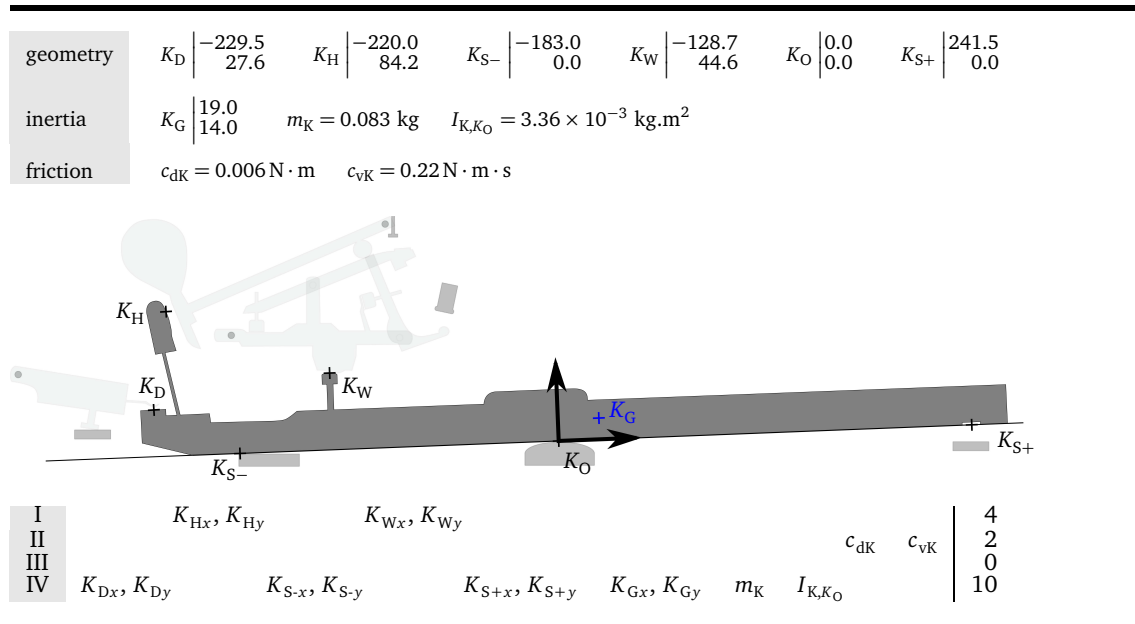


Figure 4.9 – Key frame, measurements (lengths in (mm)).

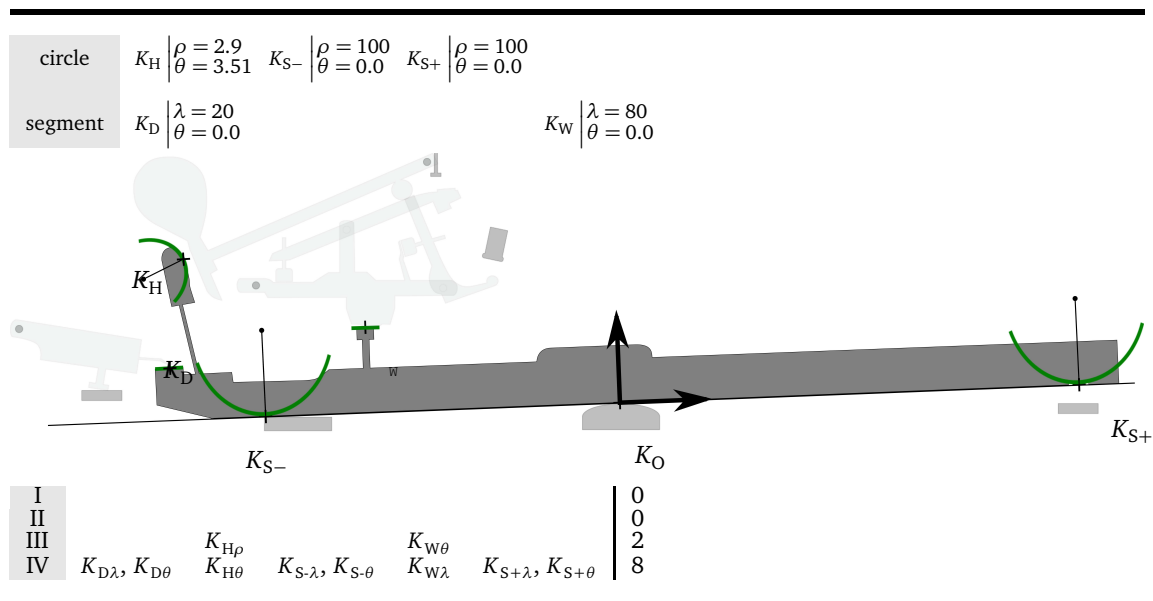



Figure 4.10 – Contacts description, key (lengths in (mm), angles in (rad)).

4.5.3. Whippen

external forces	inertia	felt reactions	hinge frictions	Coulomb friction	coupling springs
gravity	yes	jack key lever	yes	no	ground

Table 4.7 – Elements involved in the whippen’s dynamics.

geometry	$W_O \begin{vmatrix} 0.0 \\ 0.0 \end{vmatrix}$	$W_L^W \begin{vmatrix} 16.1 \\ 2.0 \end{vmatrix}$	$L_O \begin{vmatrix} 47.5 \\ 29.8 \end{vmatrix}$	$W_K \begin{vmatrix} 59.0 \\ -20.8 \end{vmatrix}$	$W_J \begin{vmatrix} 75.8 \\ 20.8 \end{vmatrix}$	$J_O^W \begin{vmatrix} 99.1 \\ 0.0 \end{vmatrix}$
inertia	$W_G \begin{vmatrix} 53.0 \\ 7.0 \end{vmatrix}$	$m_W = 19.8 \times 10^{-3} \text{ kg}$		$I_{W,W_O} = 3.97 \times 10^{-4} \text{ kg.m}^2$		
friction	$c_{dW} = 0.0992 \text{ N} \cdot \text{m}$		$c_{vW} = 4.93 \times 10^{-5} \text{ N} \cdot \text{m} \cdot \text{s}$			




The diagram shows a side view of the whippen frame. A coordinate system is centered at the pivot point O , with the x -axis pointing right and the y -axis pointing up. Force vectors are shown: W_O (up), W_L (right), W_K (down), W_J (right), and W_G (down). Lengths L_O and J_O are also indicated.

I				$J_{O_x}^W, J_{O_y}^W$		c_{dW}	c_{vW}	0
II								4
III								0
IV	W_{Lx}, W_{Ly}	$L_{O_x}^W, L_{O_y}^W$	W_{Kx}, W_{Ky}	W_{Jx}, W_{Jy}		m_W	I_{W,W_O}	10

Figure 4.11 – Whippen frame, measurements (lengths in (mm)).

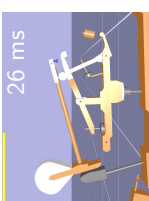
circle	$W_L \begin{vmatrix} \rho = 100 \\ \theta = -1.57 \end{vmatrix}$	$W_K \begin{vmatrix} \rho = 60 \\ \theta = 1.57 \end{vmatrix}$	$W_J \begin{vmatrix} \rho = 100 \\ \theta = 3.44 \end{vmatrix}$
--------	--	--	---



The diagram shows the whippen frame with contact points. Green arcs indicate the contact geometry for W_L , W_K , and W_J . The contact points are labeled W_O , W_L , W_K , and W_J .

I				0
II				0
III		$W_{K\rho}$		1
IV	$W_{L\rho}, W_{L\theta}$	$W_{K\theta}$	$W_{J\rho}, W_{J\theta}$	5

Figure 4.12 – Contacts description, whippen (lengths in (mm), angles in (rad)).

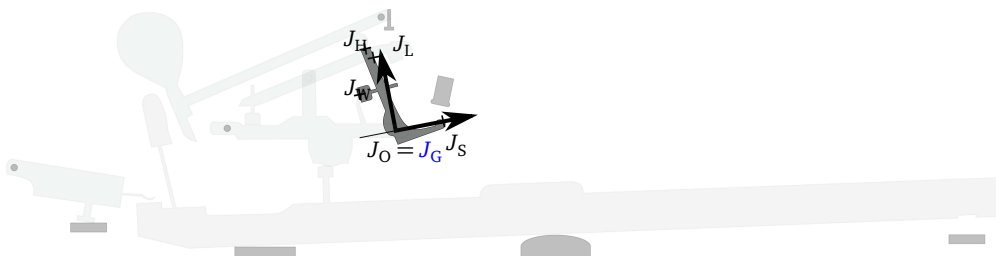


4.5.4. Jack

external forces	inertia	felt reactions	hinge frictions	Coulomb friction	coupling springs
gravity	yes	escapement button lever hammer knuckle whippen	yes	escapement button hammer knuckle	lever

Table 4.8 – Elements involved in the jack’s dynamics.

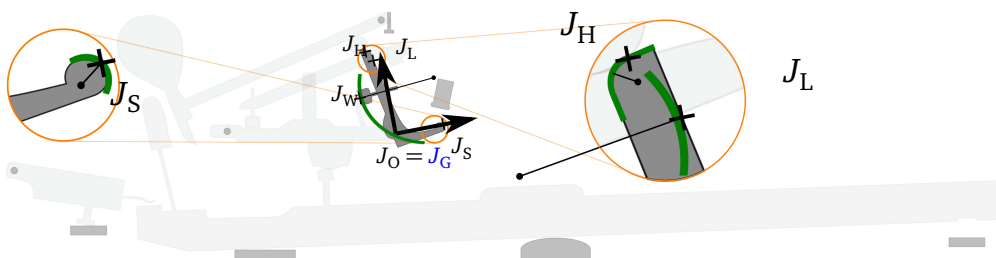
geometry	$J_W \left \begin{array}{l} -13.4 \\ 24 \end{array} \right.$	$J_H^W \left \begin{array}{l} -8.0 \\ 48.8 \end{array} \right.$	$J_L \left \begin{array}{l} -3.4 \\ 43.7 \end{array} \right.$	$J_O \left \begin{array}{l} 0.0 \\ 0.0 \end{array} \right.$	$J_S \left \begin{array}{l} 26.8 \\ 0.0 \end{array} \right.$
inertia	$J_G \left \begin{array}{l} 0.0 \\ 0.0 \end{array} \right.$	$m_J = 5.0 \times 10^{-3} \text{ kg}$	$I_{J,J_O} = 5.0 \times 10^{-6} \text{ kg.m}^2$		
friction	$c_{dJ} = 9.9 \times 10^{-4} \text{ N} \cdot \text{m}$		$c_{vJ} = 4.93 \times 10^{-5} \text{ N} \cdot \text{m} \cdot \text{s}$		



I	J_{Wx}										1
II		J_{Hx}, J_{Hy}		J_{Sx}, J_{Sy}							4
III											0
IV	J_{Wy}		J_{Lx}, J_{Ly}		J_{Gx}, J_{Gy}	m_J	I_{J,J_O}	c_{dJ}	c_{vJ}		9

Figure 4.13 – Jack frame, measurements (lengths in (mm)).

circle	$J_W \left \begin{array}{l} \rho = 8 \\ \theta = 1.63 \end{array} \right.$	$J_H \left \begin{array}{l} \rho = 0.5 \\ \theta = 0.92 \end{array} \right.$	$J_L \left \begin{array}{l} \rho = 100 \\ \theta = 3.27 \end{array} \right.$	$J_S \left \begin{array}{l} \rho = 2.4 \\ \theta = 2.07 \end{array} \right.$
--------	---	---	---	---



I				0
II		$J_{H\theta}$		1
III		$J_{H\rho}$	$J_{S\rho}, J_{S\theta}$	3
IV	$J_{W\rho}, J_{W\theta}$		$J_{L\rho}, J_{L\theta}$	4

Figure 4.14 – Contacts description, jack (lengths in (mm), angles in (rad)).

4.5.5. Lever

external forces	inertia	felt reactions	hinge frictions	Coulomb friction	coupling springs
gravity	yes	ground jack hammer knuckle whippen	yes	no	jack

Table 4.9 – Elements involved in the lever’s dynamics.

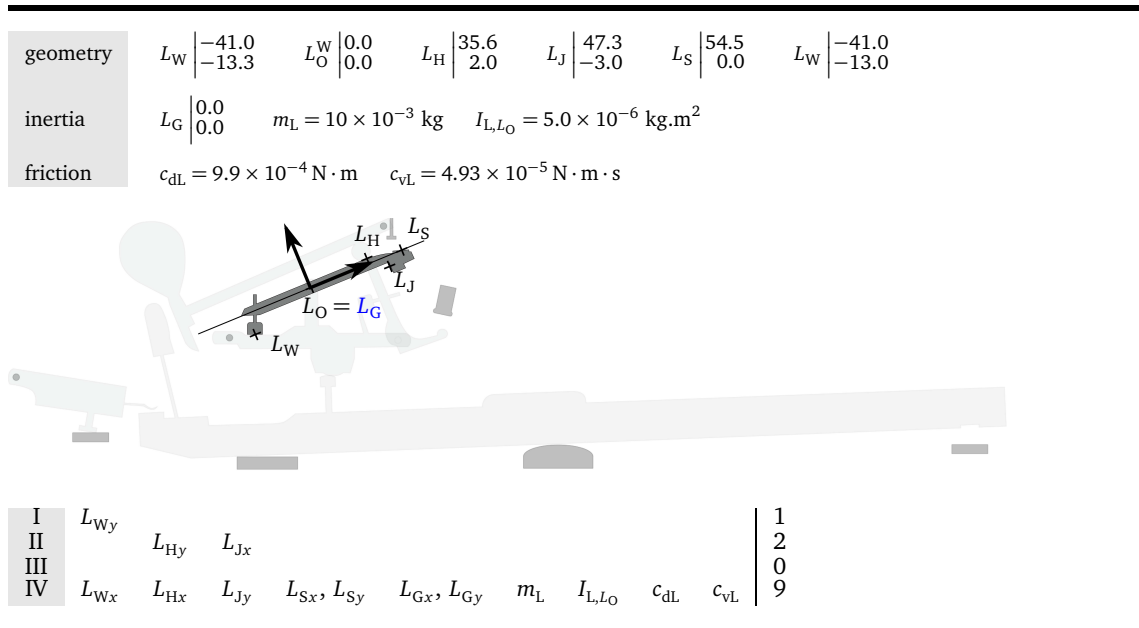


Figure 4.15 – Lever frame, measurements (lengths in (mm)).

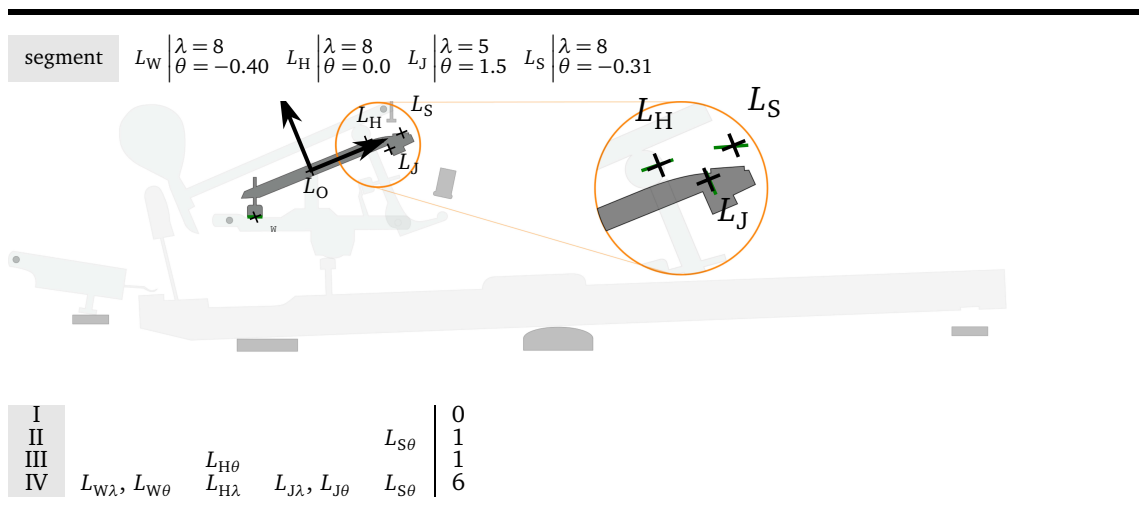
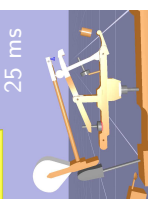


Figure 4.16 – Contacts description, lever (lengths in (mm), angles in (rad)).



4.5.6. Hammer

external forces	inertia	felt reactions	hinge frictions	Coulomb friction	coupling springs
gravity	yes	lever jack string key (backcheck)	yes	key (backcheck)	no

Table 4.10 – Elements involved in the hammer’s dynamics.

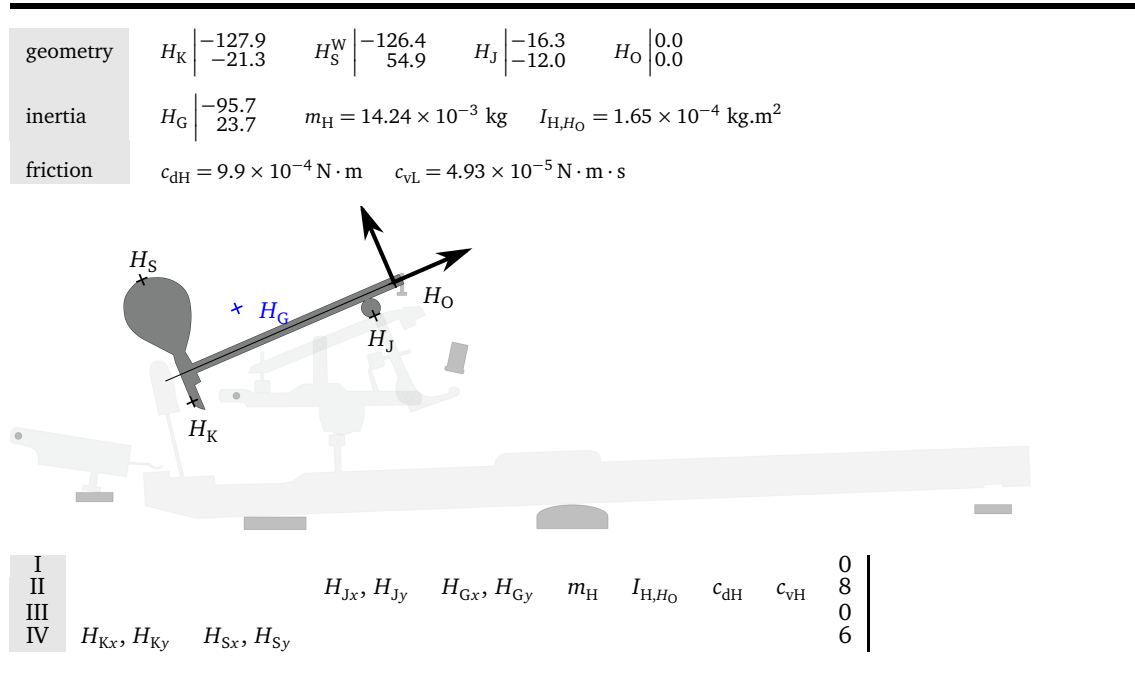


Figure 4.17 – Hammer frame, measurements (lengths in (mm)).

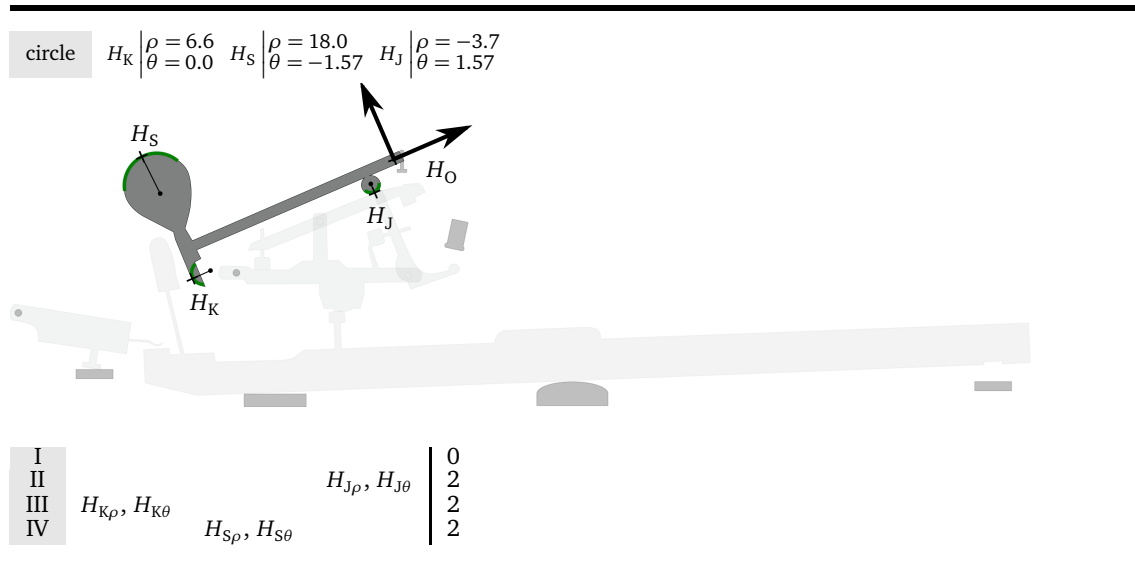


Figure 4.18 – Contacts description, hammer (lengths in (mm), angles in (rad)).

4.5.7. Damper

external forces	inertia	felt reactions	hinge frictions	Coulomb friction	coupling springs
gravity	yes	key ground	yes	no	

Table 4.11 – Elements involved in the damper’s dynamics.

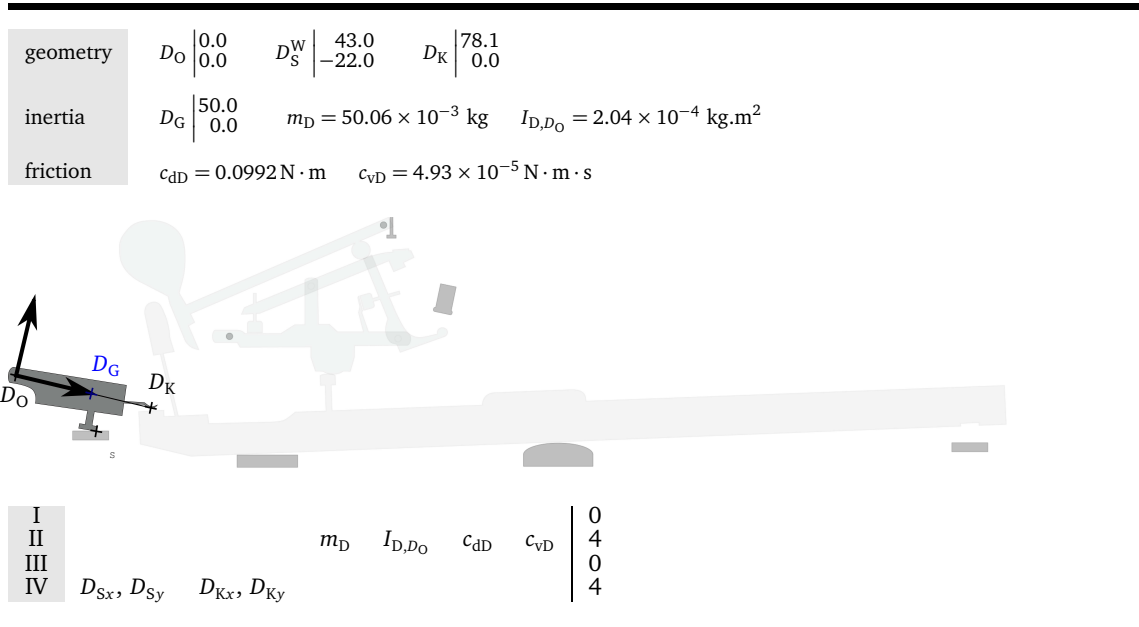


Figure 4.19 – Damper frame, measurements (lengths in (mm)).

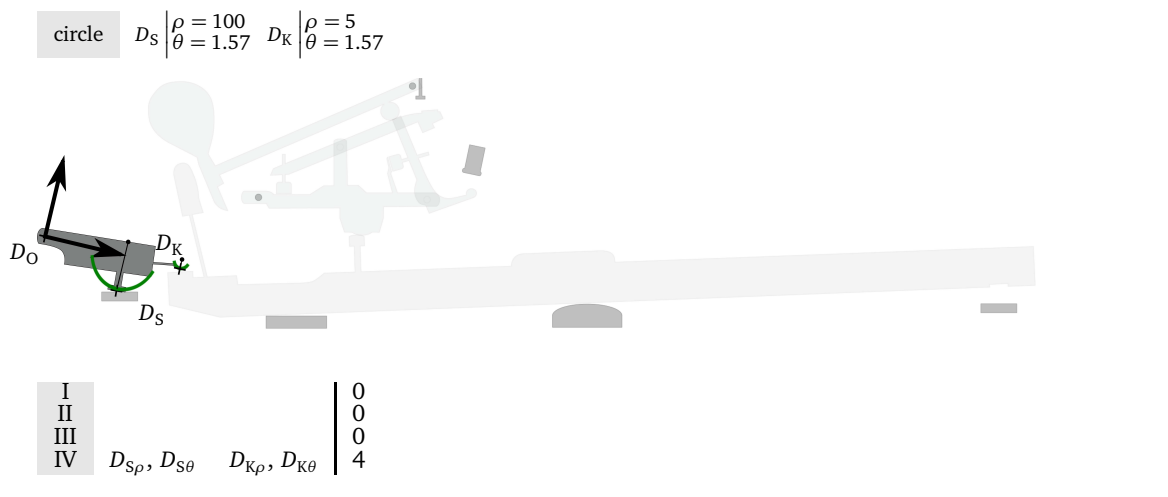
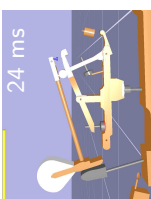


Figure 4.20 – Contacts description, damper (lengths in (mm), angles in (rad)).



4.5.8. Ground

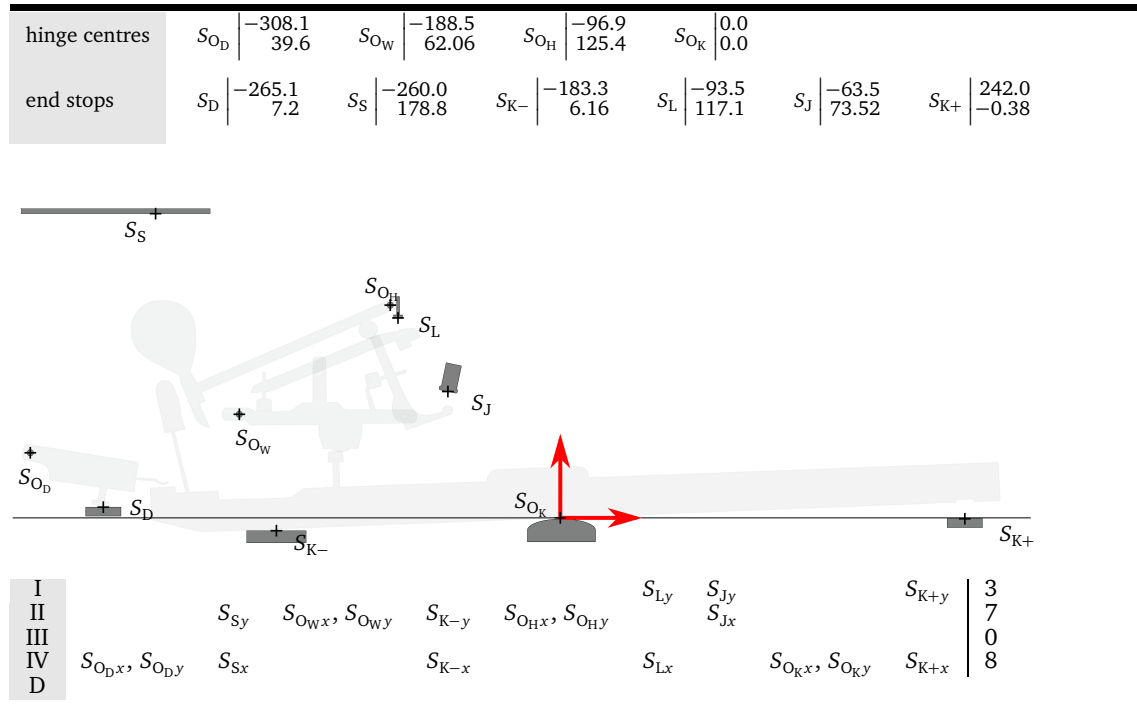


Figure 4.21 – Ground frame, measurements (lengths in (mm)).

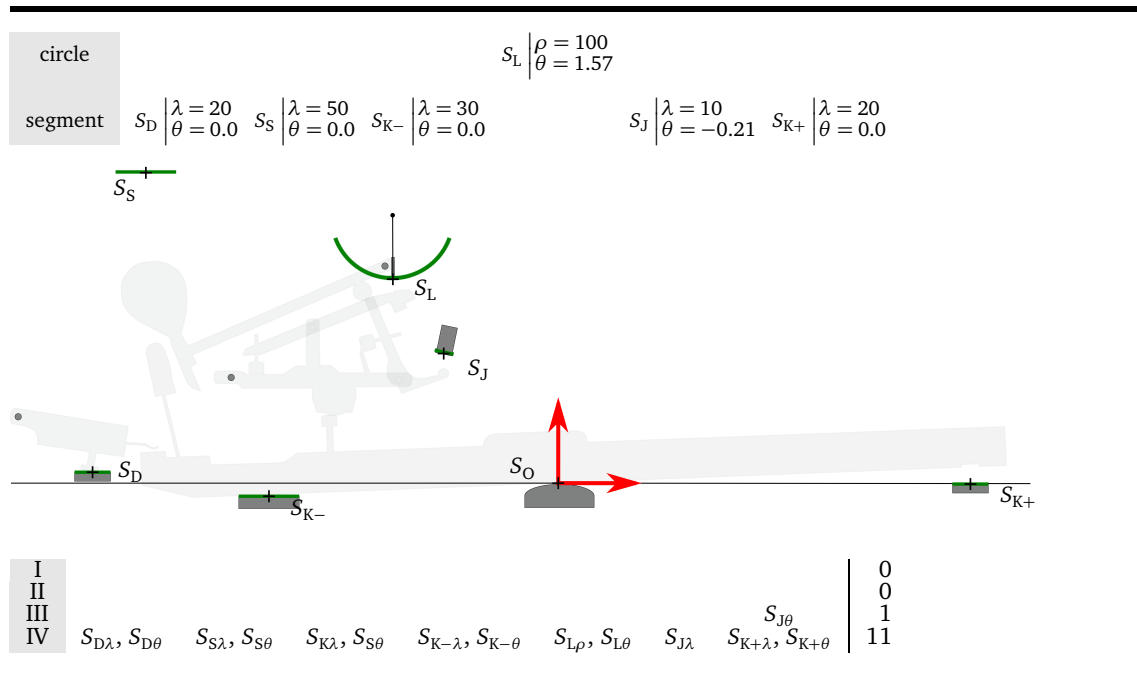


Figure 4.22 – Contacts description, ground (lengths in (mm), angles in (rad)).

4.5.9. Initial positions of the frames

The positions of each frame is determined by:

- its origin, given in paragraphs 4.5.2 to 4.5.8;
- its angle at rest, given in Figure 4.23.

initial angles $\theta_D(0) = -0.23$ $\theta_W(0) = -0.03$ $\theta_L(0) = 0.40$ $\theta_H(0) = 0.40$ $\theta_J(0) = 0.22$ $\theta_K(0) = 0.03$

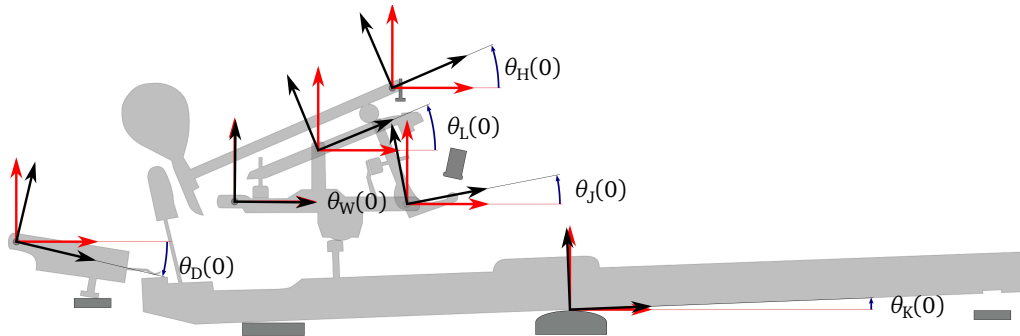


Figure 4.23 – Initial positions of the frames (in (rad)).

4.5.10. Viscoelastic and elastic behaviours

Viscoelastic behaviour of felts

The parameters of the felt laws which were used are the ones measured by Lozada. Those of the hammer knuckle and lever-ground are:

$$\begin{cases} k_{JH} = 7 \times 10^9 \text{ SI} \\ r_{JH} = 3 \\ b_{JH} = 5 \times 10^7 \text{ SI} \end{cases} \quad (4.9)$$

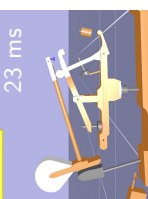
The parameters of the other felts laws are:

$$\begin{cases} k_{\alpha\beta} = 1.6 \times 10^{10} \text{ SI} \\ r_{\alpha\beta} = 2.7 \\ b_{\alpha\beta} = 5 \times 10^7 \text{ SI} \end{cases} \quad (4.10)$$

The viscoelastic part is expected to be significantly smaller than the elastic part. Typically, for a compression of 1 mm imposed at a displacement linear in time in 0.1 s, denoting by W_{elastic} the stored energy and by W_{viscous} the dissipated energy,

$$\frac{W_{\text{elastic}}}{W_{\text{viscous}}} = \frac{\int_0^{10^{-3}} k x^r dx}{\int_0^{0.1} b x^2 \dot{x}^2 dt} = 22 \quad (4.11)$$

The viscous part was not neglected as the ratio was not judged sufficiently greater than 1.



Elastic behaviour of rotational springs

The parameters of the linear law of the coupling springs were measured in [Lozada, 2007] and they are given in Table 4.12.

coupling spring	κ (N.m)	θ_0 (rad)
whippen-ground	0.0355	0.419
jack-whippen	0.0299	0.980
lever-whippen	0.1171	0.725

Table 4.12 – Parameters of the linear elastic law of the coupling springs.

4.6. Matrix formulation of the dynamics

The last part of this chapter consists in writing the dynamics of the piano action in a single matrix equation. The multiple purposes are:

- to give the equations of the dynamics;
- to write them in a synthetic form which is easy to analyse and implement;
- to introduce the formalism and the notations used in Chapter 5.

4.6.1. Equation

The dynamical equations of the rigid bodies are written in a usual form in multibody dynamics:

$$\mathbf{M}(\mathbf{x})\ddot{\mathbf{x}} + \mathbf{N}(\mathbf{x}, \dot{\mathbf{x}})\dot{\mathbf{x}} + \mathbf{c}_v\dot{\mathbf{x}} + \mathbf{c}_d\mathbf{sign}(\dot{\mathbf{x}}) + \left(\frac{\partial \boldsymbol{\delta}}{\partial \mathbf{x}}(\mathbf{x})\right)^T \mathbf{F}(\boldsymbol{\delta}) + \mathbf{F}^*(\mathbf{x}, t) + \mathbf{T}(\boldsymbol{\delta}, \dot{\mathbf{x}}) + \boldsymbol{\kappa}(\mathbf{x} - \mathbf{x}_0) = \mathbf{0} \quad (4.12)$$

\mathbf{x} is the vector of generalised coordinates, chosen such that:

$$\mathbf{x} = \left[\theta_K \quad \theta_W \quad \theta_J \quad \theta_L \quad \theta_H \quad \theta_D \right]^T \in \mathbb{R}^{6 \times 1} \quad (4.13)$$

In Equation (4.12), each term is a generalised force, that is here a moment. Each of them is made explicit in 4.6.2. To be compared to the ones in [Lozada, 2007], this equation needs to be completed by the equations of the gaps $\boldsymbol{\delta}$ which depends on the contacts' description (see 4.2.4) and are purely geometrical. The main differences with [Lozada, 2007] are the contacts' geometry and the writing of Coulomb friction.

This equation contains some non-smooth terms, that is functions which are not differentiable with respect to velocity: **sign** and **T** (related to dry/Coulomb friction). This makes its solving more complicated, as discussed in Chapter 5.

4.6.2. Details of the terms

All the physical elements listed in Section 4.3 are included in Equation (4.12). Their mathematical transcription is made explicit in the same order.

External forces

The generalised external forces, i.e. the moment of the external forces is denoted by $\mathbf{F}^*(\mathbf{x}, t)$:

$$\mathbf{F}^*(\mathbf{x}, t) = - \left(\mathbf{F}_{\text{gravity}}^*(\mathbf{x}, t) + \mathbf{F}_{\text{player} \rightarrow \text{key}}^*(\mathbf{x}, t) \right) \quad (4.14)$$

where $\mathbf{F}_{\text{gravity}}^*$ and $\mathbf{F}_{\text{player} \rightarrow \text{key}}^*(\mathbf{x}, t)$ are the moments of the gravity and of the force exerted by the pianist, respectively.

The generalised forces of gravity are:

$$\mathbf{F}_{\text{gravity}}^*(\mathbf{x}, t) = \begin{bmatrix} \underline{K_O K_G}(\mathbf{x}) \wedge m_K \underline{g} \\ \underline{W_O W_G}(\mathbf{x}) \wedge m_W \underline{g} \\ \underline{J_O J_G}(\mathbf{x}) \wedge m_J \underline{g} \\ \underline{L_O L_G}(\mathbf{x}) \wedge m_L \underline{g} \\ \underline{H_O H_G}(\mathbf{x}) \wedge m_H \underline{g} \\ \underline{D_O D_G}(\mathbf{x}) \wedge m_D \underline{g} \end{bmatrix} \cdot \underline{e}_z \in \mathbb{R}^{6 \times 1} \quad (4.15)$$

where \underline{g} is the acceleration of the gravity. The generalised forces exerted by the pianist are:

$$\mathbf{F}_{\text{player} \rightarrow \text{key}}^*(\mathbf{x}, t) = \begin{bmatrix} \underline{K_O K_{S+}}(\mathbf{x}) \wedge \underline{F_p}(t) \\ 0 \\ 0 \\ 0 \\ 0 \\ 0 \end{bmatrix} \cdot \underline{e}_z \in \mathbb{R}^{6 \times 1} \quad (4.16)$$

where $\underline{F_p}(t)$ denotes the force exerted by the player on the key at K_p .

Inertia

The linear terms of inertia $\mathbf{M}(\mathbf{x})\ddot{\mathbf{x}}$ in (4.12) are given by the generalised mass matrix \mathbf{M} :

$$\mathbf{M}(\mathbf{x}) = \begin{bmatrix} I_{K,K_O} & 0 & 0 & 0 & 0 & 0 \\ 0 & I_{W,W_O} + W_O W_J^2 I_{J,J_O} + W_O W_L^2 I_{L,L_O} & M_{WJ}(\mathbf{x}) & M_{WL}(\mathbf{x}) & 0 & 0 \\ 0 & M_{WJ}(\mathbf{x}) & I_{J,J_O} & 0 & 0 & 0 \\ 0 & M_{WL}(\mathbf{x}) & 0 & I_{L,L_O} & 0 & 0 \\ 0 & 0 & 0 & 0 & I_{H,H_O} & 0 \\ 0 & 0 & 0 & 0 & 0 & I_{D,D_O} \end{bmatrix} \quad (4.17)$$



M_{WJ} and M_{WL} can be calculated from the Lagrangian, similarly to what is demonstrated on the example of the double pendulum detailed in Appendix B.

The other (nonlinear) terms of inertia are $\mathbf{N}(\mathbf{x}, \dot{\mathbf{x}})\dot{\mathbf{x}}$ where

$$\mathbf{N}(\mathbf{x}, \dot{\mathbf{x}}) = \begin{bmatrix} 0 & 0 & 0 & 0 & 0 & 0 \\ 0 & 0 & N_{WJ}(\mathbf{x}, \dot{\mathbf{x}}) & N_{WL}(\mathbf{x}, \dot{\mathbf{x}}) & 0 & 0 \\ 0 & N_{JW}(\mathbf{x}, \dot{\mathbf{x}}) & 0 & 0 & 0 & 0 \\ 0 & N_{LW}(\mathbf{x}, \dot{\mathbf{x}}) & 0 & 0 & 0 & 0 \\ 0 & 0 & 0 & 0 & 0 & 0 \\ 0 & 0 & 0 & 0 & 0 & 0 \end{bmatrix} \quad (4.18)$$

The only non-zero components in Equation (4.18) are those concerning bodies which are not in an inertial frame, i.e. the jack and the lever (they are linked to the whippen). N_{WJ} , N_{WL} , N_{JW} and N_{LW} are calculated using the following equation:

$$[\mathbf{N}(\mathbf{x}, \dot{\mathbf{x}})\dot{\mathbf{x}}]_i = \frac{1}{2} \sum_{j,k} \dot{x}_k \left(\frac{\partial M_{ij}}{\partial x_k} + \frac{\partial M_{ik}}{\partial x_j} - \frac{\partial M_{kj}}{\partial x_i} \right) \dot{x}_j \quad (4.19)$$

where $M_{\alpha\beta}$ denotes the component of the α -th line and β -th column of \mathbf{M} and \dot{x}_k denotes the k -th component of $\dot{\mathbf{x}}$.

Felt reactions

In accordance with the notations of Table 4.2, denoting by δ_γ the compression length of the felt of the contact γ , the vector $\boldsymbol{\delta} \in \mathbb{R}^{14 \times 1}$ gathers all the lengths of compression:

$$\boldsymbol{\delta}^T = \left[\delta_{KS^+} \quad \delta_{KW} \quad \delta_{KS^-} \quad \delta_{KH} \quad \delta_{KD} \quad \delta_{WJ} \quad \delta_{WL} \quad \delta_{JG} \quad \delta_{JL} \quad \delta_{JH} \quad \delta_{LG} \quad \delta_{LH} \quad \delta_{HG} \quad \delta_{DG} \right] \quad (4.20)$$

where the dependencies with respect to \mathbf{x} have been omitted. These dependencies are purely geometrical.

$\mathbf{F}(\boldsymbol{\delta}) \in \mathbb{R}^{14 \times 1}$ is the vector of the felts reaction forces such that its i -th component is

$$[\mathbf{F}(\boldsymbol{\delta})]_i = k_i \delta_i^{r_i} + b_i \delta_i^2 \dot{\delta}_i \quad (4.21)$$

The lever arms of the felt reactions forces are gathered in

$$\left(\frac{\partial \boldsymbol{\delta}}{\partial \mathbf{x}}(\mathbf{x}) \right) \in \mathbb{R}^{14 \times 6} \quad (4.22)$$

and the reaction forces are given by

$$\left(\frac{\partial \boldsymbol{\delta}}{\partial \mathbf{x}}(\mathbf{x}) \right)^T \mathbf{F}(\boldsymbol{\delta}) \in \mathbb{R}^{6 \times 1} \quad (4.23)$$

The details of the calculations are given for the key in paragraph 4.6.3.

Viscous and dry friction in hinges

The matrices of viscous and dry joint friction coefficients $\mathbf{c}_v \in \mathbb{R}^{6 \times 6}$ and $\mathbf{c}_d \in \mathbb{R}^{6 \times 6}$ are diagonal matrices given by:

$$\mathbf{c}_d = \begin{bmatrix} c_{dK} & 0 & 0 & 0 & 0 & 0 \\ 0 & c_{dW} & 0 & 0 & 0 & 0 \\ 0 & 0 & c_{dJ} & 0 & 0 & 0 \\ 0 & 0 & 0 & c_{dL} & 0 & 0 \\ 0 & 0 & 0 & 0 & c_{dH} & 0 \\ 0 & 0 & 0 & 0 & 0 & c_{dD} \end{bmatrix}, \quad \mathbf{c}_v = \begin{bmatrix} c_{vK} & 0 & 0 & 0 & 0 & 0 \\ 0 & c_{vW} & 0 & 0 & 0 & 0 \\ 0 & 0 & c_{vJ} & 0 & 0 & 0 \\ 0 & 0 & 0 & c_{vL} & 0 & 0 \\ 0 & 0 & 0 & 0 & c_{vH} & 0 \\ 0 & 0 & 0 & 0 & 0 & c_{vD} \end{bmatrix} \quad (4.24)$$

sign is the component-wise sign function:

$$\mathbf{sign} : \mathbf{y} \in \mathbb{R}^{6 \times 1} \mapsto \begin{bmatrix} \text{sign}(y_1) \\ \text{sign}(y_2) \\ \vdots \\ \text{sign}(y_6) \end{bmatrix} \quad (4.25)$$

and **sign** is the set-valued function defined by:

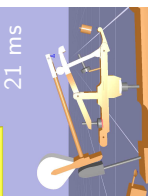
$$\mathbf{sign} : y \in \mathbb{R} \mapsto \begin{cases} -1 & \text{if } y < 0 \\ [-1, 1] & \text{if } y = 0 \\ 1 & \text{if } y > 0 \end{cases} \quad (4.26)$$

It is not a function as it assigns more than one scalar to 0. Its treatment is discussed in Chapter 5.

Coulomb friction

Coulomb frictions are included in the generalised forces $\mathbf{T}(\boldsymbol{\delta}, \dot{\mathbf{x}})$ which can be written

$$\mathbf{T}(\boldsymbol{\delta}, \dot{\mathbf{x}}) = \begin{bmatrix} T_{KH} \\ 0 \\ T_{JG} + T_{JH} \\ 0 \\ T_{HK} + T_{HJ} \\ 0 \end{bmatrix} \quad (4.27)$$



Each moment can be made explicit, similarly to T_{KH} , by changing the appropriate letters:

$$T_{KH}(\mathbf{x}, \boldsymbol{\delta}) = \begin{cases} 0 & \text{if } \|F_{KH}(\boldsymbol{\delta})\| = 0 \\ v_{KH} \frac{\partial \delta_{KH}}{\partial \mathbf{x}}(\mathbf{x}) F_{KH}(\boldsymbol{\delta}) & \text{if } \|F_{KH}(\boldsymbol{\delta})\| > 0 \end{cases} \quad (4.28)$$

Coupling springs

The actions of the two coupling springs are modelled by a generalised force of the form $\boldsymbol{\kappa}(\mathbf{x} - \mathbf{x}_0)$. This moment can be detailed:

$$\boldsymbol{\kappa}(\mathbf{x} - \mathbf{x}_0) = \begin{bmatrix} 0 & 0 & 0 & 0 & 0 & 0 \\ 0 & \kappa_{WG} & 0 & 0 & 0 & 0 \\ 0 & 0 & \kappa_{JW} & 0 & 0 & 0 \\ 0 & 0 & 0 & \kappa_{LW} & 0 & 0 \\ 0 & 0 & 0 & 0 & 0 & 0 \\ 0 & 0 & 0 & 0 & 0 & 0 \end{bmatrix} \begin{bmatrix} \theta_K \\ \theta_W \\ \theta_J \\ \theta_L \\ \theta_H \\ \theta_D \end{bmatrix} - \begin{bmatrix} 0 \\ \kappa_{WG} \theta_0^{WG} \\ \kappa_{JW} \theta_0^{JW} \\ \kappa_{LW} \theta_0^{LW} \\ 0 \\ 0 \end{bmatrix} \quad (4.29)$$

4.6.3. Example for the key

In the present paragraph, the dynamics of the key is written explicitly, from Equation (4.12).

The first line of the matrix equation (4.12) is:

$$\begin{aligned} [\mathbf{M}(\mathbf{x})\ddot{\mathbf{x}}]_1 + [\mathbf{N}(\mathbf{x}, \dot{\mathbf{x}})\dot{\mathbf{x}}]_1 + [\mathbf{c}_v\dot{\mathbf{x}}]_1 + [\mathbf{c}_d \mathbf{sign}(\dot{\mathbf{x}})]_1 + \left[\left(\frac{\partial \boldsymbol{\delta}}{\partial \mathbf{x}}(\mathbf{x}) \right)^T \mathbf{F}(\boldsymbol{\delta}) \right]_1 \\ + [\mathbf{F}^*(\mathbf{x}, t)]_1 + [\mathbf{T}(\boldsymbol{\delta}, \dot{\mathbf{x}})]_1 + [\boldsymbol{\kappa}(\mathbf{x} - \mathbf{x}_0)]_1 = 0 \end{aligned} \quad (4.30)$$

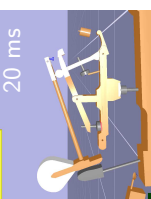
Each term can be calculated as described above:

- $[\mathbf{M}(\mathbf{x})\ddot{\mathbf{x}}]_1 = J_K \ddot{\theta}_K$;
- $[\mathbf{N}(\mathbf{x}, \dot{\mathbf{x}})\dot{\mathbf{x}}]_1 = 0$, as the key is directly linked to the ground with a hinge joint;
- $[\mathbf{c}_v\dot{\mathbf{x}}]_1 = c_{vK} \dot{\theta}_K$;
- $[\mathbf{c}_d \mathbf{sign}(\dot{\mathbf{x}})]_1 = c_{dK} \mathbf{sign} \dot{\theta}_K$;
- $\left[\left(\frac{\partial \boldsymbol{\delta}}{\partial \mathbf{x}}(\mathbf{x}) \right)^T \mathbf{F}(\boldsymbol{\delta}) \right]_1 =$
 $\frac{\partial \delta_{KS^+}}{\partial \theta_K}(\mathbf{x}) \mathbf{F}(\delta_{KS^+}(\mathbf{x})) + \frac{\partial \delta_{KW}}{\partial \theta_K}(\mathbf{x}) \mathbf{F}(\delta_{KW}(\mathbf{x})) + \frac{\partial \delta_{KS^-}}{\partial \theta_K}(\mathbf{x}) \mathbf{F}(\delta_{KS^-}(\mathbf{x})) + \frac{\partial \delta_{KH}}{\partial \theta_K}(\mathbf{x}) \mathbf{F}(\delta_{KH}(\mathbf{x}))$

as explained and detailed in Appendix C ;

- $(\mathbf{F}^*(\mathbf{x}, t))_1 = (\underline{K}_0 \underline{K}_G(\mathbf{x}) \wedge m_K \underline{g}) \cdot \underline{e}_z + (\underline{K}_0 \underline{K}_{S^+}(\mathbf{x}) \wedge \underline{F}_P(t)) \cdot \underline{e}_z$
- $(\mathbf{T}(\boldsymbol{\delta}, \dot{\mathbf{x}}))_1 = T_{KH}$ made explicit in Equation (4.28);

- $(\kappa(\mathbf{x} - \mathbf{x}_0))_1 = 0$.



The purpose of this chapter is to set forth the methods which were used for the simulation of the model described in Chapter 4. This simulation requires the solving of Equation (4.12) page 68 which is recalled:

$$\mathbf{M}(\mathbf{x})\ddot{\mathbf{x}} + \mathbf{N}(\mathbf{x}, \dot{\mathbf{x}})\dot{\mathbf{x}} + \mathbf{c}_v \dot{\mathbf{x}} + \mathbf{c}_d \mathbf{sign}(\dot{\mathbf{x}}) + \left(\frac{\partial \bar{\delta}}{\partial \mathbf{x}}(\mathbf{x}) \right)^T \mathbf{F}(\bar{\delta}) + \mathbf{F}^*(\mathbf{x}, t) + \mathbf{T}(\bar{\delta}, \dot{\mathbf{x}}) + \boldsymbol{\kappa}(\mathbf{x} - \mathbf{x}_0) = \mathbf{0}$$

This equation describes the piano's dynamics but does not yield the contact description, included in the function $\bar{\delta}$.

Two terms require a special treatment as they are not *functions*:

- Coulomb frictions in hinges $\mathbf{c}_d \mathbf{sign}(\dot{\mathbf{x}})$ is a vector of *set-valued functions* of $\dot{\mathbf{x}}$ (see Eq. (5.1));
- generalised tangential forces associated to Signorini-Coulomb laws $\mathbf{T}(\bar{\delta}, \dot{\mathbf{x}})$ is a vector of *set-valued functions* of $\dot{\mathbf{x}}$ (see (4.7)).

It implies that Equation (4.12) is not mathematically correct: its sums (single-valued) functions and set-valued functions. It can be appropriately written by:

- redefining the functions as singleton-valued functions instead of scalar-valued functions;
- replacing $= 0$ with $\ni 0$.

Nevertheless, the resulting equation is not an Ordinary Differential Equation and cannot be solved using numerical methods for ODEs. The dynamical equation of the piano action can be solved in two ways.

It can be approximated as an ODE by regularising it. Such an approach was performed in all the piano action simulations until now. This approach has major numerical drawbacks, see Section 5.1. An illustration of these drawbacks is given on the simple example of a pendulum subject to dry friction.

An other way of solving the dynamical equation is to accept the non-smoothness of the equation and use appropriate tools for non-smooth equations, see Section 5.2. This is the solution we chose. An overview of the numerical methods which were used is given. An illustration of such methods for non-smooth dynamical systems is presented for the pendulum with dry friction problem in 5.2.3. The results are compared to that of the regularisation approach. For the non-smooth simulation of the complete model, we used the computer program XDE described in Section 5.3. A few adjustments of the model had to be done (Section 5.4). Also, some additional features had to be implemented in XDE (Section 5.5).

5.1. Limitations of the regularising approach

In this section, the solving complications induced by the regularisation of non-smooth terms in the dynamics of the piano action are highlighted. The example of a pendulum with dry friction in the hinge joint is given. The way these complications have been overcome are presented in Section 5.2.

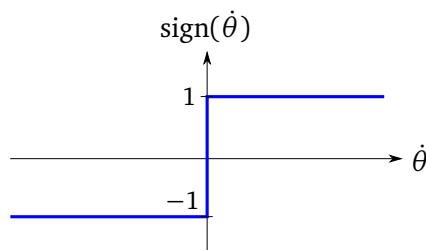
5.1.1. Changing Equation (4.12) into a regular ODE

Regularising the non-smooth friction laws

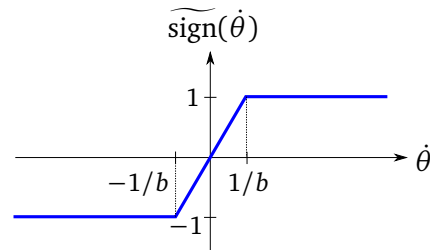
A way of solving Equation (4.12) is to approximate the components of **sign** and **T**, which are set-valued functions, with single-valued functions. One possibility of such an approximation is presented in Figure 5.1(b), where b is the slope of the piecewise-linear regularised approximation of **sign** in the neighbourhood of 0 .

$$\text{sign}(\dot{\theta}) = \begin{cases} 1 & \text{if } \dot{\theta} > 0 \\ [-1, 1] & \text{if } \dot{\theta} = 0 \\ -1 & \text{if } \dot{\theta} < 0 \end{cases} \quad (5.1)$$

$$\widetilde{\text{sign}}(\dot{\theta}) = \begin{cases} 1 & \text{if } \dot{\theta} > 1/b \\ b \dot{\theta} & \text{if } \dot{\theta} \in [-1/b, 1/b] \\ -1 & \text{if } \dot{\theta} < -1/b \end{cases} \quad (5.2)$$



(a) Multi-valued sign function (Eq. (5.1))



(b) Example of regularisation of sign (Eq. (5.2))

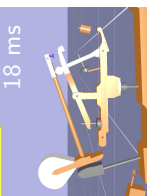
Figure 5.1 – Plots of multi-valued sign and single-valued $\widetilde{\text{sign}}$ functions.

Once (4.12) has been regularised, it is possible to solve it with numerical methods based on continuous Ordinary Differential Equations (ODEs). Up to now, all the simulations of piano actions in the literature used such approaches [Hirschhorn et al., 2006; Izadbakhsh et al., 2008; Lozada, 2007; Vyasarayani et al., 2009] for the treatment of friction, when it was taken into consideration.

Treatment of friction and observed difficulties in published piano action simulations

In [Lozada, 2007], neither the damper nor the repetition lever were implemented, in order to simplify the simulation. Three contacts were also simplified to make the solving easier. Friction was regularised in Simulink. Increasing oscillations were observed in the hammer acceleration and the calculated reaction force of the key on finger diverged, for time steps of 1 ms as well as 0.1 ms. These behaviours were believed to be due to numerical instabilities.

In [Hirschhorn et al., 2006; Vyasarayani et al., 2009], the friction laws were approximated with a Cull and Tucker model, which is a smooth regularisation of Coulomb friction [Cull and Tucker, 1999]. The model was manually adjusted in [Vyasarayani et al., 2009]. There is no mention of the time steps used. [Izadbakhsh et al., 2008] does not describe how friction is modelled, but it is believed to be also treated with a Cull and Tucker friction model, as in [Izadbakhsh, 2006]. In this master thesis, the time step is not indicated but we believe it to be small, as 75 min were required on a 2.4 GHz PC computer, including the calculation of the hammer shank deformation.



Drawbacks of regularisation

The regularisation of non-smooth laws makes the solving easier, but induces several complications.

Firstly, regularising friction does not ensure the convergence to a physical solution: a body subject to regularised friction has only one possible equilibrium position, which is the same as in the frictionless case (see Figure 5.4 for the example of the pendulum). For example, the minimum weight needed to initiate the motion of the key is 70 g, because of gravity and dry friction. Without dry friction or with the regularisation, it would be only of 15 g.

In 2000, Stewart affirmed that equations for rigid-body dynamics such as (4.12) (i.e. discontinuous ODEs) needed to be solved using the differential inclusion formalism, if high accuracy was desired [Stewart, 2000]. It is also indicated that the regularisation of non-smooth laws leads to stiff equations. This could explain the computational cost of simulations in [Izadbakhsh, 2006].

Later, more details about regularisation drawbacks are given in [Acary and Brogliato, 2008]. It is reported that regularising singularities in ODEs may impair:

- the efficiency, since calculating accurate stick-slip transitions leads to stiff equations which require a very small time step;
- the local order of consistency, which is the error in one time step;
- the global order of accuracy (the integer n such that the error varies with the time step to the power n);
- stability results.

In 5.1.2, these observations and statements are verified on an elementary example involving regularised dry friction. This enables the comparison of the regularisation approach with the non-smooth methods presented in Section 5.2, where the same elementary example is studied without regularising the contact law.

5.1.2. Example of a pendulum with regularised dry friction

The free oscillations of a pendulum with regularised dry friction are studied here.

The pendulum is studied for parameters' values of the same order of magnitude as these of the piano action model. To make the discussion easier, the equations are made dimensionless.

The considered pendulum is a compound pendulum of mass m . Its inertia around its centre of rotation O is denoted by I and the distance between its centre of gravity and O is l , see Figure 5.2 where these notations are applied in the case of the hammer. The pendulum is subject to dry friction of coefficient c_d and gravity. Its coordinate θ is chosen equal to 0 at the (stable) equilibrium in the frictionless case. The equation of its dynamics is

$$I \ddot{\theta} + c_d \text{sign}(\dot{\theta}) + mgl \sin(\theta) = 0 \quad (5.3)$$

and the values of the parameters are given in Chapter 4. For example, the case of the hammer would lead to $m = m_H$, $I = I_{H,H_0}$, $l = ||\underline{H_O H_G}||$ and $c_d = c_{dH}$.

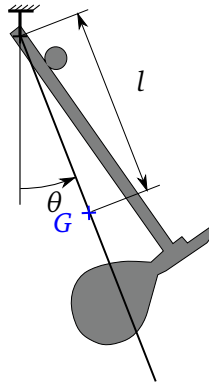


Figure 5.2 – Scheme of the hammer studied as a freely oscillating pendulum.

The derivatives in Equation (5.3) are derivatives with respect to the physical time t . Here, a dimensionless time is introduced, defined as:

$$\tau = \frac{t}{T} \quad (5.4)$$

where

$$T = 2\pi \sqrt{\frac{I}{mgl}} \quad (5.5)$$

is the period of the pendulum in the frictionless case, $\tilde{\theta}$ is the angle of the pendulum as a function of the dimensionless time, and $\dot{\tilde{\theta}}$ is the derivative of $\tilde{\theta}$. Equation (5.3) can therefore be written:

$$\ddot{\tilde{\theta}} + \Upsilon^2 \text{sign}(\dot{\tilde{\theta}}) + 4\pi^2 \sin(\tilde{\theta}) = 0 \quad (5.6)$$

introducing

$$\Upsilon = 2\pi \sqrt{\frac{c_d}{mgl}} \quad (5.7)$$

This second order differential equation is written as a matrix first order differential equation:

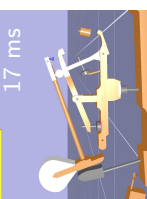
$$\begin{bmatrix} \dot{\tilde{\theta}} \\ \ddot{\tilde{\theta}} \end{bmatrix} = \begin{bmatrix} 0 & 1 \\ 0 & 0 \end{bmatrix} \cdot \begin{bmatrix} \tilde{\theta} \\ \dot{\tilde{\theta}} \end{bmatrix} + \begin{bmatrix} 0 \\ -\Upsilon^2 \text{sign}(\dot{\tilde{\theta}}) - 4\pi^2 \sin(\tilde{\theta}) \end{bmatrix} \quad (5.8)$$

or equivalently

$$\dot{\mathbf{U}} = \mathbf{A}\mathbf{U} + \mathbf{F}(\mathbf{U}) \quad (5.9)$$

with

$$\mathbf{U} = \begin{bmatrix} \tilde{\theta} \\ \dot{\tilde{\theta}} \end{bmatrix}, \quad \mathbf{A} = \begin{bmatrix} 0 & 1 \\ 0 & 0 \end{bmatrix}, \quad \mathbf{F}(\mathbf{U}) = \begin{bmatrix} 0 \\ -\Upsilon^2 \text{sign}(U_2) - 4\pi^2 \sin(U_1) \end{bmatrix} \quad (5.10)$$



Regularisation of dry friction

For the present study, Coulomb friction is approximated by the function $\widetilde{\text{sign}}$ (see Equation (5.11)) plotted in Figure 5.1(b):

$$\widetilde{\text{sign}}(\tilde{\theta}) = \begin{cases} 1 & \text{if } \tilde{\theta} > \frac{1}{\Psi} \\ \Psi \tilde{\theta} & \text{if } \tilde{\theta} \in \left[\frac{1}{\Psi}, \frac{1}{\Psi}\right] \\ -1 & \text{if } \tilde{\theta} < -\frac{1}{\Psi} \end{cases} \quad (5.11)$$

This function is the dimensionless approximation of sign corresponding to Equation (5.2), where the parameter Ψ has been introduced:

$$\Psi = \frac{b}{T} \quad (5.12)$$

This parameter somehow measures the degree of the regularisation approximation.

The function $\widetilde{\text{sign}}$ converges pointwise to a discontinuous (single-valued) function equal to 0 in 0 and $|x|/x$ elsewhere. Numerically, this limit can be identified to the sign function because $\dot{\theta}$ will never exactly equal 0. This means that the numerical simulation of the regularised model converges to that of the original model, when $\Psi \rightarrow \infty$. Obviously, increasing Ψ increases the stiffness of the numerical solving as it is going to be proved for the present example.

Linearisation of \mathbf{F} at $\mathbf{U} = {}^T [0 \ 0]$ for the study of stability and stiffness

To make the study of numerical stability and conditioning easier and analytical, the dynamics of the pendulum is studied for small angles and small velocities. The linearisation of \mathbf{F} yields an equation which can be discretised with an implicit scheme, and yet solved without using any root-finding algorithms such as Newton's. Indeed, applying an implicit scheme after the linearisation of \mathbf{F} is equivalent to applying a linearly-implicit one.

It is assumed that the results for the linearised case can be extrapolated to the non-linear case.

$$\mathbf{F}(\mathbf{U}) = \begin{bmatrix} 0 \\ -\Upsilon^2 \text{sign}(U_2) - 4\pi^2 \sin(U_1) \end{bmatrix} \begin{bmatrix} \sim \\ 0 \\ 0 \end{bmatrix} \begin{bmatrix} 0 \\ -\Upsilon^2 \Psi U_2 - 4\pi^2 U_1 \end{bmatrix} \quad (5.13)$$

because $\sin(\tilde{\theta}) \underset{0}{\sim} \tilde{\theta}$ and $\text{sign}(\tilde{\theta}) \underset{0}{\sim} \Psi \tilde{\theta}$.

Equation (5.9) becomes:

$$\dot{\mathbf{U}}(t) = \mathbf{B} \cdot \mathbf{U}(t) \quad \text{with} \quad \mathbf{B} = \begin{bmatrix} 0 & 1 \\ -4\pi^2 & -\Upsilon^2 \Psi \end{bmatrix} \quad (5.14)$$

Time step of the time-discretisation

Two elementary one-level time-discretisations are studied: explicit and linearly-implicit Euler methods. Such discretisations introduce a numerical parameter which is the time step h . Here, a third dimensionless parameter is defined:

$$\Theta = \frac{T}{h} \tag{5.15}$$

This parameter Θ is tightly related to the computational cost, as it determines how many calculations are needed to simulate one physical time unit.

Summary of the three dimensionless parameters

Three dimensionless parameters have been introduced in Equations (5.7), (5.12) and (5.15). They are gathered in Table 5.1. The Π -theorem states that $\tilde{\theta}$ can be written as a function of Υ , Ψ and Θ .

notation	expression	meaning
Υ	$2\pi \sqrt{\frac{c_d}{mgl}}$	importance of friction with regard to gravity
Ψ	$\frac{b}{T}$	measure of the approximation of sign
Θ	$\frac{T}{h}$	quantifies the number of calculations to simulate one period

Table 5.1 – Summary of the three dimensionless parameters.

T is the period of the frictionless pendulum:

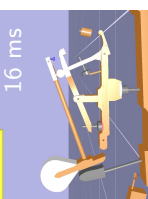
$$T = 2\pi \sqrt{\frac{I}{mgl}} \tag{5.16}$$

Υ is a physical parameter which quantifies how important friction is compared to the effect of gravity. The value of Υ is shown for each body in Table 5.2 using the values given in Chapter 4. The jack and the lever have infinite Υ because their centres of gravity are supposed equal to their centres of rotation.

Ψ was introduced for the regularisation of Coulomb friction. It gives a measure of the approximation: the higher Ψ , the better the approximation. Θ relates the physical time to the numerical one. A larger Θ increases the accuracy but impairs the computational efficiency.

body	key	whippen	jack	lever	hammer	damper
Υ	3.51	1.98	∞	∞	1.68	1.26

Table 5.2 – Value of Υ for each body.



Explicit scheme

In this paragraph, Euler's explicit scheme is implemented and studied. The vector $\dot{\mathbf{U}}$ is discretised using with the non-dimensional time step $1/\Theta$:

$$\dot{\mathbf{U}}_n = \Theta(\mathbf{U}_{n+1} - \mathbf{U}_n) \quad (5.17)$$

This explicit scheme in Equation (5.14) yields:

$$\mathbf{U}_{n+1} = \left(\mathbf{1} + \frac{1}{\Theta}\mathbf{B}\right) \cdot \mathbf{U}_n \quad (5.18)$$

The dynamics of the pendulum can then be solved with some initial conditions \mathbf{U}_0 :

$$\mathbf{U}_0 = \begin{bmatrix} \theta_0 \\ \dot{\theta}_0 \end{bmatrix} \quad \text{and} \quad \forall n \in \mathbb{N}, \mathbf{U}_n = \begin{bmatrix} 1 & \frac{1}{\Theta} \\ -\frac{4\pi^2}{\Theta} & 1 - \frac{\Upsilon^2 \Psi}{\Theta} \end{bmatrix}^n \cdot \mathbf{U}_0 \quad (5.19)$$

The matrix relating \mathbf{U}_{n+1} to \mathbf{U}_n is denoted by \mathbf{C} . The eigenvalues of \mathbf{C} are the roots of

$$\det(\mathbf{C} - X \mathbf{1}) = \det \left(\begin{bmatrix} 1 - X & \frac{1}{\Theta} \\ -\frac{4\pi^2}{\Theta} & 1 - \frac{\Upsilon^2 \Psi}{\Theta} - X \end{bmatrix} \right) = (1 - X) \left(1 - \frac{\Upsilon^2 \Psi}{\Theta} - X \right) + \frac{4\pi^2}{\Theta^2} \quad (5.20)$$

The solutions are:

$$\begin{cases} X = 1 - \frac{\Upsilon^2 \Psi}{2\Theta} \pm \frac{1}{2\Theta} \sqrt{\Upsilon^4 \Psi^2 - 16\pi^2} & \text{if } \Psi \Upsilon^2 \geq 4\pi \\ X = 1 - \frac{\Upsilon^2 \Psi}{2\Theta} \pm \frac{i}{2\Theta} \sqrt{16\pi^2 - \Upsilon^4 \Psi^2} & \text{if } \Psi \Upsilon^2 < 4\pi \end{cases} \quad (5.21)$$

Equations (5.21) show that A-stability¹ requires that $\Psi \Upsilon^2 \ll \Theta$. If not, the spectral radius of \mathbf{C} would be greater than 1 and the numerical scheme would be unstable, see Figure 5.3 (blue curve). Accurate stick-slip transitions require large Ψ which can lead to very large Θ , especially when dry friction is important (large Υ). The computation can therefore be very costly.

Linearly-implicit scheme

The following implicit discretisation of $\dot{\mathbf{U}}$

$$\dot{\mathbf{U}}_{n+1} = \Theta(\mathbf{U}_{n+1} - \mathbf{U}_n) \quad (5.22)$$

¹See [Dahlquist, 1963; Hairer, 2010].

in (5.14) leads to the following linearly-implicit scheme² (5.26):

$$\mathbf{U}_{n+1} = \left(\mathbf{1} - \frac{1}{\Theta} \mathbf{B} \right)^{-1} \cdot \mathbf{U}_n \quad (5.26)$$

The dynamics of the pendulum can then be solved with some initial conditions \mathbf{U}_0 :

$$\mathbf{U}_0 = \begin{bmatrix} \theta_0 \\ \dot{\theta}_0 \end{bmatrix} \quad \text{and} \quad \forall n \in \mathbb{N}, \mathbf{U}_n = \begin{bmatrix} 1 & -\frac{1}{\Theta} \\ \frac{4\pi^2}{\Theta} & 1 + \frac{\Upsilon^2 \Psi}{\Theta} \end{bmatrix}^{-n} \cdot \mathbf{U}_0 \quad (5.27)$$

for Θ big enough for $(\mathbf{1} - \frac{1}{\Theta} \mathbf{B})$ to be invertible.

The eigenvalues of the matrix \mathbf{D} which relates \mathbf{U}_{n+1} to \mathbf{U}_n are strictly smaller than 1, which illustrates that the (linearly-)implicit scheme is unconditionally A-stable. It also implies that the only equilibrium position in the neighbourhood of $\mathbf{U}^T = [0, 0]$ is $[0, 0]$, which is the consequence of having regularised dry friction.

Also, the condition number of \mathbf{D} , defined here with the infinity norm and given by

$$\text{cond}(\mathbf{D}) = \|\mathbf{D}\|_{\infty} \|\mathbf{D}^{-1}\|_{\infty} \quad (5.28)$$

can be easily calculated. The calculation yields

$$\text{cond}(\mathbf{D}) \underset{\Psi \rightarrow \infty}{\sim} \frac{\Psi \Upsilon^2}{\Theta} \quad (5.29)$$

so that for a good approximation of sign (large Ψ), the time step has to be small (large Θ). This is even more valid if the friction is significant (large Υ).

Results and discussion

The angle plots are presented for the explicit and the linearly-implicit Euler schemes, calculated without the small angles assumption. In the following plots, the "exact" solution (green) is calculated with the non-smooth numerical method described in Section 5.2.

²Denoting by f the approximation of the time-derivative, the implicit Euler scheme consists in estimating \mathbf{U}_{n+1} from \mathbf{U}_n the following way:

$$\mathbf{U}_{n+1} - \frac{1}{\Theta} f(\mathbf{U}_{n+1}) - \mathbf{U}_n = 0 \quad (5.23)$$

Equation (5.23) is a non-linear algebraic equation, which can be solved with a root-finding algorithm such as the Newton method. The linearly-implicit scheme is equivalent to applying the first step of the Newton method, with an initial value chosen as \mathbf{U}_n .

The first step of a Newton method yields:

$$\mathbf{U}_n - \frac{1}{\Theta} f(\mathbf{U}_n) - \mathbf{U} + \left(1 - \frac{1}{\Theta} \partial_{\mathbf{U}} f(\mathbf{U}_n) \right) (\mathbf{U}_{n+1} - \mathbf{U}_n) = 0 \quad (5.24)$$

i.e.

$$\left(1 - \frac{1}{\Theta} \partial_{\mathbf{U}} f(\mathbf{U}_n) \right) (\mathbf{U}_{n+1} - \mathbf{U}_n) = \frac{1}{\Theta} f(\mathbf{U}_n) \quad (5.25)$$

which is the definition of the linearly-implicit scheme and leads to (5.26). A numerically-oriented discussion on this scheme is proposed in [Deuffhard, 1987]. Here, \mathbf{F} has been regularised so the implicit and linearly-implicit schemes yield the same results.



It has been verified that for small angles³, this solution and the analytical one match perfectly.

In Figure 5.3, we can see that:

- the explicit scheme may lead to an instability, even with $\Theta = 100$;
- $\Theta = 100$ leads to an excellent estimation of the solution when $\Upsilon = 1$.

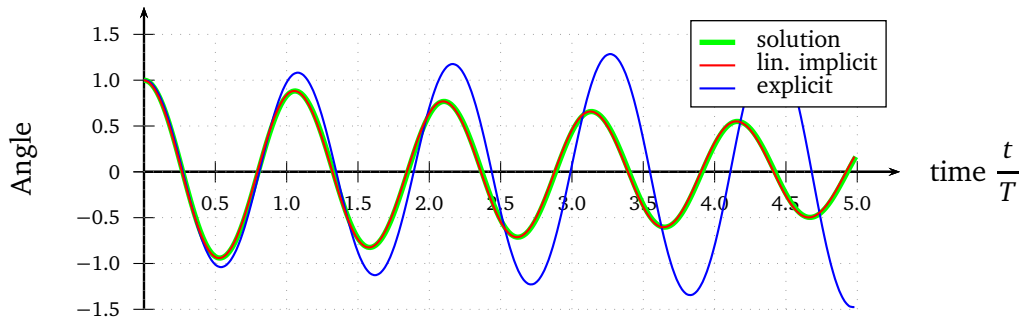


Figure 5.3 – Example of instability of the explicit scheme. $(\tilde{\theta}_0, \tilde{\dot{\theta}}_0) = (1, 0)$ and $(\Theta, \Psi, \Upsilon) = (100, 10, 1)$.

Figure 5.4 illustrates the convergence to the only possible equilibrium position for the regularised scheme: $\tilde{\theta} = 0$. Here, the regularisation factor Ψ is low and, in spite of a huge number of time steps ($\Theta = 10000$), the calculated angles using the regularised approach remains unsatisfactory.

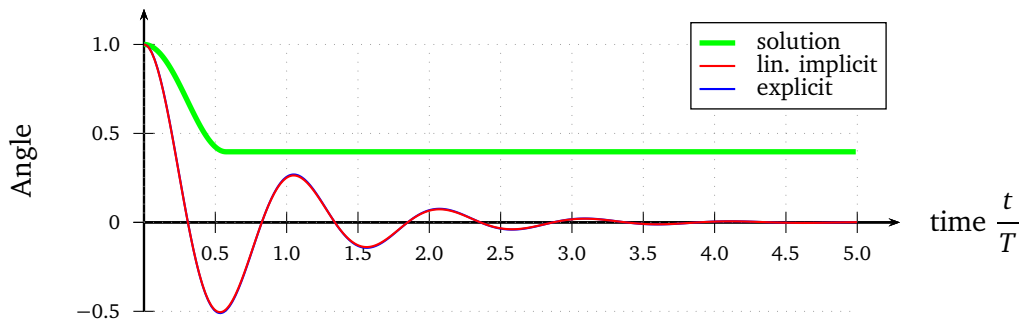


Figure 5.4 – Example of non-physical convergence due to regularisation. $(\tilde{\theta}_0, \tilde{\dot{\theta}}_0) = (1, 0)$ and $(\Theta, \Psi, \Upsilon) = (1000, 0.1, 5)$.

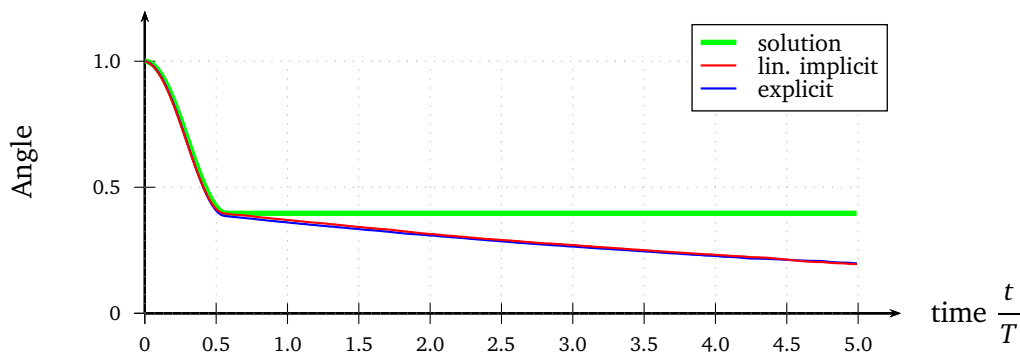


Figure 5.5 – Example of non-convergence due to too small Θ . $(\tilde{\theta}_0, \tilde{\dot{\theta}}_0) = (1, 0)$ and $(\Theta, \Psi, \Upsilon) = (250, 10000, 5)$.

³For small angles, the dynamics of the pendulum can be analytically calculated.

The larger Ψ , the better the friction law is approximated. The compensation is that the time step must be very small to get an acceptable result. Figure 5.5 shows that even with $\Theta = 250$, the estimation of the angle after five periods is half of the solution.

In Figure 5.6, one can observe the well-know phenomenon called *chattering*. Both the explicit and linearly-implicit regularised schemes show high-frequency oscillations. Note that this chattering would not be observed with a (non-linear) implicit Euler scheme.

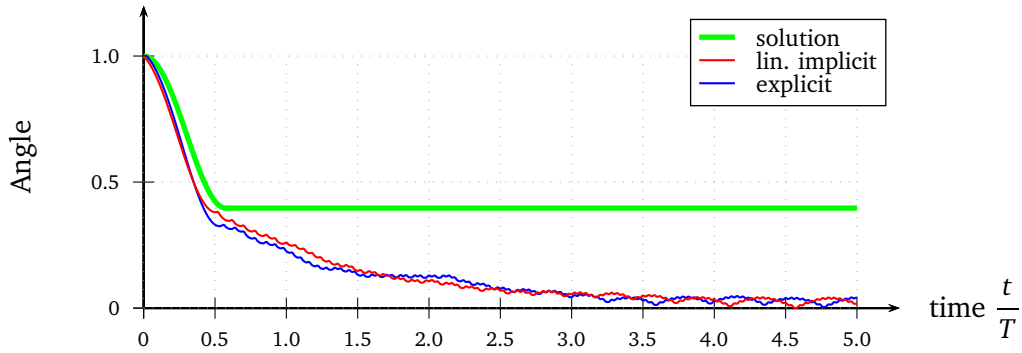


Figure 5.6 – *Chattering of regularised schemes.* $(\tilde{\theta}_0, \tilde{\dot{\theta}}_0) = (1, 0)$ and $(\Theta, \Psi, \Upsilon) = (50, 10000, 5)$.

Eventually, an order of magnitude of the appropriate time step required for⁴ $\Upsilon = 5$ can be deduced from Figure 5.7. To simulate correctly the free oscillations of the pendulum for a duration of $5T$, Θ has to be chosen as several thousands. In Section 5.2, it will be shown that with non-smooth methods, $\Theta = 20$ is sufficient. The computational cost is about 100 times less for this problem.

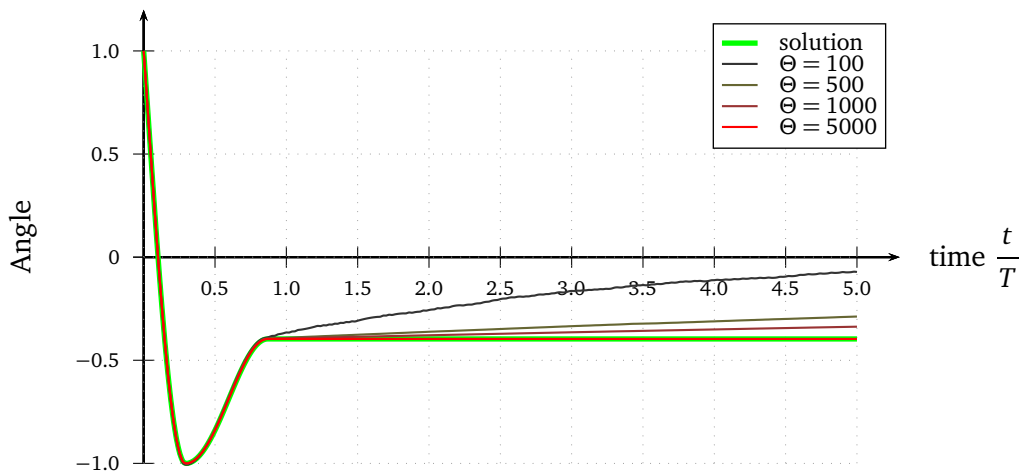
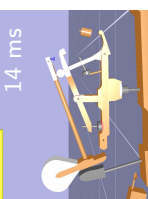


Figure 5.7 – *Convergence of the implicit scheme.* $(\tilde{\theta}_0, \tilde{\dot{\theta}}_0) = (1, -10)$ and $(\Theta, \Psi, \Upsilon) = (\cdot, 10000, 5)$.

5.2. Formulation of the piano action as a non-smooth dynamical multibody system

In Section 5.1, the drawbacks of regularising the non-smooth laws of the piano action's dynamics have been described. They have then been illustrated on the simple example of

⁴To be compared to the values of Υ for each rigid body of the piano action, see Table 5.2.



a pendulum subject to dry friction. The characteristic number of time steps required for a good approximation of the motion of a pendulum, with properties similar to that of the bodies of the piano action, was about a few thousands per period for five pseudo-periods.

Here, an overview of the non-smooth methods which were used for the simulation of the piano action is first given. They were implemented in the computer program XDE presented in Section 5.3. Then, such methods are applied to the previous example of the simple pendulum subject to dry friction. The aim is to quantify the efficiency of such methods compared to the regularisation approach for the piano action, without considering collisions.

5.2.1. Non-smooth formulation

Equation (4.12)⁵ is written as a Measure Differential Inclusion (MDI) (see [Acary and Brogliato, 2008]):

$$\begin{cases} \mathbf{M}(\mathbf{x}) d\mathbf{v} = \mathbf{F}^\circ(\mathbf{x}, \dot{\mathbf{x}}, t) dt + \mathbf{H}(\mathbf{x}) d\mathbf{i} \\ \mathbf{v}^+ = (\dot{\mathbf{x}})^+ \\ (\mathbf{g}(\mathbf{x}), \mathbf{H}^T(\mathbf{x}) \cdot \mathbf{v}^+, d\mathbf{i}) \in K \end{cases} \quad (5.30)$$

The first line formulates the dynamics of the piano action. \mathbf{F}° gathers all the smooth terms which are not related to contact nor unilateral constraints:

$$\mathbf{F}^\circ(\mathbf{x}, \dot{\mathbf{x}}, t) = -\mathbf{N}(\mathbf{x}, \dot{\mathbf{x}}) \dot{\mathbf{x}} - \mathbf{c}_v \dot{\mathbf{x}} - \mathbf{F}^*(\mathbf{x}, \dot{\mathbf{x}}, t) - \kappa(\mathbf{x} - \mathbf{x}_0) \quad (5.31)$$

where the felt reaction forces have been included in \mathbf{F}^* .

dt is the Lebesgue measure, $d\mathbf{v}$ and $d\mathbf{i}$ are vector-valued measures corresponding to the "accelerations" (smooth or not) and the impulses, respectively. Their components are of the form:

$$\begin{aligned} d\mathbf{v} &= \gamma dt + (\mathbf{v}^+ - \mathbf{v}^-) d\mathbf{v} + d\mathbf{v}_s \\ d\mathbf{i} &= f dt + p d\mathbf{v} + d\mathbf{i}_s \end{aligned} \quad (5.32)$$

The measure $d\mathbf{i}$ includes the reactions associated with non-smooth laws. The prefactors of dt are the smooth acceleration (γ) and the smooth forces (f) which are not included in \mathbf{F}° . The measure $d\mathbf{v}$ is a countable sum of Dirac deltas, weighted by the value of discontinuity in velocity ($\mathbf{v}^+ - \mathbf{v}^-$) or in force (p). The last parts ($d\mathbf{v}_s$ and $d\mathbf{i}_s$) are neglected singular measures, assuming that all the physical quantities involved are regular enough.

The geometric operator $\mathbf{H}^T(\mathbf{x})$ yields the relative velocities in the contact frame.

The third line formulates the non-smooth laws and the unilateral constraints as an inclusion in a set K . As previously, the vector of the compression of the felts is denoted by $\boldsymbol{\delta} \in \mathbb{R}^{14 \times 1}$. Felts are treated as material compliances so that each felt is modelled as an additional body, which is linked to the body it belongs to with a prismatic joint. Such

⁵We recall Equation (4.12):

$$\mathbf{M}(\mathbf{x}) \ddot{\mathbf{x}} + \mathbf{N}(\mathbf{x}, \dot{\mathbf{x}}) \dot{\mathbf{x}} + \mathbf{c}_v \dot{\mathbf{x}} + \mathbf{c}_d \text{sign}(\dot{\mathbf{x}}) + \left(\frac{\partial \boldsymbol{\delta}}{\partial \mathbf{x}}(\mathbf{x}) \right)^T \mathbf{F}(\boldsymbol{\delta}) + \mathbf{F}^*(\mathbf{x}, t) + \mathbf{T}(\boldsymbol{\delta}, \dot{\mathbf{x}}) + \kappa(\mathbf{x} - \mathbf{x}_0) = \mathbf{0}$$

a treatment of the felts adds fourteen degrees of freedom to the system. The vector of generalised coordinates \mathbf{x} is therefore completed with the additional DOFs:

$$\mathbf{x} = \begin{bmatrix} \mathbf{x}_{\text{hinges}} \in \mathbb{R}^{6 \times 1} \\ \mathbf{x}_{\text{felts}} \in \mathbb{R}^{14 \times 1} \end{bmatrix} \in \mathbb{R}^{20 \times 1} \quad (5.33)$$

Details and implications of this choice are given in 5.4.2.

Three of the contacts between felts and other bodies are modelled with a Signorini-Coulomb law (see Figure 4.4 page 54). All the other ones are modelled with a Signorini law. For reasons described later on and related to the modelling of the felts, the contact between the bodies are inelastic.

In addition to the felts' compressions δ , a gap function g is associated to each of the fourteen contact zones (see 5.4). The vector of the fourteen gaps is denoted by \mathbf{g} . The condition of non-interpenetration between the bodies and the felts is written as

$$\mathbf{g}(\mathbf{x}) \in \mathbb{R}^{+14} \quad (5.34)$$

so that all the gaps remain positive. The normal reaction impulses \mathbf{r}_N , included in $p dv$, are written as an inclusion to the normal cone of \mathbb{R}^{+14} :

$$-\mathbf{r}_N \in \mathcal{N}_{\mathbb{R}^{+14}}(\mathbf{g}(\mathbf{x})) \quad (5.35)$$

so that for each contact zone:

- if $g > 0$, $r_N = 0$: the normal reaction force is zero when there is no contact;
- if $g = 0$, $r_N \geq 0$: the normal reaction force is positive if there is contact.

The tangential forces \mathbf{r}_T , included in $d\mathbf{i}$ and given by the Coulomb friction law (see Chapter 4) are written for each contact as

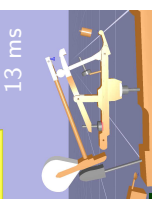
$$(\mathbf{H}^T(\mathbf{x})\mathbf{v})_{\alpha_1, \alpha_2} \in \mathcal{N}_{\mathcal{B}(\mu(\mathbf{r}_N)_i)}((\mathbf{r}_T)_{\beta_1, \beta_2}) \quad (5.36)$$

where $\mathbf{H}^T(\mathbf{x})\mathbf{v}$ are the velocities in the contact frame, μ is the Coulomb friction coefficient and $\mathcal{B}(\mu \mathbf{r}_N)$ is the disk of radius $\mu \mathbf{r}_N$. The generic indices depend on the numbering and are such that α_1, α_2 yield the relative tangential velocities corresponding to the i -th contact, and β_1 and β_2 give the tangential forces of the same i -th contact.

The dry friction in hinges is written as an inclusion in $\mathbf{c}_d \mathbf{sign}(\mathbf{x})$.

5.2.2. Numerical methods used to solve the non-smooth equations

In XDE, Equation (5.30) is solved as described in [Merlhiot, 2011]. The following definitions are introduced:



$$\forall \alpha \in [0, 1], \begin{cases} t_{n+\alpha} & = t_n + \alpha \Delta t \\ \mathbf{x}_{n+\alpha}(\mathbf{k}_x) & = \mathbf{x}_n + \alpha \Delta t \mathbf{k}_x \\ \mathbf{v}_{n+\alpha}(\mathbf{k}_v) & = \mathbf{v}_n + \alpha \Delta t \mathbf{k}_v \end{cases} \quad (5.37)$$

and

$$\mathbf{r} \mid \int_{t_k}^{t_{k+1}} \mathbf{H}(\mathbf{x}_{n+\gamma}(\mathbf{k}_x)) d\mathbf{i} \approx \mathbf{H}(\mathbf{x}_{n+\gamma}(\mathbf{k}_x)) \mathbf{r} \quad (5.38)$$

The smooth dynamics and the differential inclusions are time-discretised using a time-stepping scheme as follows:

$$\begin{cases} \mathbf{M}(\mathbf{x}_{n+\theta}(\mathbf{k}_x)) \mathbf{k}_v = \mathbf{F}^\circ(\mathbf{x}_{n+\theta}(\mathbf{k}_x), \mathbf{v}_{n+\theta}(\mathbf{k}_v), t_{n+\theta}) + \mathbf{H}(\mathbf{x}_{n+\gamma}(\mathbf{k}_x)) \mathbf{r} \\ \mathbf{v}_{n+\theta}(\mathbf{k}_v) = \mathbf{k}_x \\ (\mathbf{g}(\mathbf{x}_{n+\gamma}(\mathbf{k}_x)), \mathbf{H}^T(\mathbf{x}_{n+\gamma}(\mathbf{k}_x)) \mathbf{v}_{n+\gamma}(\mathbf{k}_v), \mathbf{r}) \in F \end{cases} \quad (5.39)$$

Each iteration is solved in a global Newton loop. First, the contact kinematics and the smooth forces \mathbf{F}° are linearised, which leads to an algebraic inclusion with unknowns $(\mathbf{k}_v, \mathbf{r})$, known as a One-Step Non-Smooth Problem [Acary and Brogliato, 2008]. This OS-NSP is reformulated using an augmented Lagrangian approach [Studer, 2009] and solved by an iterative projective Gauss-Seidel-like method. More details are given in [Merlhiot et al., 2012].

5.2.3. Example of a pendulum with dry friction

The dynamics of the pendulum described in 5.1.2, where Coulomb friction had been regularised, is now solved with a non-smooth approach.

The dynamics equation of the pendulum (5.6) is recalled:

$$\ddot{\tilde{\theta}} + \Upsilon^2 \text{sign}(\dot{\tilde{\theta}}) + 4\pi^2 \sin(\tilde{\theta}) = 0$$

It can be written in a form similar to (5.30):

$$\begin{cases} \ddot{\tilde{\theta}} = -4\pi^2 \sin(\tilde{\theta}) - \Upsilon^2 \lambda \\ \lambda \in \text{sign}(\dot{\tilde{\theta}}) \end{cases} \quad (5.40)$$

5.2.4. Implicit scheme

Similarly to 5.1.2, the linearly-implicit Euler scheme is applied to $\tilde{\theta}$:

$$\tilde{\theta}_{k+1} = \Theta(\tilde{\theta}_{k+1} - \tilde{\theta}_k) \quad (5.41)$$

so that

$$\begin{cases} \tilde{\theta}_{k+1} = \tilde{\theta}_k - 4\pi^2 \sin(\tilde{\theta}_k) - \Upsilon^2 \lambda_{k+1} \\ \lambda_{k+1} \in \text{sign}(\tilde{\theta}_{k+1}) \end{cases} \quad (5.42)$$

Note that the effect of gravity was treated explicitly (written as a function of $\tilde{\theta}_k$). This has no significant influence on the results because the effect of gravity does not change much from one step to another, but it simplifies the resolution which does not require a Newton-like root-finder algorithm.

It can be proved⁶ that:

$$\lambda_{k+1} \in \text{sign}(\tilde{\theta}_{k+1}) \iff \lambda_{k+1} = \text{proj}_{[-1,1]} \left(-\frac{q_k}{W_k} \right) \quad (5.43)$$

where q_k and W_k are defined by

$$\tilde{\theta}_{k+1} = q_k + W_k \lambda_{k+1} \quad (5.44)$$

and $\text{proj}_{[-1,1]}$ is the projector on $[-1, 1]$ defined by

$$\text{proj}_{[-1,1]}(\alpha) = \begin{cases} -1 & \text{if } \alpha < -1 \\ \alpha & \text{if } \alpha \in [-1, 1] \\ 1 & \text{if } \alpha > 1 \end{cases} \quad (5.45)$$

Similarly to Equation (5.9), the overall equations can be written as a matrix equation:

$$\begin{bmatrix} \tilde{\theta}_{k+1} \\ \tilde{\theta}_{k+1} \end{bmatrix} = (\Theta \mathbf{I} - \mathbf{A})^{-1} \left(\Theta \begin{bmatrix} \tilde{\theta}_k \\ \tilde{\theta}_k \end{bmatrix} + \begin{bmatrix} 0 \\ -4\pi^2 \sin(\tilde{\theta}_k) - \Upsilon^2 \text{proj}_{[-1,1]} \left(\frac{\Theta}{\Upsilon^2} [\tilde{\theta}_k - \frac{4\pi^2}{\Theta} \sin(\tilde{\theta}_k)] \right) \end{bmatrix} \right) \quad (5.46)$$

or generically:

$$\mathbf{U}_{k+1} = \mathbf{D}^{-1} [\Theta \mathbf{U}_k + \mathbf{F}(\mathbf{U}_k)] \quad (5.47)$$

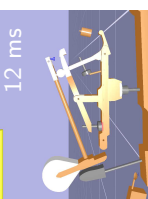
5.2.5. Results

Some results are represented in Figure 5.8 for $\Upsilon = 5$. One can see that dry friction actually blocks the pendulum even for low Θ , whereas this was never observed in Figure 5.7.

A comparison of the results calculated with the regularised and the non-smooth approach is given in Figure 5.9 with the same time step. For the same computational cost, the non-smooth scheme yields a very good solution. The regularised scheme leads to an inappropriate and chattering solution.

The comparison of the convergence speeds is presented more precisely in Figure 5.10 with values of Υ which are typical for the piano action. The measure of the difference between each calculated solution and the exact solution was defined by the mean of the difference for each time step. It appears that Υ is a good indicator of the relative benefit offered by the nonsmooth approach, relatively to the regularised one: the larger Υ , the larger

⁶Case by case, for example.



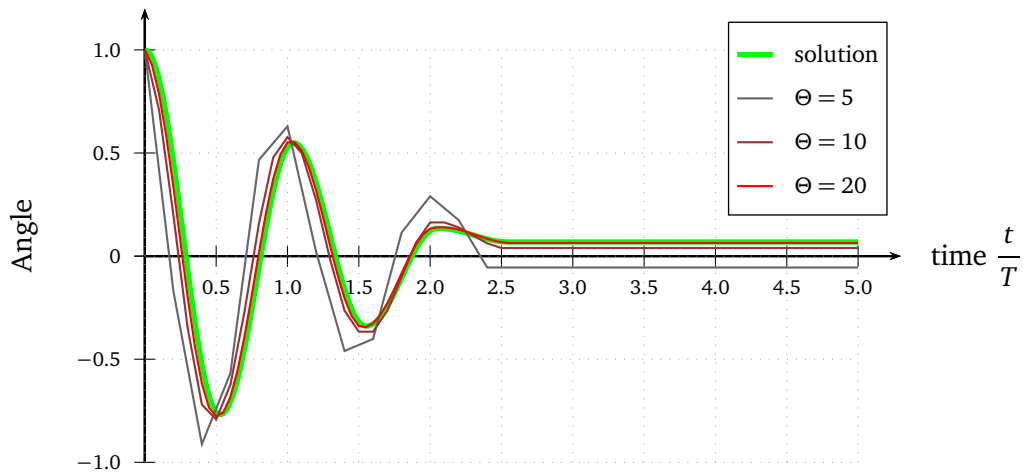


Figure 5.8 – Convergence of the non-smooth scheme. $(\tilde{\theta}_0, \tilde{\theta}'_0) = (1, 0)$ and $(\Theta, \Upsilon) = (\cdot, 5)$.

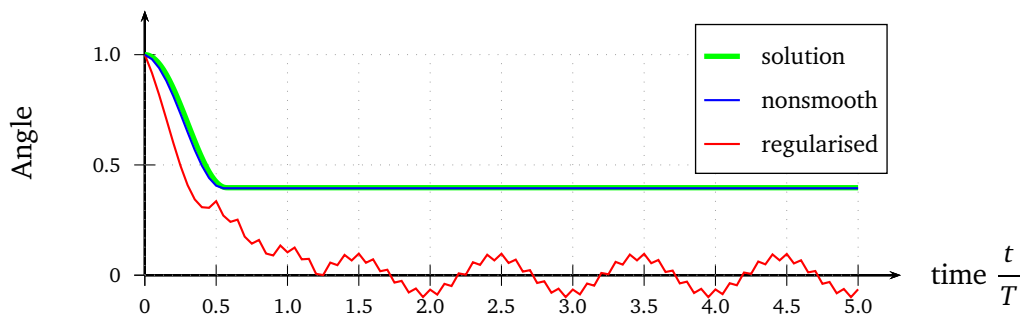


Figure 5.9 – Comparison of the regularised and non-smooth approaches. $(\tilde{\theta}_0, \tilde{\theta}'_0) = (1, 0)$ and $(\Theta, \Psi, \Upsilon) = (20, 10000, 5)$.

the relative advantage of the nonsmooth approach is. Also, the nonsmooth approach is systematically more efficient.

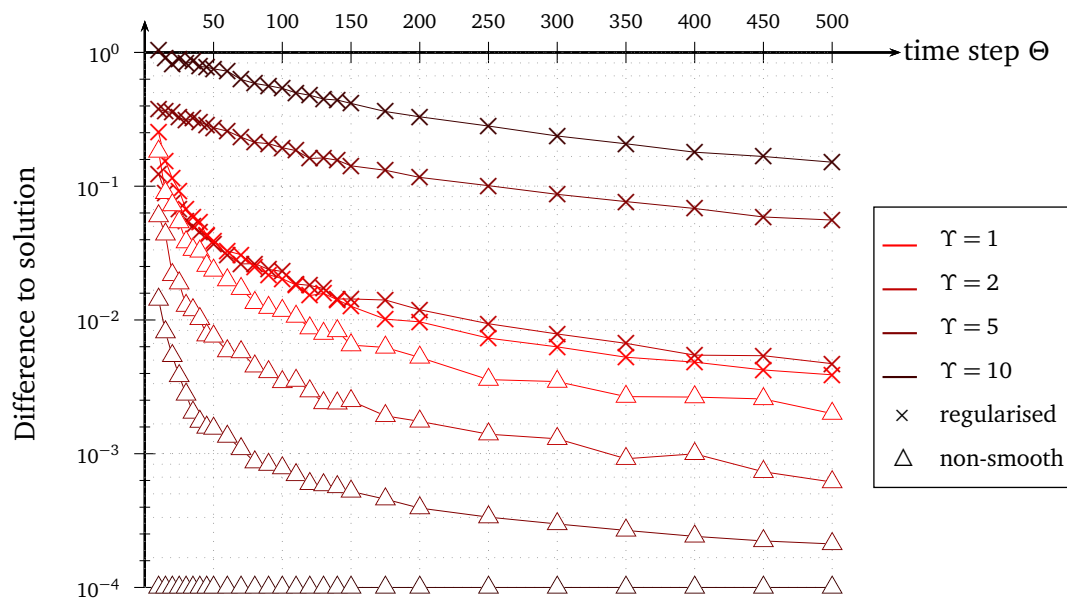


Figure 5.10 – Convergence of the regularised scheme (\times) and the non-smooth scheme (Δ) for several Υ . $(\tilde{\theta}_0, \tilde{\theta}'_0) = (1, 0)$ and $\Psi = 10000$.

The conclusion of this brief study is that in order to calculate the effect of dry friction on the bodies of the piano action, without considering contacts, the presented non-smooth method is significantly more efficient and robust than the regularising approach. For $\Upsilon = 2$, an relative error of 1 % is reached with $\Theta = 40$ with the non-smooth method, and with $\Theta = 250$ with the regularised one. For $\Upsilon = 5$, the same relative error is reached with $\Upsilon = 15$ with the non-smooth method⁷, whereas $\Upsilon \gg 500$ is required otherwise. This matters even more as on the complete mechanism, the regularising approach may require time steps which are largely below the characteristic time of the piano action, estimated as approximately 1 ms (this corresponds to $\Theta \approx 1000$). The time step would then have to be reduced for numerical reasons instead of physical ones.

The impairment of numerical properties induced by a regularised approach, as observed in this simple study, appeared clear enough to make us choose non-smooth numerical methods. It is noteworthy that a simple regularised approach has been used in the study of the pendulum with dry friction, but more sophisticated regularised models exist.

5.3. eXtended Dynamic Engine (XDE)

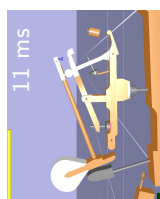
The numerical methods described in 5.2.2 were implemented in the computer program XDE, which stands for eXtended Dynamic Engine. The part we used is XDE Physics, which is a C++ development kit consisting in a kernel for interactive mechanical simulation of rigid multibody systems with kinematic constraints, intermittent contacts and dry friction.

XDE was developed at CEA LIST, mainly for industrial virtual prototyping and simulation for robotics. Its main features which were useful for the simulation of the piano action are:

- the simulation of rigid multibody systems with intermittent friction using efficient numerical methods;
- the modelling and parametrisation of multibody systems with kinematic constraints;
- the parametrisation and the formulation of the dynamics of multibody systems based on Lie groups;
- the implementation of numerical integration for such parametrisations;
- the modelling of frictional contact with nonsmooth contact laws: Signorini and Signorini-Coulomb laws;
- the nonsmooth formulation of the dynamics for multibody systems with nonsmooth contact laws, by means of measure differential inclusions;
- the implementation of time integration using time-stepping methods;
- the implementation of nonsmooth time-stepping-compatible methods for collision detection, with efficient geometrical estimation of contacts.

More information is provided in [Merlhiot, 2012].

⁷Indeed, the error with the non-smooth method gets smaller when friction increases, in this case of free oscillations.



5.4. Adjustments of the model for its implementation

In order to implement the complete model of the piano action described in Chapter 4, some modifications of the model were required.

5.4.1. Actuation of the key

As it was not possible to use the key position as an input of the simulation in XDE, a Kelvin-Voigt viscoelastic model was inserted between the (virtual) key and the (virtual) finger, as shown in Figure 5.11. It was then possible to control the position of the free end of the Kelvin-Voigt model.

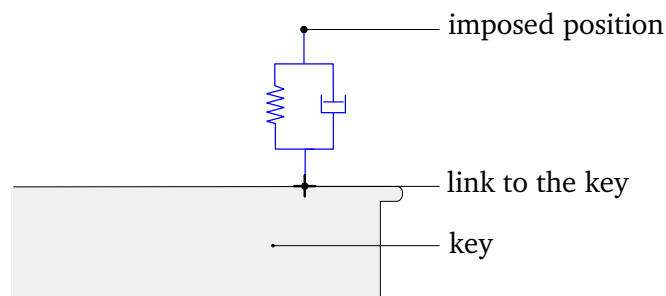


Figure 5.11 – *Scheme of the Kelvin-Voigt model added for the simulation.*

An infinite stiffness in the Kelvin-Voigt model would lead to a position-driven simulation but the numerical stiffness would be too high to be solved properly. In the experiments, a viscoelastic material was added to correspond to a Kelvin-Voigt model. Its choice and the values of its parameters are discussed in 3.3, page 41.

The simulated system is composed of the piano action and this PD corrector.

5.4.2. Felt laws

There are (at least) two possible ways of implementing the felt laws:

1. as a compliant contact in the normal direction, with a Hertz-like penalisation;
2. as a material compliance, by introducing new bodies corresponding to the felts, new degrees of freedom, and by assigning a Signorini law to each of the contacts.

This first option was ruled out for several reasons. The first one is that unilateral constraints are not ensured when a linearly implicit scheme is used together with penalised contacts, because the linearisation can lead to negative reaction forces. Similarly, it is hard to ensure compressive dissipation only. This would be improved using non-linear implicit schemes, but the computational cost is likely to increase significantly. Moreover, for the piano action, several contacts can occur within the relaxation time of a felt (consider for instance, the quick use of the double escapement). The correct estimation of the corresponding dissipation would require to keep the history of the compression of each felt. Such a feature would have to be implemented.

We chose to add one body per felt, introducing fourteen new degrees-of-freedom in total. This solution introduces collisions between felts and other bodies. In XDE, collisions are

modelled with an inelastic contact. Since the mass of each felt is very low compared to that of the rotating bodies, the corresponding dissipation is negligible.

A rigid body (disk or segment) was associated to each felt in accordance with the contact description (see Table 4.2). This additional rigid body was given a mass m_{felt} corresponding to the characteristic mass of the felt material involved during collision⁸. It was linked to the body it belonged to with a prismatic joint. The felt law was applied between the fix part of the prismatic joint and its sliding part.

This model is illustrated in Figure 5.12 on the example of the hammer colliding with the string.

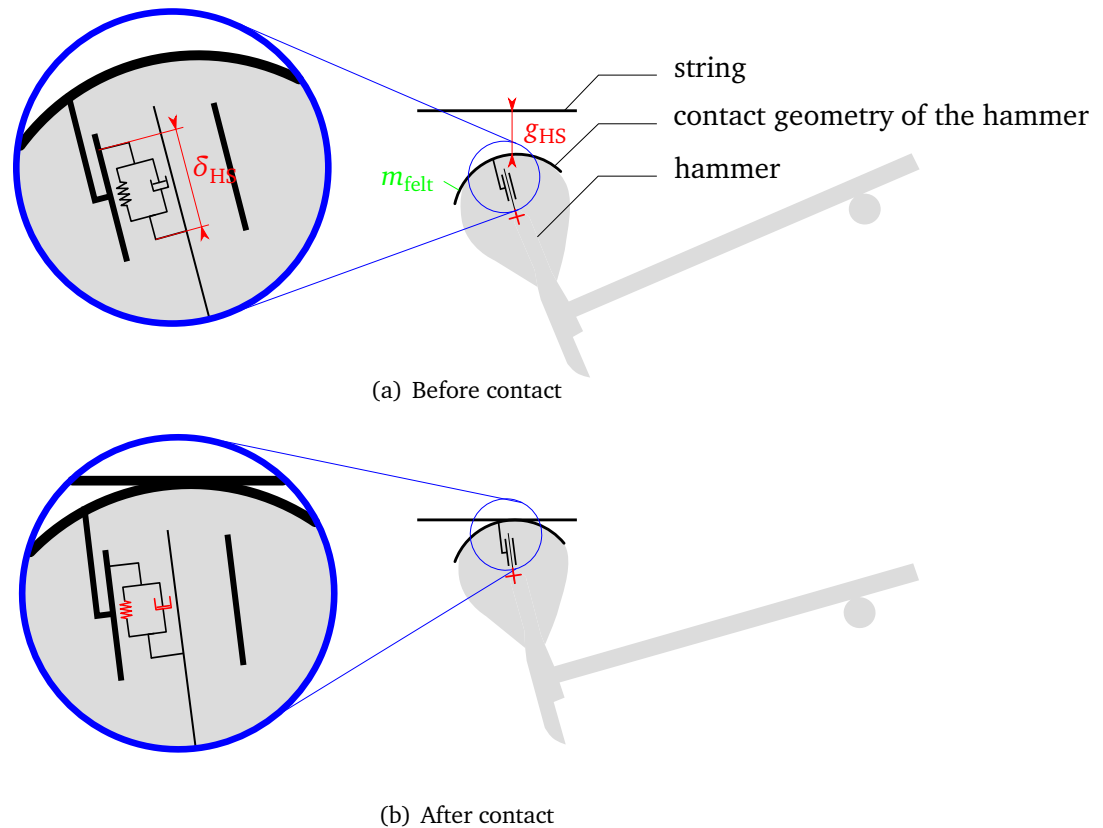


Figure 5.12 – Description of the contact with prismatic joint and felt law, illustrated with the hammer-string contact.

It is noteworthy that introducing an additional degree of freedom for each felt (14 DOFs in total) does not perceptibly change the computation times.

5.5. Adjustments of XDE for the simulation

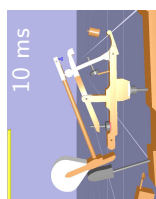
5.5.1. Implementation of the felt laws

The model used for the felt is such that its reaction force F obeys:

$$\forall \delta \geq 0, \forall \dot{\delta}, \quad F(\delta, \dot{\delta}) = k \delta^r - b \dot{\delta} \delta^2$$

where δ is the compression of the felt (see 4.5.10).

⁸This parameter was included in the parameters category III (see 4.4.1).



In XDE, the only implemented law is linear viscoelastic (Kelvin-Voigt model). To implement the felt laws, we change the stiffness k_{lin} and the viscosity b_{lin} of the linear model at each time step. This also required the addition of an external force f_{lin} (joint actuator) at each iteration.

The value of k_{lin} , b_{lin} and f_{lin} were determined from the differentiation of F , which is $\mathcal{C}^1(\mathbb{R}, \mathbb{R})$ as $r > 1$. The calculation yields:

$$\begin{aligned}
 F(\delta_{n+1}, \dot{\delta}_{n+1}) &= F(\delta_n, \dot{\delta}_n) + (\delta_{n+1} - \delta_n) \frac{\partial F}{\partial \delta}(\delta_n, \dot{\delta}_n) + (\dot{\delta}_{n+1} - \dot{\delta}_n) \frac{\partial F}{\partial \dot{\delta}}(\delta_n, \dot{\delta}_n) \\
 &= (k \delta_n^r + b \dot{\delta}_n \delta_n^2) + (kr \delta_n^{r-1} + 2b \delta_n \dot{\delta}_n)(\delta_{n+1} - \delta_n) + (b \delta_n^2)(\dot{\delta}_{n+1} - \dot{\delta}_n) \\
 &= \underbrace{k \delta_n^r - kr \delta_n^r - 2b \delta_n^2 \dot{\delta}_n}_{\text{actuator joint effort}} + \underbrace{(kr \delta_n^{r-1} + 2b \delta_n)}_{\text{proportional gain}} \delta_{n+1} + \underbrace{(b \delta_n^2)}_{\text{derivative gain}} \dot{\delta}_{n+1}
 \end{aligned} \tag{5.48}$$

so that

$$\begin{cases} k_{\text{lin}} = (kr \delta_n^{r-1} + 2b \delta_n) \\ b_{\text{lin}} = (b \delta_n^2) \\ f_{\text{lin}} = k(1-r) \delta_n^r - 2b \delta_n^2 \dot{\delta}_n \end{cases} \tag{5.49}$$

An illustration is given in Figure 5.13, where the dissipative part has been omitted.

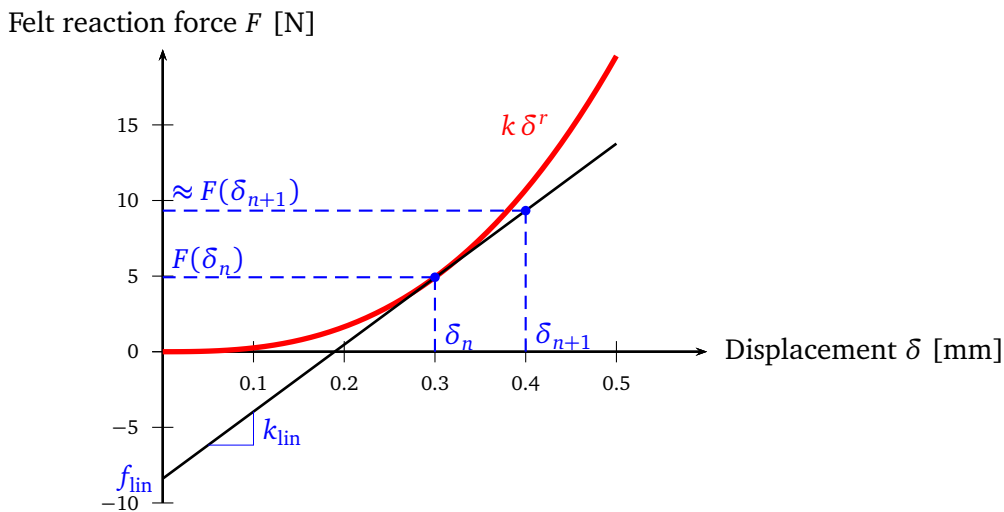


Figure 5.13 – Illustration of the implementation of the felt law as a linear model with adjustable parameters (the dissipative part has been omitted).

5.5.2. Ensuring the repeatability of the simulation

The simulating program is divided in several elements, which are Orocos Agents (Open RObot COntrol Software, [Orocos, 2013]), see Figure 5.14. Each element is a block with a specific function:

physic engine – Contains the mechanical and the solving parts.

clock – Initiates the simulation. It also allows to regulate the speed of the simulation.

position input – Imports the position command to be applied at the following step.

joint positions export Exports the generalized coordinates at each time step.

felt law Sets the parameters of the linear viscoelastic laws so that it models the felts, see 5.5.1.

To ensure the repeatability of the simulations, a synchronisation is implemented so that each block can only run when its input ports receive a signal from the previous one, meaning that the previous block has finished its task. The initial start is given by a clock. In Figure 5.14, the connexions between the blocks is shown. The red dots indicates eventual ports, i.e. ports which activates the block to which they are connected every time a new data is written in them. On the contrary, green dots symbolises periodical ports, i.e. ports where the data is read periodically, whether it is a new one or not.

Doing so slowed down the simulation time significantly (factor ≈ 20), but ensured an absolute repeatability. This loss of time could be completely compensated with an appropriate low-level implementation (in the physics kernel).

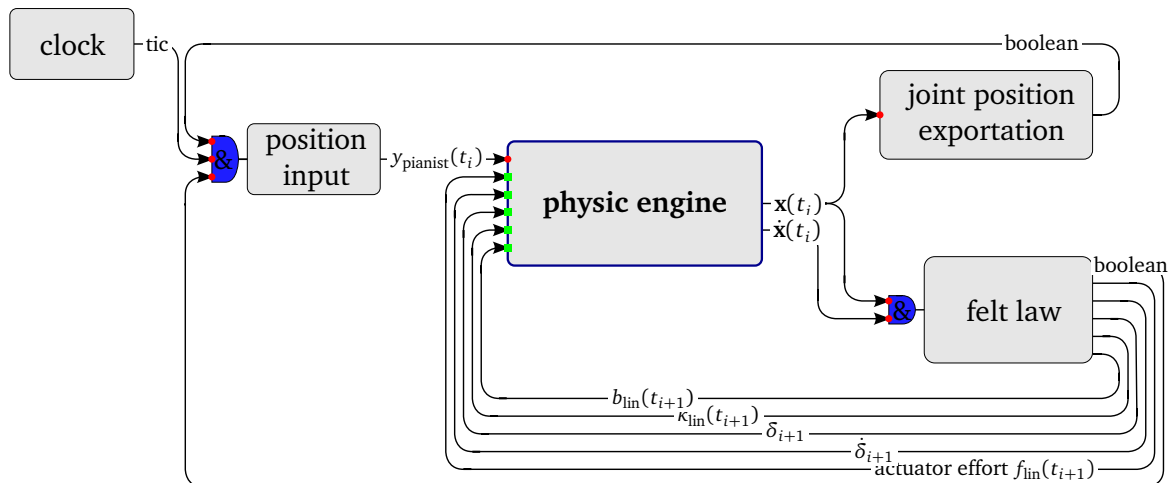
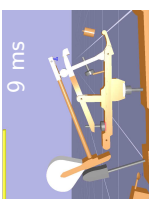


Figure 5.14 – Synchronized connexions of Orocos agents.

5.6. Simulating in practice

In practice, XDE was run in a Python framework. After the implementation of the modifications described in 5.5, some additional Python scripts were written so that all the simulations would be controlled from MATLAB. It communicated with Python by means of text files, see Figure 5.15. In total, the Python scripts used to control XDE for the simulation of the piano action are made of more than 2000 lines.

The results of the simulation were written by Python in other text files, which were interpreted by MATLAB.



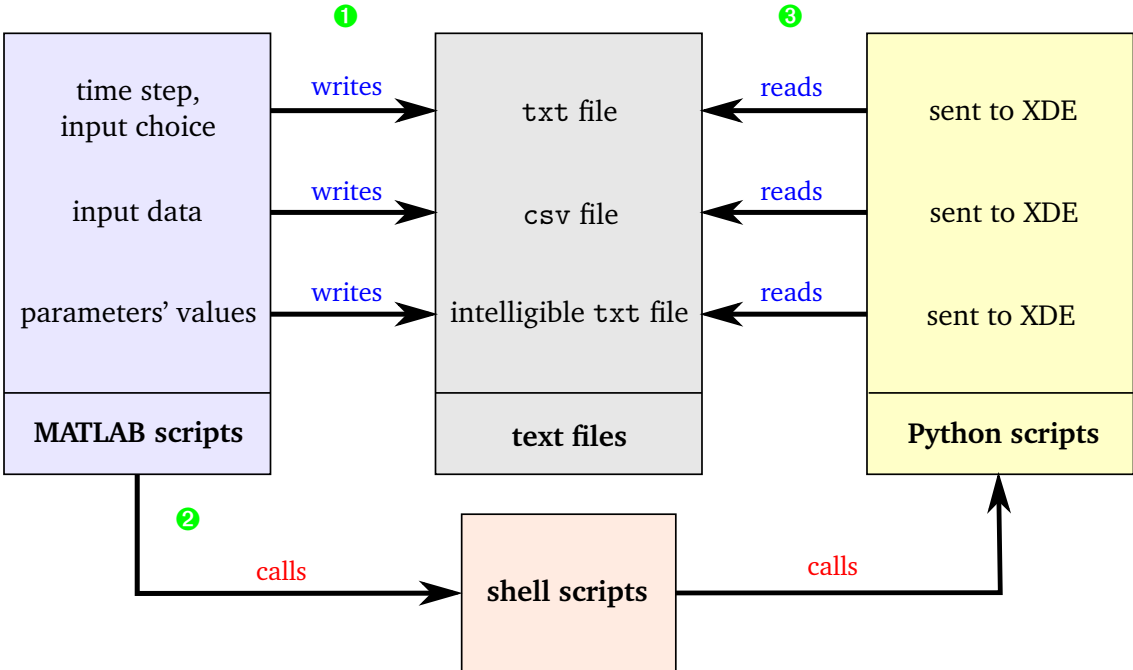
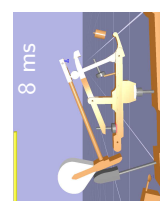


Figure 5.15 – Simulations principle.

Overview In this chapter, the model of Chapter 4 is simulated using the methods described in Chapter 5. The simulations consist in predicting the reaction force of the key on the finger in response to a position, as explained in Chapter 2. The simulation results are compared to the experimental results of Chapter 3.

Contents

6.1. Regulation of the virtual piano action	98
6.2. Position-driven simulations	98
6.2.1. Key	98
6.2.2. All bodies	102
6.2.3. Visualisation of the simulations	104
6.3. Force-driven simulations	106
6.4. Discussion	107
6.4.1. Position-driven	107
6.4.2. Force-driven	110
6.5. A sensitivity analysis	113
6.5.1. Choice of the cost functional	113
6.5.2. Parameters of category I	113
6.5.3. Parameters of Category II	117
6.5.4. Parameters of Category III	118
6.5.5. Parameters of Category IV	119
6.5.6. Discussion and conclusion	119



The model of the piano action presented in Chapter 4 is simulated using the methods described in Chapter 5. The first results were promising but kinematic observations of the simulations highlighted a few misadjustments of some parameters' values. Section 6.1 expounds how the virtual piano action has been numerically regulated. Results for *piano* and *forte* keystrokes are given in 6.2 and 6.3 for position-driven¹ and force-driven simulations, respectively. Testing the effect of significant changes led to the same conclusion of Chapter 2. The discussion is focused on the upward phase because the sustain and the release of the key matter less, from the haptical point of view.

Finally, a sensitivity analysis of the (simulated) reaction forces, to the parameters of categories I, II and III, is carried out for the *piano* and *forte* dynamics.

6.1. Regulation of the virtual piano action

First, simulations were run with the values of the parameters given in Chapter 4, for several keystroke dynamics. The comparison between kinematic measurements and the calculated kinematics showed that the virtual escapement occurred a bit too late. As done in real life by piano technicians, this was corrected by regulating the virtual piano action, here by lowering the let-off button.

Applying the full procedure (see Appendix A), the regulation of the virtual action yielded the following modifications:

- the jack regulating screw (jack-whippen contact) was moved horizontally² by 0.4 mm;
- the backcheck (key-hammer contact) was moved horizontally by -7×10^{-4} m;
- the capstan screw (key-whippen contact) was lowered by 0.2 mm;
- the let-off button (support-jack contact) was screwed to leave an additional gap of 1.9 mm.

Except for the let-off button, these modifications lie within the margin of uncertainties of the lengths measurements (see Chapter 3). They can be perceived as *virtual lutherie*: the virtual action is treated as a real action.

The results presented in Sections 6.2 and 6.3 were calculated using these adjustments.

6.2. Position-driven simulations

The damper is not considered, as it is not a key element in the global dynamics.

6.2.1. Key

We remind that, because it was technically not possible to use the key position as an input of the simulation in XDE, a Kelvin-Voigt viscoelastic model has been inserted between the (virtual) key and the (virtual) finger. It was then possible to control the position of the free end of the Kelvin-Voigt model in the simulation (see 3.3 and 5.4.1). A piston has been inserted between the (real) key and the (real) finger, modelled by the Kelvin-Voigt model.

For the key, two different positions were therefore considered in the experiments:

¹Contrary to the simulations of Chapter 2, the acceleration measurements are not used in the present chapter.

²As in Chapter 4, the x -axis is positive in the direction of the pianist.

- the measured position of the upper face of the piston Y_{meas} ;
- the measured position of the key y_{meas} ;

The measured signals Y_{meas} and y_{meas} were downsampled at 2 kHz. The signal Y_{meas} was used as an input for the simulation. The summary of the relationships between the different physical quantities is given in Figure 6.1.

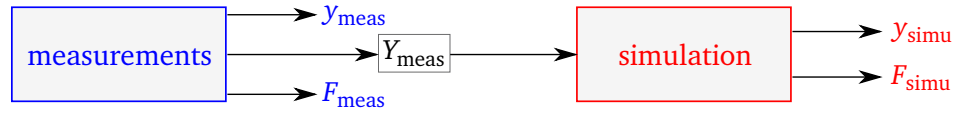


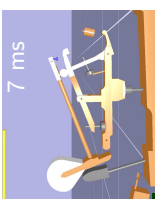
Figure 6.1 – Scheme of the measured and simulated physical quantities (position-driven).

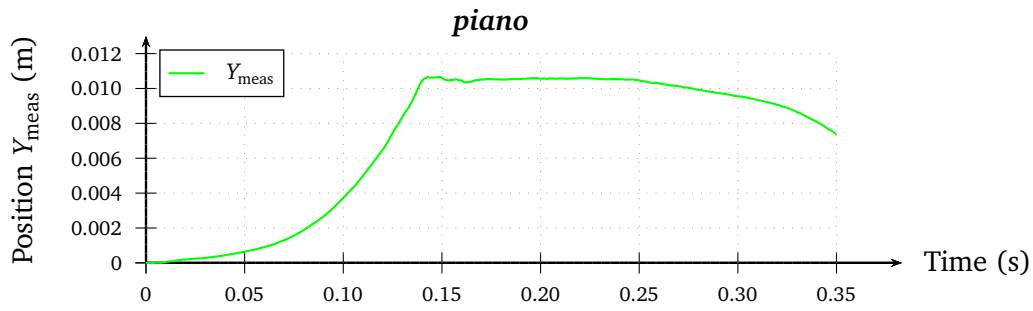
The input Y_{meas} is plotted in Figures 6.2(a) and 6.3(a) for *piano* and *forte* dynamics, respectively.

The main result is the comparison between the simulated reaction force of the key on the pianist (F_{simu}). It is represented together with F_{meas} for both *piano* and *forte* keystrokes in Figures 6.2(b) and 6.3(b), respectively.

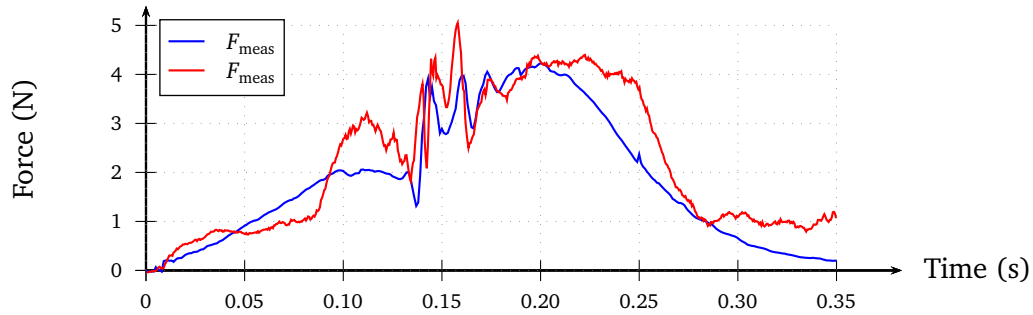
The comparison between y_{meas} and y_{simu} aims at making sure that measured and simulated displacements of the key are similar, see Figure 6.2(c) for *piano* and 6.3(c) for *forte*.

The comparisons between measured and simulated quantities are discussed in Section 6.4.

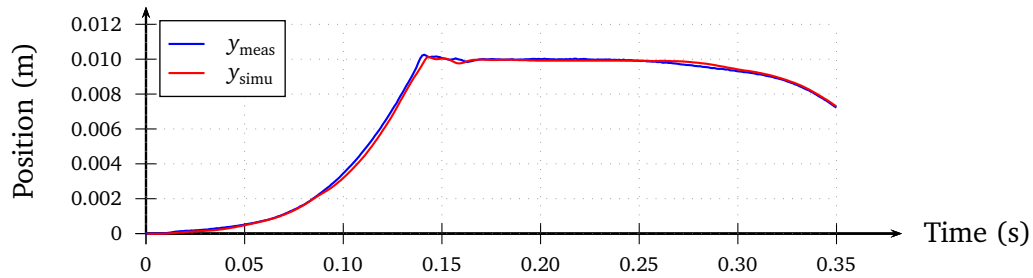




(a) Input-position of the simulation Y_{meas} .

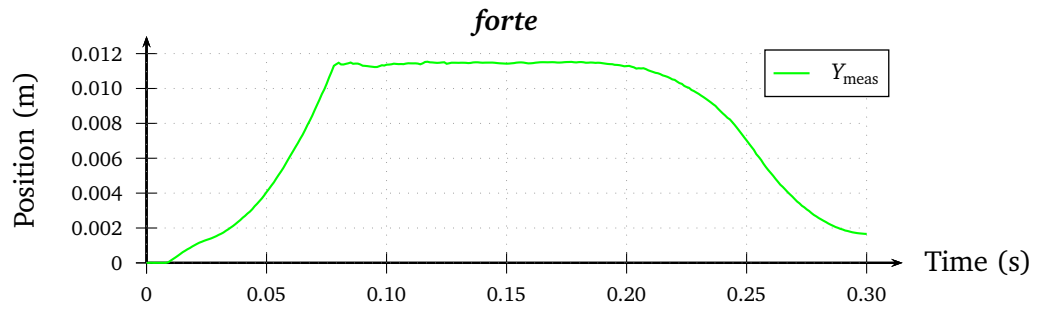
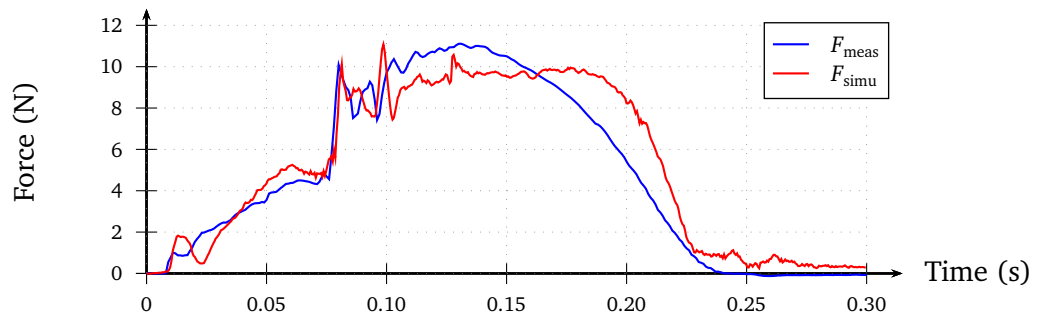


(b) Measured and simulated reaction forces of the key on the pianist's finger.

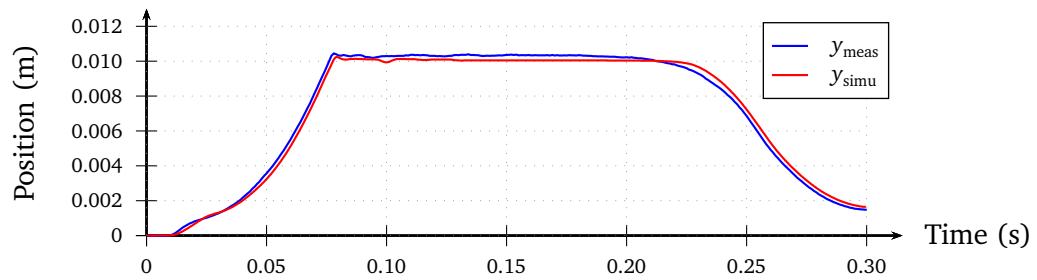


(c) Simulated and measured position of the key.

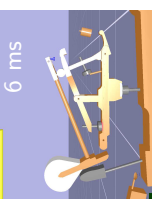
Figure 6.2 – Simulation results for a piano keystroke (input: displacement).

(a) Input-position of the simulation Y_{meas} .

(b) Measured and simulated reaction force of the key on the pianist's finger.



(c) Measured and simulated position of the key.

Figure 6.3 – Simulation results for a forte keystroke (input: displacement).

6.2.2. All bodies

Here, we compare the angular positions of each rigid body measured with the video tracking and calculated from the simulation, for the *piano* blow. The tracking is not very accurate (see Chapter 3) but gives valuable indications.

The results are shown in Figure 6.4. For each body, notable events have been marked by a vertical segment:

- (a): Initial position, at rest.
- (b): Beginning of the rotation of the jack, which corresponds to the contact between the jack and the let-off button.
- (c): Contact of the key and the front rail punching.
- (d): Impact of the hammer and the string.
- (e): Catch of the hammer by the backcheck.
- (f): Repositioning of the jack, so that the mechanism is ready to propel the hammer again.

These events are used in the discussion 6.4.1.

For technical reasons, the impact of the hammer on the string was first considered as inelastic. This unrealistic model did not affect much the study of the haptics, because we focused on the phase before the impact of the hammer on string. Nevertheless, at the very end of the thesis, an elastic contact law has been implemented. The angles calculated with this hammer-string contact model are marked with a tilde (for instance $\tilde{\theta}_k$ is the angle of the key calculated with this law). The elastic law resulted in a higher velocity of the hammer during its check so that the hammer stopped at a slightly different angle than with the inelastic law. We corrected this by adjusting the backcheck, as done in real life. The kinematic computations, plotted in dashed green in Figure 6.4, show improvements: the hammer trajectory is much closer to the measured one. The implementation of the elastic law resulted in an overestimated computed reaction force of the key on the finger during the check. This is believed to be due to the position of the backcheck, adjusted to correspond to the measured kinematics, but not to the measured dynamics. Additional investigation would be required to better modelled the catch of the hammer.

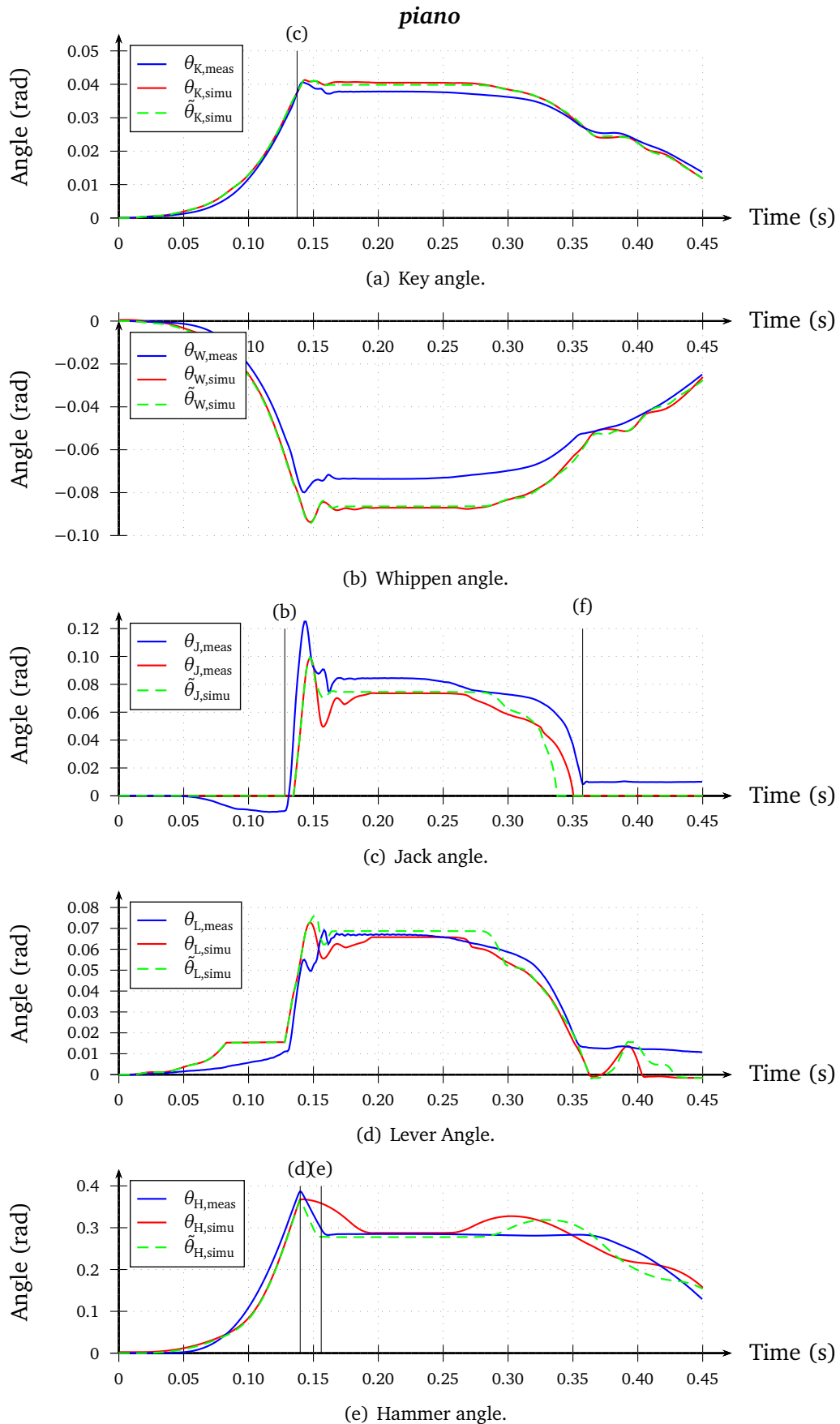
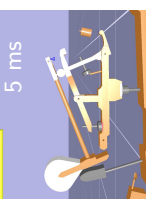


Figure 6.4 – Comparison of the position of the bodies (tracking vs simulation) for a piano keystroke. *Blue*: measurements. *Red*: simulation. *Green*: simulation with elastic hammer/string contact law.



6.2.3. Visualisation of the simulations

The visualisation of the simulations offers a good insight on the qualitative behaviour of the mechanism. We compare the real state of the piano action captured by a high-speed film and the corresponding simulation, for a *piano* keystroke. Figure 6.5 presents the states corresponding to events (a), (b), (d), (e) and (f). These events are reported on the position and force results in Figure 6.9.

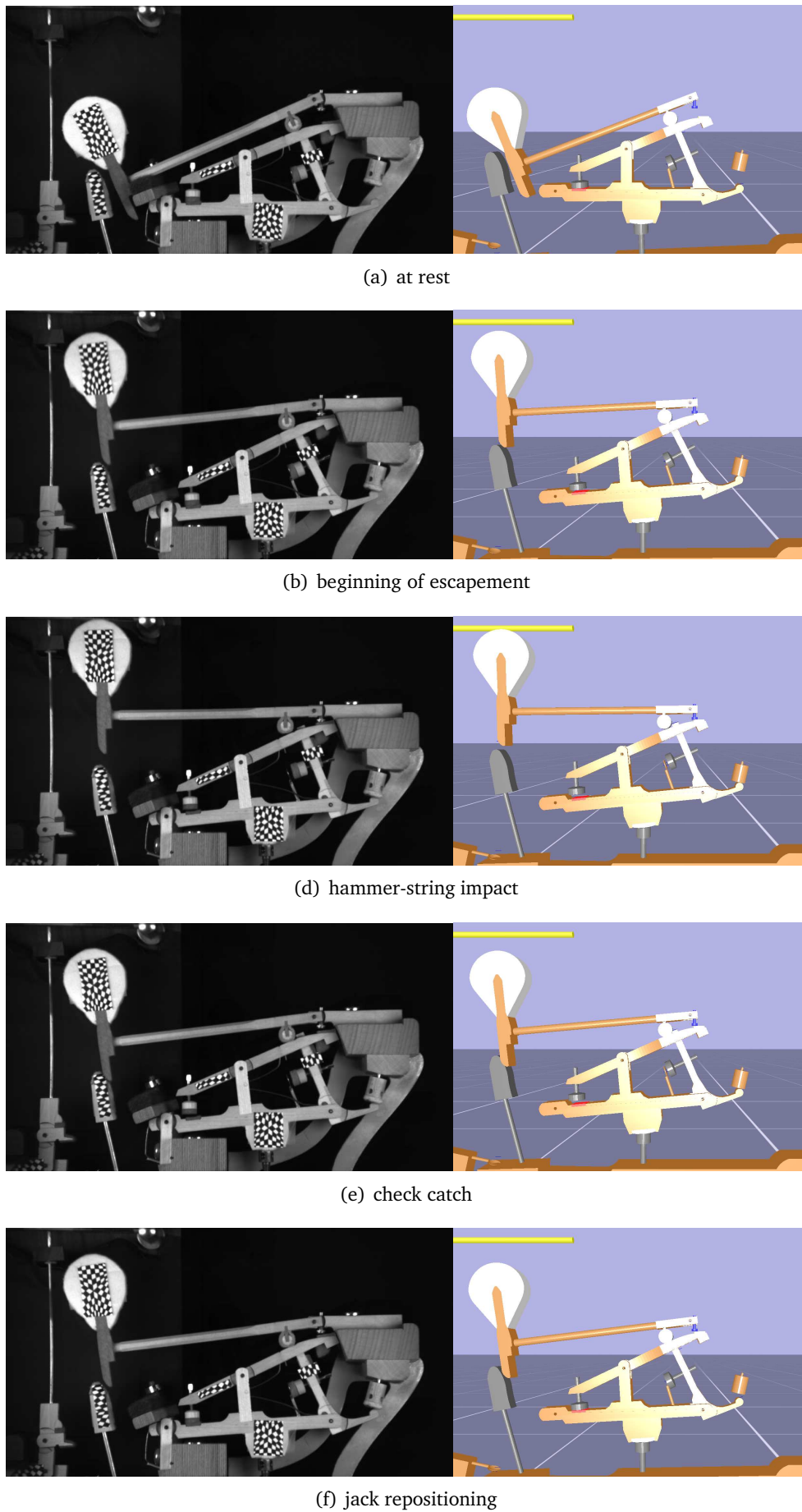
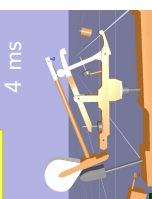


Figure 6.5 – Film and simulation screenshots comparison for notable events (see Figure 6.9).



6.3. Force-driven simulations

For force-driven simulations, the relationship between the different physical quantities is given in Figure 6.6.



Figure 6.6 – Scheme of the measured and simulated physical quantities (force-driven).

The measured force F_{meas} is used as an input for the simulations which yield a calculated displacement of the key end y_{simu} . The comparison between y_{simu} and the measured displacement of the key y_{meas} are presented for a *piano* keystroke (Figure 6.7) and for a *forte* keystroke (Figure 6.8).

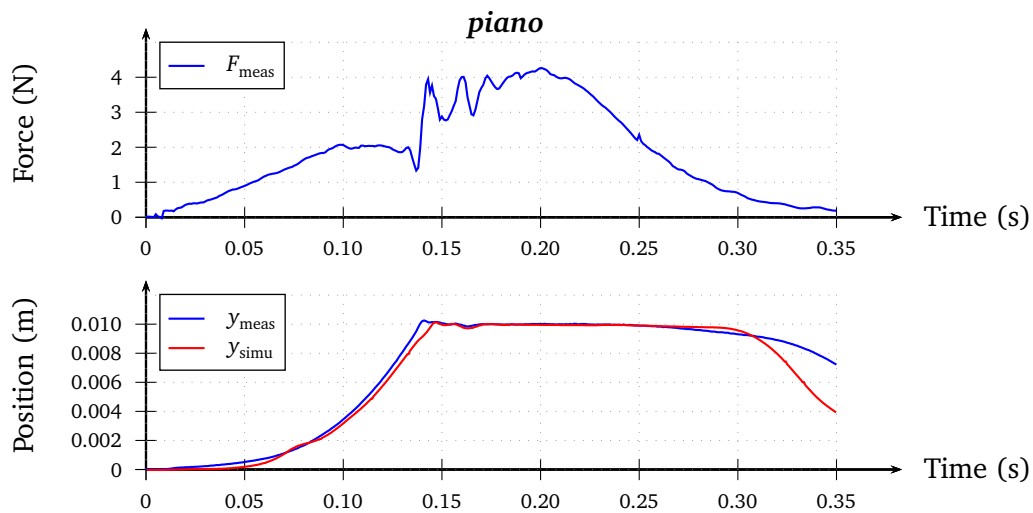


Figure 6.7 – Simulation results for a piano keystroke (input: force).

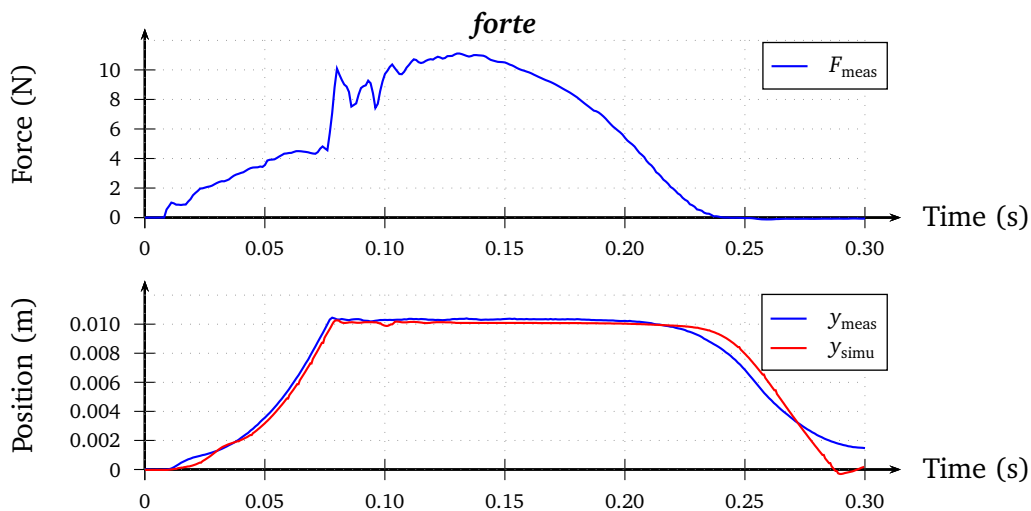


Figure 6.8 – Simulation results for a forte keystroke (input: force).

6.4. Discussion

6.4.1. Position-driven

Using the above-described measurements, it was possible to capture the following events, which are the main elements of the motion of the grand piano action:

- (a): start from the resting position;
- (b): jack - let-off button punching (support) contact;
- (c): key - front rail punching contact;
- (d): impact on the string;
- (e): catch of the hammer;
- (f): return of the jack to its initial position.

The instants of these events are reported in Figure 6.9 (key positions – top – and reaction forces of the key on the pianist – bottom). There are no obvious correlations between these events in the position diagrams. On the reverse, (b), (c) and (e) can be correlated with some patterns of the force diagrams.

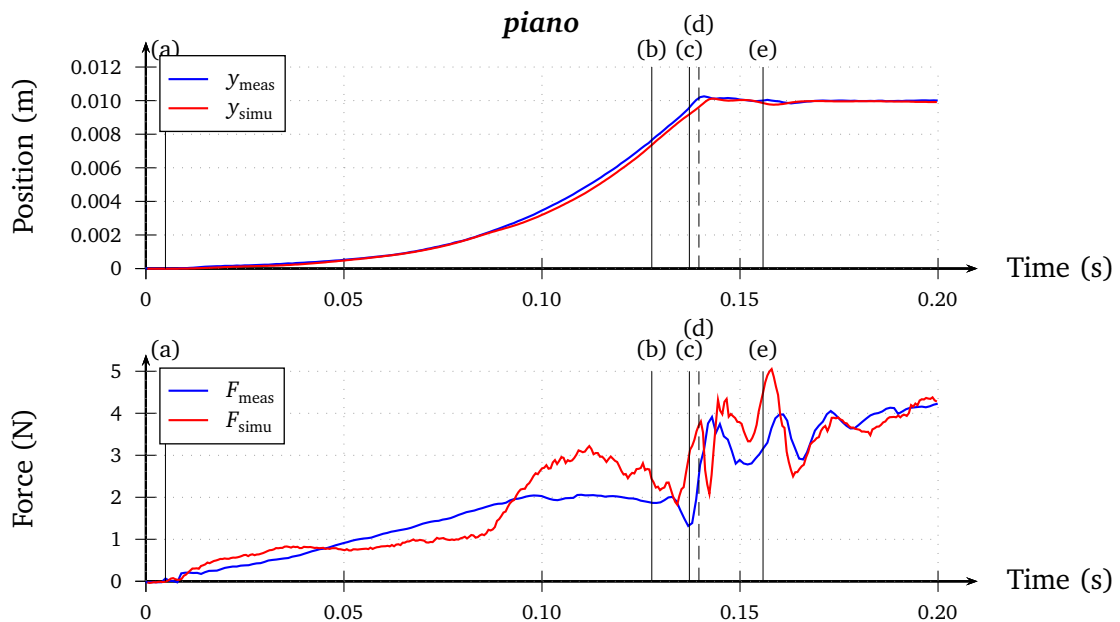
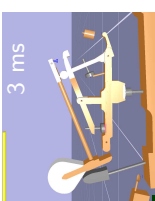


Figure 6.9 – Notable events during a piano keystroke.

The instant when the jack meets the let-off button (b) is followed by a small hump and a rather sharp decrease of the force. This pattern was systematically observed, whatever the keystroke dynamics. This is one of the major elements of the regulation of the action, extensively commented (see e.g. [Porter, 2009]) and known as *aftertouch*. The simulations render this pattern in both *piano* and *forte*. One can note that the hump is of low amplitude compared to the other irregularities. A representation of $\frac{dF}{dt}$ would better emphasise this pattern. This suggests that $\frac{dF}{dt}$ could represent, in some way, the haptical point of view, better than $F(t)$.

The instant when the contact between the key and the front rail punching (c) occurs, was deduced from the geometrical measurements of the key (see Chapter 4) and corresponds



to a displacement of the key of $y = 9.8 \text{ mm}$. It appears on the measured force F_{meas} as a local minimum in time: since the hammer has just escaped, the reaction of the key decreases until it meets the front rail. Then, because of the large stiffness of the felt, the reaction increases. The amplitude of this force increase is accurately calculated in *piano* and *forte* dynamics. For the *piano* keystroke, the position of the local minimum is shifted by a about five milliseconds.

After hitting the string, the hammer is caught back by the backcheck. It transfers some of its kinetic energy to the key, pushing the finger end upwards. Again, the experimental diagram does not exhibit a strong time-variation in F but a strong variation in $\frac{dF}{dt}$. Since the return of the hammer is not simulated realistically (because of the hammer-string impact law, see bottom of Figure 6.4), it is not surprising that this pattern is not visible in the diagram of the simulated reaction forces. As a matter of fact, the simulated force increases during the check, but simulations without the backcheck showed the same increase. It can be deduced from the sensitivity analysis to come (Section 6.5) that the heightening of the force is related to the lever meeting the drop screw.

Most of the other irregularities observed in the measurements are also observed in the simulations. In particular, both *piano* and *forte* measurements exhibit two peaks and a smaller third one after the contact of the key and front rail punching: from $t = 0.14 \text{ s}$ to $t = 0.20 \text{ s}$ and from $t = 0.8 \text{ s}$ to $t = 0.12 \text{ s}$, in the *piano* and *forte* keystrokes, respectively. This is believed to be due to oscillations of the key, under the reaction of the front rail punching. For the *piano* keystroke, the frequency of these oscillations is about 70 Hz . The corresponding force is about $F_{\text{meas}} \approx 3.5 \text{ N}$. The position of the key is nearly constant during the oscillations. The stiffness of the non-linear felt law of the front rail punching can therefore be linearised in an apparent linear stiffness k_{lin} around the compression δ . From the felt law (4.4) comes:

$$k_{\text{lin}} \approx \frac{\partial F}{\partial \delta}(\delta) = 1.6 \times 10^{10} \times 2.7 \times \delta^{1.7} \quad (6.1)$$

For $F = 3.5 \text{ N}$, the felt law (the dissipative part is neglected) yields $\delta = 0.26 \text{ mm}$. The oscillating mass is composed of two elements:

- the key (with the force sensor and the piston);
- a part of the musculoskeletal system of the pianist (finger, hand, arm).

The oscillations' frequency f_{lin} of the linear spring, which approximates the front rail punching non-linear behaviour, is given by:

$$f_{\text{lin}} = \frac{1}{2\pi} \sqrt{\frac{k_{\text{lin}}}{m_{\text{eq}}}} \quad (6.2)$$

The contribution in mass of the pianist is very hard to evaluate. If we ignore it, then $m_{\text{eq}} = 62 \text{ g}$ and Equation (6.2) gives $f_{\text{lin}} = 121 \text{ Hz}$ in *piano* dynamics, which is the same order of magnitude of the frequency of the observed oscillations (70 Hz). Moreover, ignoring the contribution in mass of the pianist results in an underestimated m_{eq} , and therefore in overestimating f_{lin} .

The similar reasoning can be done for the *forte* keystroke. The observed frequency is roughly 90 Hz , the force oscillates around 9 N which corresponds to a compression of the

accurate time with the elastic one. Also, the shapes of the position curves are very similar, except for the hammer when the coefficient of restitution of its contact with the string was underestimated.

The escapement velocities of the hammer are perfectly estimated in the simulations, see Table 6.1. The escapement velocity for the *forte* dynamics is usually larger [Askenfelt and Jansson, 1991] because, as mentioned in Chapter 3, *forte* normally corresponds to higher forces.

	measurements	simulation
<i>piano</i>	$1.01 \text{ m} \cdot \text{s}^{-1}$	$1.00 \text{ m} \cdot \text{s}^{-1}$
<i>forte</i>	$1.56 \text{ m} \cdot \text{s}^{-1}$	$1.56 \text{ m} \cdot \text{s}^{-1}$

Table 6.1 – *Escapement velocities, measured and simulated.*

Time steps and real time applicability The characteristic time of the piano action is about a few milliseconds. All the simulation results presented in the thesis⁴ have been calculated with a time step of $h = 0.5 \text{ ms}$ ($f = 2 \text{ kHz}$). The computed forces for different frequencies are shown in Figure 6.10, for a *piano* keystroke. The results for $f = 2 \text{ kHz}$ and $f = 10 \text{ kHz}$ are very similar. A simulation frequency of $f = 2 \text{ kHz}$ is therefore assumed to be appropriate. On the reverse, choosing $f = 0.4 \text{ kHz}$ induces significant discrepancies.

Simulating 1s of motion of the piano action took about 20s with a laptop computer equipped with an Intel Core i5 processor. This factor 20, between the computation time and the real time, can be improved applying two independent modifications.

- Before implementing the felt laws and ensuring the synchronisation (see 5.5.2), which artificially but considerably slowed down the computation, simulations were computed nearly in real time (factor 1.2). It is therefore very likely that the low-level implementation of the felt laws, in XDE’s kernel, will lead to a factor close to 1.2 from real time, reducing the computation time by more than 15 times.
- Even if the model of the piano action is plane, XDE works only in 3D. The simulation does not take advantage of this possible simplification. A gain of a factor greater than 3 is expected.

All in all, because the time step of 0.5ms is small enough to simulate realistic forces, and because with a few programming effort, the simulation could run a few times faster than real time, it is very reasonable to consider that the simulations of the grand piano action can be applied to real time tasks.

6.4.2. Force-driven

As it can be foreseen according to the conclusions of Chapter 2, the simulated positions are very similar to the measured ones during the attack phase. The return of the key to its resting position is not accurately simulated in *piano*. This does not seem to be due to a systematic error because the results are far better in *forte*. The discrepancy could be due to errors in the measurements (see Section 3.5).

⁴Except those of Figure 6.10, of course.

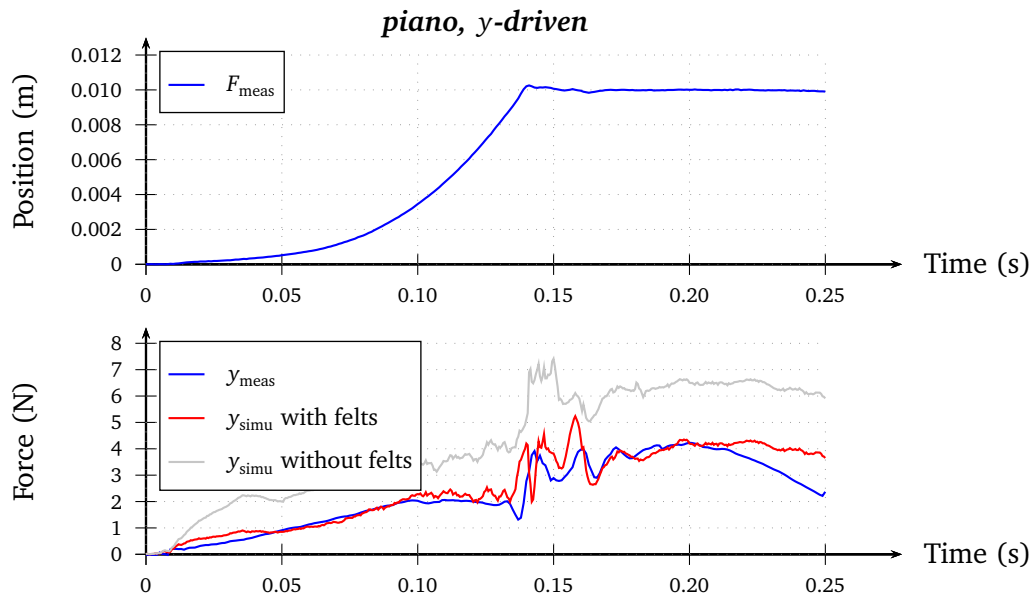


Figure 6.12 – Simulation results for a piano keystroke without felts (input: displacement).

The conclusion of Chapter 2, according to which the simulation should be driven by the measured position of the key in order to account for the validity of a dynamic model of the piano action, is retrieved in the case of the complete model.

6.5. A sensitivity analysis

In this section, we study the sensitivity of the simulated reaction force of the key on the finger, relatively to the model parameters. A cost functional is defined in 6.5.1. The sensitivity to the parameters defined in Chapter 4 is then presented, category by category (see 4.4.1). Given the large number of parameters, their analysis were only carried out independently for each parameter. The parameters which are adjusted in a real regulation of a piano action (category I) are studied in detail. Those of category II and III are briefly described and classified, depending on how they are influential.

6.5.1. Choice of the cost functional

The cost functional⁵ \mathcal{J} is defined as:

$$\mathcal{J}[F_{\text{simu}}] := \frac{\sum_{t_i=t_b}^{t_e} |F_{\text{meas}}(t_i) - F_{\text{simu}}(t_i)|}{\sum_{t_i=t_b}^{t_e} |F_{\text{meas}}(t_i)|} \quad (6.4)$$

where t_i is the time of the i -th measurement. The instant of the beginning of the motion of the key is denoted by t_b ($t_b = 0$ s). The instants of the releasing of the key t_e were identified from the force curves and estimated as $t_e = 0.22$ s for the *piano* keystroke, and $t_e = 0.13$ s in *forte*. The frequency of the measurements is 50 kHz. For the calculation of the cost functional \mathcal{J} , the measurement signals were downsampled at the frequency of the simulation: 2 kHz.

The 1-norm was chosen in \mathcal{J} because we did not want to penalise large discrepancies too much.

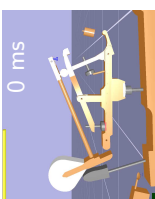
This cost functional does not account specifically for the escapement velocity of the hammer. The assumption is made that a simulation which gives a good prediction of the reaction force of the key describes the piano action well. This assumption implies that a simulation for which \mathcal{J} is small cannot lead to an irrelevant hammer velocity. The relevance of this choice is discussed later.

6.5.2. Parameters of category I

The eight parameters of category I are represented in Figure 4.6 page 56. We remind that:

- S_{K+y} is the height of the front rail punching;
- K_{Wx} and K_{Wy} are the coordinates of the top of the capstan screw (which is fixed to the key and lifts the whippen);
- S_{Jy} is the vertical position of the let-off button;
- J_{Wx} is the horizontal position of the jack regulating screw (which is in contact with the whippen, in the resting position);
- S_{Ly} is the vertical position of the drop screw;
- K_{Hx} is the horizontal position of the backcheck.

⁵The term *cost functional* refers to \mathcal{J} as a function of a simulated force F_{simu} . When \mathcal{J} is considered as a function of the parameters, the expression *cost function* is used.



The value p of each of these parameters was changed independently, by steps of 0.1 mm around its measured value⁶ p_0 given in Chapter 4, and up to a range of ± 2 mm.

This corresponds to 82 simulations for each parameter of category I (41 for the *piano* keystroke and 41 for the *forte* one).

The values of the cost functional were straightforwardly calculated from the simulated force using Equation (6.4). The corresponding plots are represented in Figure 6.13 to 6.20.

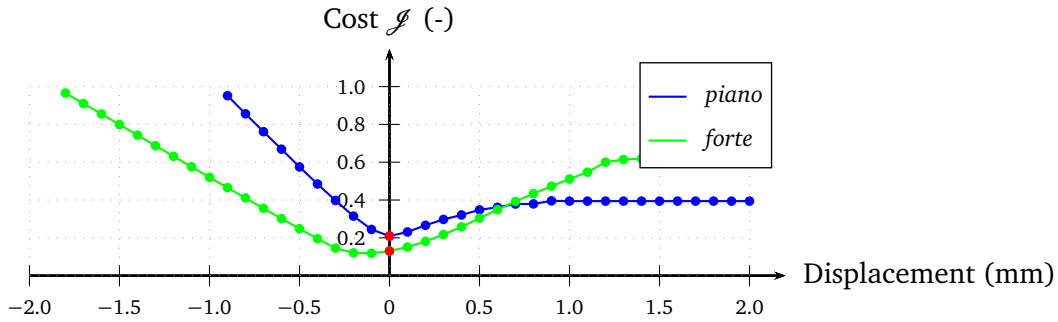


Figure 6.13 – Sensitivity of \mathcal{J} with respect to S_{K+y} .

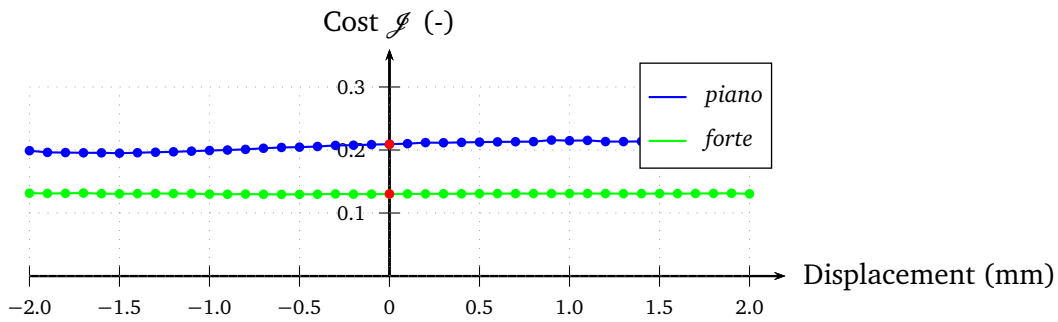


Figure 6.14 – Sensitivity of \mathcal{J} with respect to K_{Wx} .

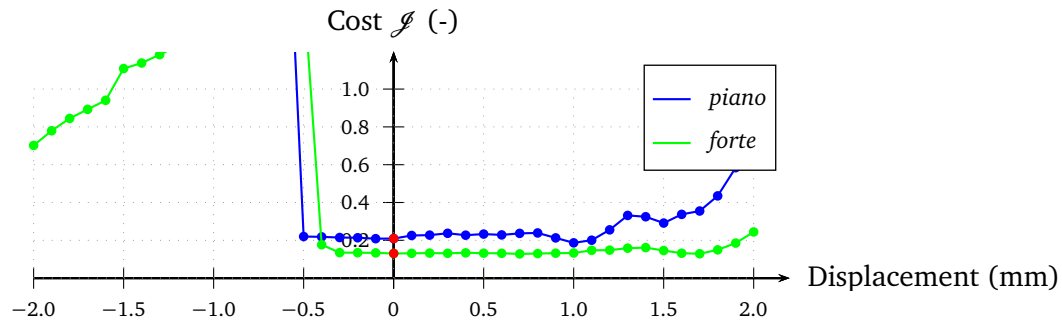


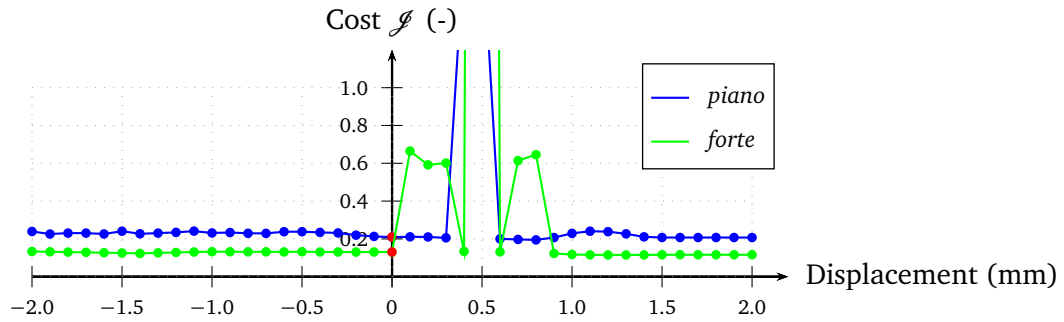
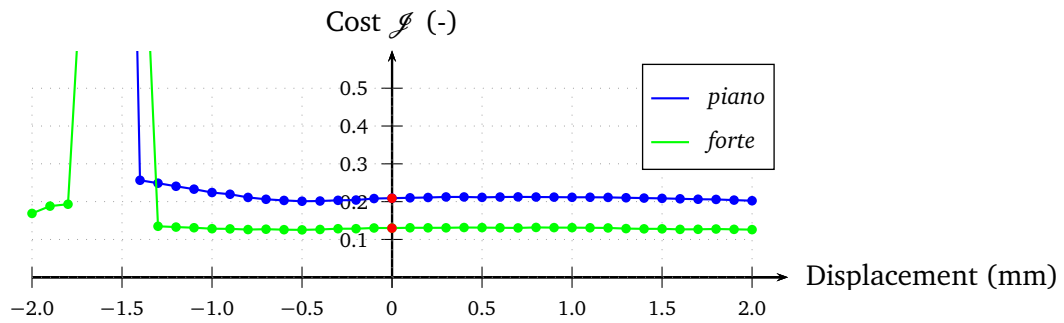
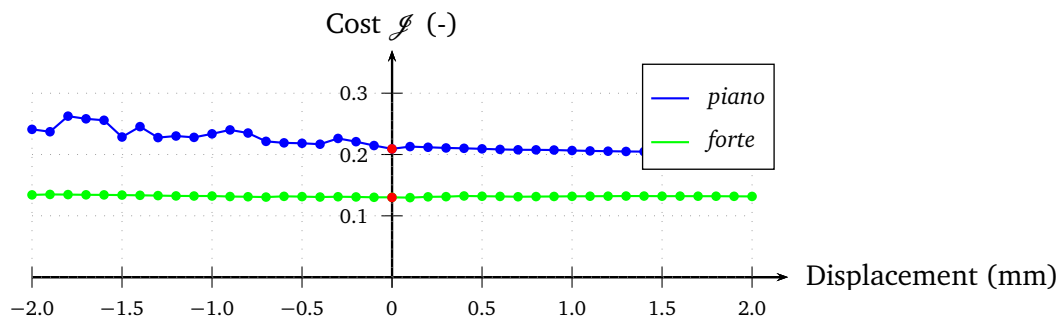
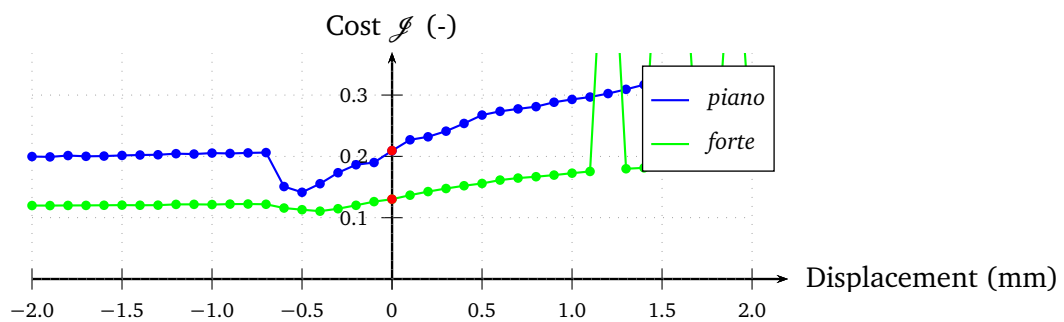
Figure 6.15 – Sensitivity of \mathcal{J} with respect to K_{Wy} .

Several shapes of the cost function are observed:

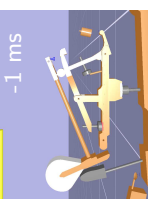
- For S_{Ly} and K_{Wx} , the sensitivity of the cost function to a small displacement is negligible. This means that varying these parameters on the piano action does not have a significant effect on the reaction force of the key. It can nevertheless have a significant effect on the functioning of the action, such as an escapement velocity not sufficient for the hammer to reach the string.

⁶This corresponds to values of p covering exactly

$$[p_0 - 2 \text{ mm}, p_0 - 1.9 \text{ mm}, \dots, p_0, \dots, p_0 + 1.9 \text{ mm}, p_0 + 2 \text{ mm}]$$

Figure 6.16 – Sensitivity of \mathcal{J} with respect to S_{Jy} .Figure 6.17 – Sensitivity of \mathcal{J} with respect to J_{Wx} .Figure 6.18 – Sensitivity of \mathcal{J} with respect to S_{Ly} .Figure 6.19 – Sensitivity of \mathcal{J} with respect to L_{Wy} .

- For K_{Wy} , S_{Jy} , J_{Wx} and K_{Hx} , the cost function is partly flat but also has large irregularities. The latter corresponds to settings of the action which lead to its blocking: for such adjustments, the force required for the key to move according to the imposed displacement is very large. It is noteworthy that a 0.5 mm change of the value of one of these parameters is enough to block the action. Also, it is interesting to notice that the measured values (in red) are always on the flat part of the cost function.
- The cost function is (locally) convex with respect to S_{K+y} and L_{Wy} . The measurement of S_{K+y} corresponds to the minimum of \mathcal{J} . The value of L_{Wy} is 0.5 mm higher than



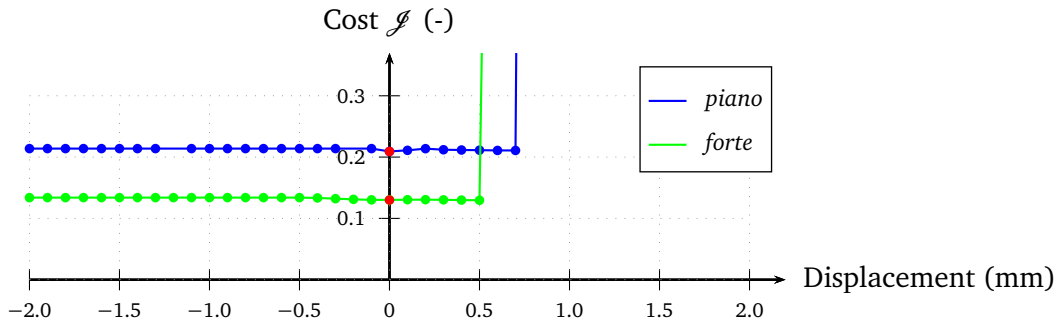


Figure 6.20 – Sensitivity of \mathcal{J} with respect to K_{Hx} .

the optimal one. Indeed, the force calculated using this optimal solution yields much better results than with the measured value, see Figure 6.21 for *piano* and 6.22 for *forte*. This optimal adjustment, originally found empirically from the sensitivity analysis, is confirmed here. The kinematics corresponding to the optimal setting of L_{Wy} are also given, in Figure 6.23. The analogue kinematic results for the non-optimal value of L_{Wy} have been given in Figure 6.4. We recall that the green dashed plots correspond to the computations with an elastic hammer/string contact law. The calculated position of the hammer shows a significant improvement and is very similar to the measured one.

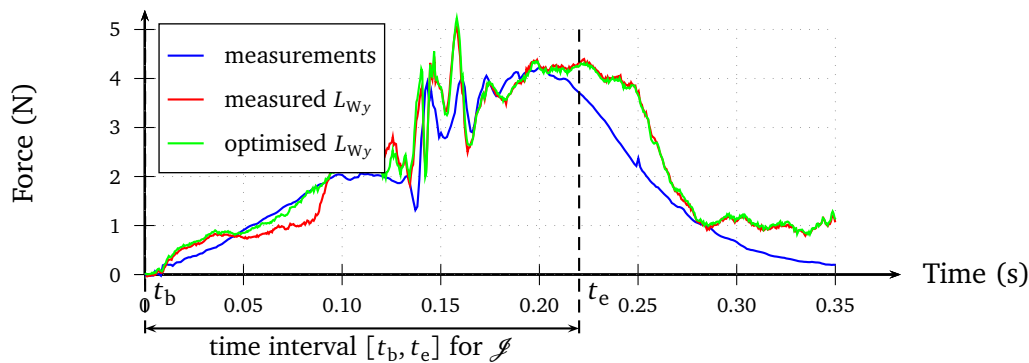


Figure 6.21 – Comparison of simulation results with measured (red) and optimised (green) values of L_{Wy} for a piano keystroke (input: displacement).

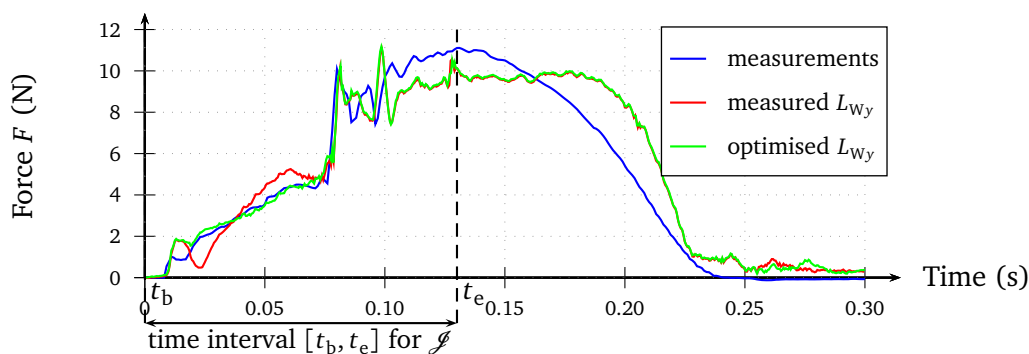


Figure 6.22 – Comparison of simulation results with measured (red) and optimised (green) values of L_{Wy} for a forte keystroke (input: displacement).

The sensitivity analysis of category I parameters allows to make some distinctions between the parameters. Some have a significant effect on the reaction force of the key (S_{K+y}, L_{Wy}). Some do not (S_{Ly}, K_{Wx}) but they may have other functions: S_{Ly} is crucial for the double escapement. It does not affect much the sensitivity analysis since during the measurements,

the key was only depressed once. Also, some parameters have no significant effect on the reaction force of the key up to a given extent, but can lead to a blocking of the piano action (K_{W_y} , S_{J_y} , J_{W_x} , K_{H_x}). Again, these parameters may have some other functions: K_{W_x} and K_{W_y} have to be adjusted to prevent the hammer from bouncing and producing a second sound by impacting the string. This has no weight in our cost function. Both S_{J_y} and J_{W_x} are critical for the escapement of the hammer, and therefore for the control offered by the piano action, but do not change significantly the reaction force of the key.

6.5.3. Parameters of Category II

Instead of reporting all the figures for these parameters, we used the characterisations introduced above (convex, flat or flat/irregular). Table 6.2 summarises those of Category II (i.e. parameters which are measurable and are likely to have an influence on the reaction force) and indicates the appropriate qualifying adjective of the corresponding cost function shape. For each parameter, the relative difference between the value of \mathcal{J} for the measured value p_0 and the minimum value of \mathcal{J} , is calculated for *piano* and *forte* keystrokes. The maximum value is given in Table 6.2 (column: $\Delta \mathcal{J} / \mathcal{J}$).

parameter	tested range	shape	typical blocking length	$\frac{\Delta \mathcal{J}}{\mathcal{J}}$
c_{sK}	[-10%, 10%]	flat	-	0.0%
c_{vK}	[-10%, 10%]	flat	-	0.2%
J_{Ox}	[-1 mm, 1 mm]	irregular/flat	0.2 mm	37%
J_{Oy}	[-1 mm, 1 mm]	irregular/flat	0.8 mm	24%
c_{sW}	[-10%, 10%]	flat	-	0.0%
c_{vW}	[-10%, 10%]	flat	-	0.0%
J_{Hx}	[-1 mm, 1 mm]	irregular	0.2 mm	18%
J_{Hy}	[-1 mm, 1 mm]	irregular/linear/irregular	0.4 mm	42%
J_{Sx}	[-1 mm, 1 mm]	irregular/flat	0.2 mm	2.5%
J_{Sy}	[-1 mm, 1 mm]	irregular/flat	0.2 mm	6.7%
L_{Hy}	[-1 mm, 1 mm]	convex	-	26%
L_{Jx}	[-1 mm, 1 mm]	flat	-	0.0%
H_{Jx}	[-1 mm, 1 mm]	flat/irregular	0.4 mm	10%
H_{Jy}	[-1 mm, 1 mm]	irregular	0.4 mm	3.0%
H_{Gx}	[-2 mm, 2 mm]	flat	-	1.4%
H_{Gy}	[-2 mm, 2 mm]	flat	-	0.6%
m_H	[-10%, 10%]	flat	-	4.7%
J_{H,H_0}	[-10%, 10%]	linear	-	8.9%
c_{sH}	[-10%, 10%]	flat	-	0.8%
c_{vH}	[-10%, 10%]	flat	-	0.1%
$H_{J\rho}$	[-10%, 10%]	flat/irregular	4%	2.7%
$H_{J\theta}$	[-10%, 10%]	irregular/flat	4%	10%
S_{Hy}	[-1 mm, 1 mm]	flat	-	0.8%
W_{Ox}	[-1 mm, 1 mm]	irregular/flat	0.4 mm	3.9%
W_{Oy}	[-1 mm, 1 mm]	flat	-	6.0%

Continued on next page

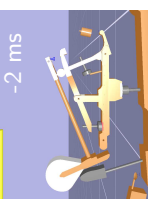


Table 6.2 – Continued from previous page

parameter	tested range	shape	typical blocking length	$\frac{\Delta \mathcal{J}}{\mathcal{J}}$
S_{K-y}	[-1 mm, 1 mm]	convex	-	0.0 %
K_{Ox}	[-1 mm, 1 mm]	flat/irregular	0.4 mm	2.0 %
K_{Oy}	[-1 mm, 1 mm]	convex	-	0.0 %
S_{Jx}	[-1 mm, 1 mm]	flat	-	0.3 %

Table 6.2 – Sensitivity of the cost function with respect to parameters of Category II.

Several results come out of the sensitivity analysis of the cost function \mathcal{J} with respect to the parameters of Category II.

- Some changes were applied to the values of the model parameters, with large amplitudes. The cost function was estimated for each set of values. For J_{Ox} , J_{Oy} , J_{Hx} , J_{Hy} and L_{Hy} , these changes led to significantly lower \mathcal{J} (between 26% and 42% lower, for the worse case between *piano* and *forte*). This is due to a mis-setting which has been highlighted previously, in the sensitivity analysis of parameters of Category I. It also shows the interdependencies of the parameters: we saw that \mathcal{J} is a convex function of L_{Wy} , now \mathcal{J} shows a similar property with the other end of the lever L_{Hy} . Also, these parameters are interestingly all related to the escapement, which is known to be very delicate.
- For the other parameters, the measured setting is very close to the minimal cost (in the sense of the parameters taken individually) and therefore the optimal setting in terms of reaction force of the key.
- Many parameters have no significant influence on the reaction force of the key. This is particularly interesting as it is a step towards a simplification of the model.
- Table 6.2 also highlights the high accuracy required for the regulation of the piano action: for many parameters, a variation of 0.2 mm leads to a completely different dynamical behaviour.

6.5.4. Parameters of Category III

parameter	tested range	shape	typical blocking length	$\frac{\Delta \mathcal{J}}{\mathcal{J}}$
$K_{H\rho}$	[-10 %, 10 %]	flat	-	0.5 %
$K_{W\theta}$	[0.5 rad, 0.5 rad]	irregular/convex	0.3 rad	17 %
$W_{K\rho}$	[-10 %, 10 %]	flat	-	0.8 %
$J_{H\lambda}$	[-10 %, 10 %]	flat	-	0.8 %
$J_{S\rho}$	[-10 %, 10 %]	flat	-	0.0 %
$J_{S\theta}$	[0.5 rad, 0.5 rad]	flat	-	0.0 %
$L_{H\theta}$	[0.5 rad, 0.5 rad]	convex	0.0 mm	18 %
$H_{K\rho}$	[-10 %, 10 %]	flat	-	0.0 %
$H_{K\theta}$	[0.5 rad, 0.5 rad]	irregular	0.2 rad	0.0 %

Continued on next page

Table 6.3 – Continued from previous page

parameter	tested range	shape	typical blocking length	$\frac{\Delta \mathcal{J}}{\mathcal{J}}$
$S_{J\theta}$	[0.5 rad, 0.5 rad]	flat	-	0.3 %
felts masses	[-50 %, 1000 %]	flat	-	<1.6 %
ν_{KH}	[-20 %, 20 %]	flat	-	0.9 %
ν_{JH}	[-20 %, 20 %]	slope	-	4.9 %
ν_{JS}	[-20 %, 20 %]	flat	-	0.5 %

Table 6.3 – Sensitivity of the cost function with respect to parameters of Category III.

6.5.5. Parameters of Category IV

It has been shown that many parameters of Categories II and III do not have a significant influence on the reaction force of the key. This was not known before running the simulations.

The parameters of Category IV are supposed *a priori* to have no significant effect on this force either. This is an assumption. It was verified studying the variation of \mathcal{J} with respect to seven parameters arbitrarily chosen and as different as possible: m_K , J_{K,K_0} , K_{Gx} , K_{Gy} , $K_{W\lambda}$, c_{sJ} and $H_{S\rho}$. The cost function was flat in all these independent directions and the maximum cost was only 3 % higher than the minimum cost.

This tends to validate the assumption.

6.5.6. Discussion and conclusion

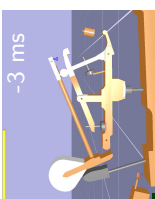
A sensitivity analysis was carried out for all the parameters of Categories I, II and III taken independently, using the cost functional (6.4).

The analysis showed that for many geometrical parameters, a change of less than a millimetre can lead to the blocking of the action, thus preventing the hammer from escaping properly.

Considering the parameter space and \mathcal{J} as a function of the parameters, the cost function is convex in a few parameters' directions: the height of the front rail punching S_{K+y} , the regulation button of the repetition lever⁷ L_{Wy} , the height of the back rail cloth S_{K-y} , the height of the rotation of the key K_{Oy} and the angle which characterises the direction of the contact between the key and the whippen $K_{W\theta}$. Except for L_{Wy} , the measured value of each of these parameters corresponded to the minimum cost in the direction of the parameter.

On the contrary, the cost function is flat in many parameters' directions. This means that it is nearly impossible to find the optimal values of the parameters of the action model, from only position and force measurements of the key – at least with this cost function: the gradient of the cost function has many zero-slope directions at the point corresponding to the correct values of the parameters. In other words, common methods of convex optimisation should probably not be applied to the piano action using \mathcal{J} .

⁷And therefore also the cost function is also convex in the direction of the other end of the repetition lever, L_{Hy} .



The choice of the cost functional must be discussed. This one does not reflect whether the escapement actually occurred, nor the escapement velocity, and more generally the kinematics are not directly weighted. Using a cost functional base on the force was intended to reflect the haptical role of the action. It appears that the let-off, known to be essential to pianists' touch, only appears as a small hump in the force diagram and has therefore a low weight in the cost function. A more appropriate cost functional has yet to be found. This requires a better knowledge of what is felt by the finger.

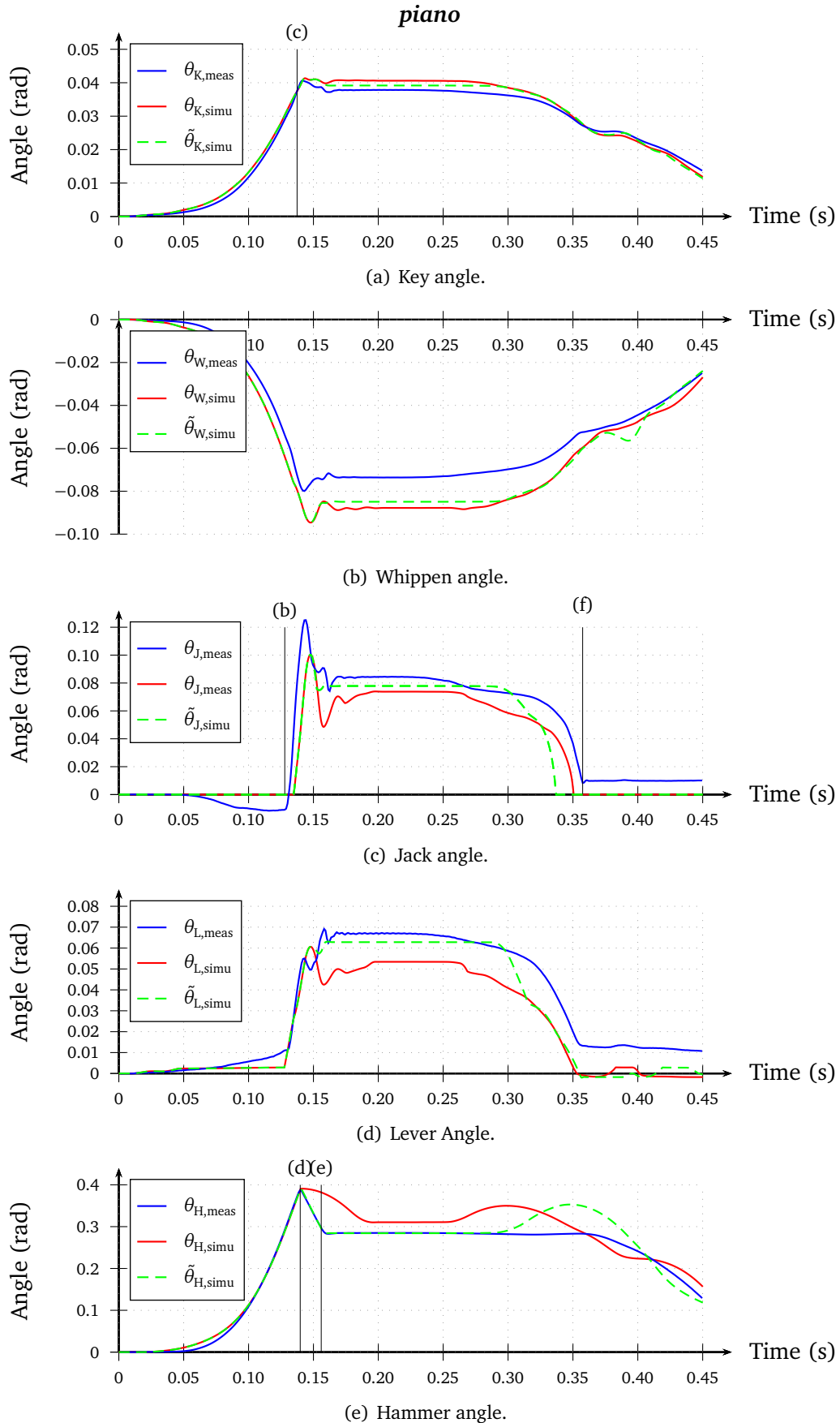
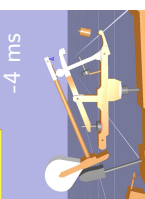


Figure 6.23 – Comparison of the position of the bodies (tracking vs simulation) for a piano keystroke with the optimised value of L_{Wy} . **Blue:** measurements. **Red:** simulation. **Green:** simulation with elastic hammer/string contact law.



Conclusion

The objective of the thesis was to propose a model of the grand piano action, and methods to simulate it, in order to render the subtle dynamics of the piano action from the key's viewpoint.

The first step consisted in an analysis of how this dynamics should be studied. The investigation was based on an elementary single-degree-of-freedom model. The conclusion is that the quality of a model for the action's dynamics, is given by the quality of the reaction forces of the key that it predicts, for given displacements of the key. On the reverse, the fact that a model predicts accurate displacements of the key, in response to force inputs, does not proof its validity. Such an assertion is a radical change with what has been done for nearly fifty years.

Then, a complete model with six degrees of freedom based the one proposed in [Lozada, 2007] has been presented. All the values of its parameters have been measured. The model includes non-smooth friction and contact laws. Instead of regularising them as it has been done up to now, we chose to treat them as such. The reasons of this choice are given, and a quantitative comparison between a regularised approach and a non-smooth approach was illustrated with a pendulum including joint dry friction. The dynamical model of the piano action, as a non-smooth multibody system, was solved with the numerical methods implemented in the computer program XDE.

The use of XDE implied a few adjustments. The felt law were manually implemented which slowed down the computations. Also, the position input was imposed in XDE by means of a PD controller placed on the virtual key. In order to make simulations and experiments truly comparable, a piston was inserted between the finger and the real key. The piston had to be adjusted carefully so that its model would correspond to a PD controller.

Using key positions as inputs, predicted forces were found to be reasonably similar to the measured ones, in both *piano* and *forte* dynamics. Most of the measured irregularities were reflected in the calculations. A sensitivity analysis of the reaction force to the numerous model's parameters has been proposed. The high-sensitivity of the reaction force to geometrical adjustments, well known by piano technicians, was rendered. The analysis also allowed to detect the misadjustment of one parameter, which is a strong indication of the model's validity, as well as the way it has been simulated. The results of the sensitivity analysis are largely conditioned by the choice of the cost function. The chosen one, which measured the difference between the simulated force and the measured force, did not render the amplitude of some events which are known to be essential for the touch of pianists, such as the let-off. Better choices of the cost function could lead to more relevant results in haptics.

The computations are about twenty times slower than real time, with a standard laptop. The calculation time is expected to be improved by a factor 50 by taking into account the

specificities of the model (felt laws, planarity). Integrating them is the last step to make the implementation of the model and its simulation methods usable in haptic devices.

The following step is the design of an interface capable of applying a force input faithfully. This is a very reasonable goal, since a lot of fruitful efforts have already been made in that direction. We are confident that it will open doors to new design methods for grand piano actions, to digital pianos with improved haptics and modulable touch, and to many diverse experiments for the understanding of what, in the piano action dynamics, allows the pianist to control the hammer so accurately.

Bibliography

- Acary, V. and Brogliato, B.** (2008). *Numerical methods for nonsmooth dynamical systems: applications in mechanics and electronics*, volume 35. Springer.
- Askenfelt, A. and Jansson, E. V.** (1990). From touch to string vibrations. i: Timing in the grand piano action. *The Journal of the Acoustical Society of America* **88**, 52.
- Askenfelt, A. and Jansson, E. V.** (1991). From touch to string vibrations. ii: The motion of the key and hammer. *The Journal of the Acoustical Society of America* **90**, 2383.
- Barbacci, A., Diener, J. et al.** (2013). A robust videogrametric method for the velocimetry of wind-induced motion in trees [submitted]. *Agricultural and Forest Meteorology* .
- Blackham, E. D.** (1965). The physics of the piano. *Scientific American* **213**, 88–99.
- Bokiau, B., Poncelet, A., Fisette, P. and Docquier, N.** (2012). Multibody model of a grand piano action aimed at understanding and demystifying the escapement principle. The 2nd Joint International Conference on Multibody System Dynamics.
- Brenon, C.** (2002). *Mécanique de la touche de piano*. Master's thesis, Université Pierre et Marie Curie, Paris VI, France.
- Cadoz, C., Lisowski, L. and Florens, J.-L.** (1990). A modular feedback keyboard design. *Computer music journal* **14**, 47–51.
- Chartrand, R.** (2011). Numerical differentiation of noisy, nonsmooth data. *ISRN Applied Mathematics* **2011**.
- Chu, L.** (1996). Haptic feedback in computer music performance. In *Proceedings of ICMC*, volume 96.
- Clementi, M.** (1803). Introduction to the art of playing on the pianoforte. .
- Closson, E. and Ames, D.** (1977). *History of the Piano*. Scholarly Press.
- Cull, S. and Tucker, R.** (1999). On the modelling of coulomb friction. *Journal of Physics A: Mathematical and General* **32**, 2103.
- Dahlquist, G. G.** (1963). A special stability problem for linear multistep methods. *BIT Numerical Mathematics* **3**, 27–43.
- Dennerlein, J. T., Mote Jr, C. and Rempel, D. M.** (1998). Control strategies for finger movement during touch-typing the role of the extrinsic muscles during a keystroke. *Experimental Brain Research* **121**, 1–6.
- Deuflhard, P.** (1987). *Uniqueness theorems for stiff ODE initial value problems*. ZIB.
- Dijksterhuis, P.** (1965). De piano. *Nederlandse Akoest. Genootschap* **7**, 50–65.
- Gillespie, B.** (1994). The virtual piano action: Design and implementation. In *Proceedings*

- of the international Computer Music Conference. INTERNATIONAL COMPUTER MUSIC ASSOCIATION.
- Gillespie, B. and Cutkosky, M.** (1992). Dynamical modeling of the grand piano action. In *Proceedings of the International Computer Music Conference*. International Computer Music Association.
- Gillespie, B. and Cutkosky, M.** (1993). Interactive dynamics with haptic display. In *2nd Ann. Symp. on Haptic Interfaces for Virtual Environment and Teleoperator Systems*, ASME/WAM, New Orleans, LA, DSC.
- Gillespie, R. B.** (1996). *Haptic display of systems with changing kinematic constraints: The virtual piano action*. Ph.D. thesis, stanford university.
- Gillespie, R. B., Yu, B., Grijalva, R. and Awtar, S.** (2011). Characterizing the feel of the piano action. *Computer Music Journal* **35**, 43–57.
- Goebel, W., Bresin, R. and Galembo, A.** (2005). Touch and temporal behavior of grand piano actions. *The Journal of the Acoustical Society of America* **118**, 1154.
- Goebel, W. and Palmer, C.** (2008). Tactile feedback and timing accuracy in piano performance. *Experimental Brain Research* **186**, 471–479.
- Hairer, G. W. E.** (2010). *Solving ordinary differential equations II*. Springer.
- Hall, D. E. and Askenfelt, A.** (1988). Piano string excitation v: Spectra for real hammers and strings. *The Journal of the Acoustical Society of America* **83**, 1627.
- Hayashi, E., Yamane, M. and Mori, H.** (1999). Behavior of piano-action in a grand piano. i. analysis of the motion of the hammer prior to string contact. *The Journal of the Acoustical Society of America* **105**, 3534.
- Hirschhorn, M., McPhee, J. and Birkett, S.** (2006). Dynamic modeling and experimental testing of a piano action mechanism. *Journal of computational and nonlinear dynamics* **1**, 47–55.
- Hirschhorn, M. C.** (2004). *Dynamic model of a piano action mechanism*. Ph.D. thesis, University of Waterloo.
- Horváth, P. and Törőcsik, D.** (2013). Magnetic issues of a haptic keyboard. *SzÁlchenyi IstvÁqn University* .
- Hunt, K. and Crossley, F.** (1975). Coefficient of restitution interpreted as damping in vibroimpact. *J. Appl. Mech.* .
- Izadbakhsh, A.** (2006). Dynamics and control of a piano action mechanism. *Master thesis* .
- Izadbakhsh, A., McPhee, J. and Birkett, S.** (2008). Dynamic modeling and experimental testing of a piano action mechanism with a flexible hammer shank. *Journal of computational and nonlinear dynamics* **3**.
- Links, H.** (2011). Modeling of a grand piano action mechanism. *Master Thesis* .
- Lozada, J.** (2007). *Modélisation, contrôle haptique et nouvelles réalisations de claviers musicaux*. Ph.D. thesis, Ecole Polytechnique.

- Lucas, B. D., Kanade, T. et al.** (1981). An iterative image registration technique with an application to stereo vision. In *IJCAI*, volume 81.
- Lutringer-Flecher, M.** (2002). *Le concept de toucher dans la pratique instrumentale du piano*. Master's thesis, Université Marc Bloch, France.
- Mamou-Mani, A. and Maniguet, T.** (2009). Investigating the history of the piano action using scientific calculus: The case of an érard grand piano from 1802 .
- Masoudi, R.** (2012). *Micromechanics of Fiber Networks Including Nonlinear Hysteresis and its Application to Multibody Dynamic Modeling of Piano Mechanisms*. Ph.D. thesis, University of Waterloo.
- Masoudi, R. and McPhee, J.** (2012). A mechanistic model of compression hysteresis in compliant interfaces in multibody dynamic simulation of a piano action mechanism. The 2nd Joint International Conference on Multibody System Dynamics.
- Merlhiot, X.** (2011). On some industrial applications of time-stepping methods for nonsmooth mechanical systems: issues, successes and challenges. In *Euromech Colloquium [516]-Nonsmooth contact and impact laws in mechanics*.
- Merlhiot, X.** (2012). Contact determination methods for nonsmooth time-stepping schemes. Presented at Summer School on Nonsmooth Mechanics: Modeling and Simulation, Aussois.
- Merlhiot, X., Le Garrec, J., Saupin, G. and Andriot, C.** (2012). The XDE mechanical kernel: Efficient and robust simulation of multibody dynamics with intermittent nonsmooth contacts. The 2nd Joint International Conference on Multibody System Dynamics.
- Mori, T.** (1997). A comparison between upright and grand pianos. volume 83. Journal of the European Acoustics Association.
- Oboe, R.** (2006). A multi-instrument, force-feedback keyboard. *Computer Music Journal* 30, 38–52.
- Oboe, R. and Poli, G. D.** (2002). Multi-instrument virtual keyboard - the mikey project.
- Oledzki, A.** (1973). Dynamics of piano mechanisms. *Mechanism and Machine Theory* 7, 373–385.
- Orocos** (2013). The Orocos Project.
- Pfeiffer, W.** (1950). *Über Dämpfer, Federn und Spielart*, volume 1. Verlag Das Musikinstrument.
- Pfeiffer, W.** (1962). *Vom Hammer*. Verlag Das Musikinstrument.
- Pfeiffer, W., Engelhardt, J. and Neupert, H.** (1967). *The piano key and whippen: An analysis of their relationships in direct blow actions*, volume 18. Verlag Das Musikinstrument.
- Pollens, S.** (2002). The gatti-kraus piano action ascribed to bartolomeo cristofori. *The Galpin Society Journal* 55, 269–278.
- Porter, L.** (2009). *The Piano the Pianist*. AuthorHouse.

- Principeaud, N. and Boutillon, X.** (2008). Reproducibility of piano playing. *The Journal of the Acoustical Society of America* **123**, 3125–3125.
- Repp, B. H.** (1999). Control of expressive and metronomic timing in pianists. *Journal of Motor Behavior* **31**, 145–164.
- Rimski-Korsakov, A.** (1937). The problem of a piano hammer striking a string (parts 1 and 2). *Zhurnal Tehnicheskoi Fiziki* **7**, 43–74.
- Rimski-Korsakov, A. and Maveev, P.** (1938). Investigation of dynamical properties of the piano key action. *SRIMI* , 159.
- Rimski-Korsakov, A. and Samoilenko, K.** (1937). Experimental determination of stiffness and friction of hammer piano felt. *Zhurnal Tehnicheskoi Fiziki* **7**, 135–150.
- Serina, E. R., Mockensturm, E., Mote Jr, C. and Rempel, D.** (1998). A structural model of the forced compression of the fingertip pulp. *Journal of biomechanics* **31**, 639–646.
- Stewart, D. E.** (2000). Rigid-body dynamics with friction and impact. *SIAM review* **42**, 3–39.
- Studer, C.** (2009). *Numerics of Unilateral Contacts and Friction*, volume 47. Springer.
- Times, N. Y.** (1904). Great piano bonfire .
- Tomasi, C. and Kanade, T.** (1991). *Detection and tracking of point features*. School of Computer Science, Carnegie Mellon Univ.
- Van den Berghe, G., De Moor, B. and Minten, W.** (1995). Modeling a grand piano key action. *Computer Music Journal* **19**, 15–22.
- Vyasarayani, C. P.** (2009). *Transient Dynamics of Continuous Systems with Impact and Friction, with Applications to Musical Instruments*. Ph.D. thesis, University of Waterloo.
- Vyasarayani, C. P., Birkett, S. and McPhee, J.** (2009). Modeling the dynamics of a compliant piano action mechanism impacting an elastic stiff string. *The Journal of the Acoustical Society of America* **125**, 4034.

Adjustment procedure of the grand piano action

In this Appendix, the regulation procedure which has been applied to our piano action is presented. It is a transcription of exchanges with two professional technicians. There are several other procedures, either specific to given actions or universal. The following one is presented as a typical universal procedure.

Main technical terms are given in Figure A.1. The different adjustments are shown in Figure A.2.

It is interesting to notice that, according to one of the professional technicians we met, it is not possible to regulate accurately an action without being able to touch it by yourself.

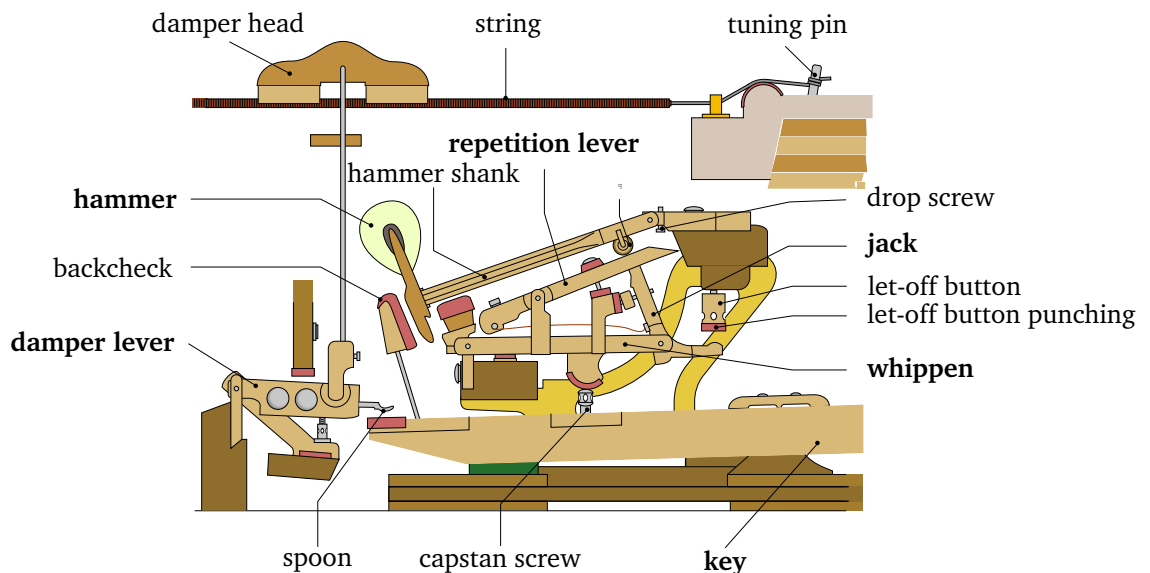


Figure A.1 – Terminology of the grand piano action [after Olek Remesz / Wikimedia Commons].

Preliminary adjustments

Key balance rail

When lifted, the key must fall down very slowly back to its normal resting position.

Escapement button

The hammer must escape as close as possible to the string, typically of 1.5 mm or less. This is adjusted with the escapement button.

Drop screw

When the key is depressed, the drop screw must be adjusted so that the hammer falls outright but not too much.

Backcheck – Hammer

The backcheck wire is adjusted so that for *forte* keystrokes, the hammer is caught a 15 mm of the string. Also, the contact has to occur at the top third of the backcheck.

Damper – Key

The spoon can be deformed so that it gets in contact with the key when the hammer is half-way through (23.5 mm).

Mass and inertial of the key

The can be changed by adding lead, so that the minimum downward weight of the action without damper is close to 50 g and the maximum upward weight is 25 g. As it is a destructive operation, it is done only if it cannot be avoided. Note that the exact weights depend on the manufacturers and the grand piano model.

Application of the Lagrangian to a double pendulum

In this appendix, the Lagrangian is applied to a double pendulum, which is one of the simplest multibody system for which not all the bodies move in a Galilean frame. The goal is to illustrate the efficiency of the Lagrangian and the physical meaning of the underlying equations.

Furthermore, the dynamics of the double pendulum has similarities with that of the whippen-jack-lever assembly as both the jack and the lever are assembled to the whippen with hinge joints, and the whippen himself is fixed to the ground with a hinge joint, see Figure B.1.

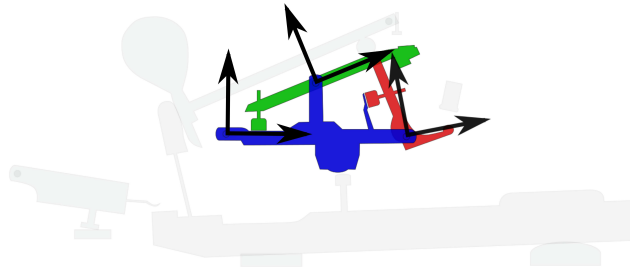


Figure B.1 – Non-inertial frame of the lever and the jack connected to the whippen with hinges joints.

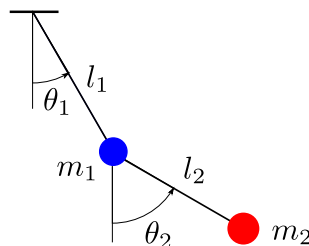


Figure B.2 – Scheme and parametrisation of the double pendulum.

The double pendulum is described in figure B.2. No external loading are considered, for simplicity. The Lagrangian \mathcal{L} is therefore equal to the kinetic energy \mathcal{T} .

Generalized coordinates The position of the masses in the ground frame is denoted by $\mathbf{X} = [\underline{X}_1 \underline{X}_2] \in \mathbb{R}^4$ where $\underline{X}_i \in \mathbb{R}^2$ is the position of the mass i in the ground frame. The double pendulum can also be described by the angles θ_1 and $\theta_2 \in \mathbb{R}$. These two scalars fully describe its state as the double pendulum is a 2-DOF mechanism. They define the vector of generalised coordinates \mathbf{x} :

$$\mathbf{x}(t) = \begin{bmatrix} \theta_1(t) \\ \theta_2(t) \end{bmatrix} \quad (\text{B.1})$$

The geometrical link between \mathbf{x} and \mathbf{X} is given by the following geometric relations:

$$\mathbf{X}(t) = \phi(\mathbf{x}(t)) \quad \text{with } \phi : \mathbf{x} = \begin{bmatrix} \theta_1 \\ \theta_2 \end{bmatrix} \in \mathbb{R}^2 \longmapsto \begin{bmatrix} l_1 \sin(\theta_1) \\ -l_1 \cos(\theta_1) \\ l_1 \sin(\theta_1) + l_2 \sin(\theta_2) \\ -l_1 \cos(\theta_1) - l_2 \cos(\theta_2) \end{bmatrix} \in \mathbb{R}^4 \quad (\text{B.2})$$

The equations of motion can then be calculated from the Euler-Lagrange equation:

$$\frac{d}{dt} \frac{\partial \mathcal{L}}{\partial \dot{\mathbf{x}}} - \frac{\partial \mathcal{L}}{\partial \mathbf{x}} = 0 \quad \text{with } \mathcal{L} = \mathcal{T} = \frac{1}{2} \mathbf{X}^T \underline{\underline{M}} \dot{\mathbf{X}} \quad \text{and} \quad \underline{\underline{M}} = \begin{bmatrix} m_1 & 0 & 0 & 0 \\ 0 & m_1 & 0 & 0 \\ 0 & 0 & m_2 & 0 \\ 0 & 0 & 0 & m_2 \end{bmatrix} \quad (\text{B.3})$$

Equation B.3 yields:

$$\left\{ \begin{array}{l} \boxed{(m_1 + m_2) l_1^2 \ddot{\theta}_1 + m_2 l_1 l_2 \cos(\theta_1 - \theta_2) \ddot{\theta}_2} - \boxed{+m_2 l_1 l_2 \sin(\theta_1 - \theta_2) \dot{\theta}_2^2} = 0 \\ \boxed{m_2 l_1 l_2 \cos(\theta_1 - \theta_2) \ddot{\theta}_1} + \boxed{-m_2 l_1 l_2 \sin(\theta_1 - \theta_2) \dot{\theta}_1^2} = 0 \end{array} \right. \quad (\text{B.4})$$

linear inertia nonlinear inertia

The prefactors of the linear accelerations are gathered in the mass matrix $\mathbf{M}(\mathbf{x})$ whereas $\mathbf{N}(\mathbf{x}, \dot{\mathbf{x}})$ gathers the nonlinear acceleration terms and their prefactors, so that the equation of motion finally comes as:

$$\mathbf{M}(\mathbf{x}) \ddot{\mathbf{x}} + \mathbf{N}(\mathbf{x}, \dot{\mathbf{x}}) \dot{\mathbf{x}} = \mathbf{0} \quad (\text{B.5})$$

Mass matrix M The generalised mass matrix is given by

$$\mathbf{M}(\mathbf{x}) = \begin{bmatrix} l_1^2 (m_1 + m_2) & l_1 l_2 m_2 \cos(\theta_1 - \theta_2) \\ l_1 l_2 m_2 \cos(\theta_1 - \theta_2) & l_2^2 m_2 \end{bmatrix} \quad (\text{B.6})$$

which is a symmetrical matrix. It is noteworthy that \mathbf{M} could also have been calculated from the kinetic energy \mathcal{T} :

$$\mathcal{T} = \frac{1}{2} \dot{\mathbf{X}}^T \underline{\underline{M}} \dot{\mathbf{X}} = \frac{1}{2} \dot{\mathbf{x}}^T \mathcal{J}_\phi(\mathbf{x})^T \underline{\underline{M}} \mathcal{J}_\phi(\mathbf{x}) \dot{\mathbf{x}} = \frac{1}{2} \dot{\mathbf{x}}^T \mathbf{M}(\mathbf{x}) \dot{\mathbf{x}} \quad \implies \mathbf{M}(\mathbf{x}) = \mathcal{J}_\phi(\mathbf{x})^T \underline{\underline{M}} \mathcal{J}_\phi(\mathbf{x}) \quad (\text{B.7})$$

where \mathcal{J}_ϕ is the Jacobian matrix of ϕ defined in (B.2) equal to

$$\mathcal{J}_\phi = \begin{bmatrix} l_1 \cos(\theta_1) & 0 \\ l_1 \sin(\theta_1) & 0 \\ l_1 \cos(\theta_1) & l_2 \cos(\theta_2) \\ l_1 \sin(\theta_1) & l_2 \sin(\theta_2) \end{bmatrix} \quad (\text{B.8})$$

Nonlinear inertial terms N The calculation of **N** yields

$$\mathbf{N}(\mathbf{x}, \dot{\mathbf{x}}) = m_2 l_1 l_2 \sin(\theta_1 - \theta_2) \begin{bmatrix} 0 & \dot{\theta}_2 \\ -\dot{\theta}_1 & 0 \end{bmatrix} \quad (\text{B.9})$$

which actually corresponds to the contribution of the variation of mass in the conservation of the momentum:

$$\frac{d}{dt}(\mathbf{M}(\mathbf{x}) \dot{\mathbf{x}}) = \mathbf{M}(\mathbf{x}) \ddot{\mathbf{x}} + \widehat{\mathbf{M}(\mathbf{x})} \dot{\mathbf{x}} = \mathbf{M}(\mathbf{x}) \ddot{\mathbf{x}} + \mathbf{N}(\mathbf{x}, \dot{\mathbf{x}}) \dot{\mathbf{x}} \quad (\text{B.10})$$

Also, it can be verified that:

$$(\mathbf{N}(\mathbf{x}, \dot{\mathbf{x}}) \dot{\mathbf{x}})_i = \frac{1}{2} \sum_{j,k} \dot{x}_k \left(\frac{\partial M_{ij}}{\partial x_k} + \frac{\partial M_{ik}}{\partial x_j} - \frac{\partial M_{kj}}{\partial x_i} \right) \dot{x}_j \quad (\text{B.11})$$

Example of the calculation of $\partial_{\mathbf{x}}\delta_{KH}$

The purpose of the appendix is to make the link between the matricial expression of the lever arms $\partial_{\mathbf{x}}\delta$ and their geometrical expression.

Since

$$\left(\left(\frac{\partial \delta}{\partial \mathbf{x}}(\mathbf{x}) \right)^T \right)_1 = \left[\frac{\partial \delta_{KS^+}}{\partial \theta_K}(\mathbf{x}) \quad \frac{\partial \delta_{KW}}{\partial \theta_K}(\mathbf{x}) \quad \frac{\partial \delta_{KS^-}}{\partial \theta_K}(\mathbf{x}) \quad \frac{\partial \delta_{KH}}{\partial \theta_K}(\mathbf{x}) \quad 0 \quad 0 \quad 0 \quad 0 \quad 0 \quad 0 \quad 0 \quad 0 \quad 0 \quad 0 \right] \quad (\text{C.1})$$

comes

$$\left(\left(\frac{\partial \delta}{\partial \mathbf{x}}(\mathbf{x}) \right)^T \mathbf{F}(\delta) \right)_1 = \frac{\partial \delta_{KS^+}}{\partial \theta_K}(\mathbf{x}) \mathbf{F}(\delta_{KS^+}(\mathbf{x})) + \frac{\partial \delta_{KW}}{\partial \theta_K}(\mathbf{x}) \mathbf{F}(\delta_{KW}(\mathbf{x})) + \frac{\partial \delta_{KS^-}}{\partial \theta_K}(\mathbf{x}) \mathbf{F}(\delta_{KS^-}(\mathbf{x})) + \frac{\partial \delta_{KH}}{\partial \theta_K}(\mathbf{x}) \mathbf{F}(\delta_{KH}(\mathbf{x})) \quad (\text{C.2})$$

The gap functions can easily be evaluated by geometrical calculations. For example,

$$\delta_{KS^+}(\mathbf{x}) = \underline{S^+ K_{S^+}} \cdot e_y \quad (\text{C.3})$$

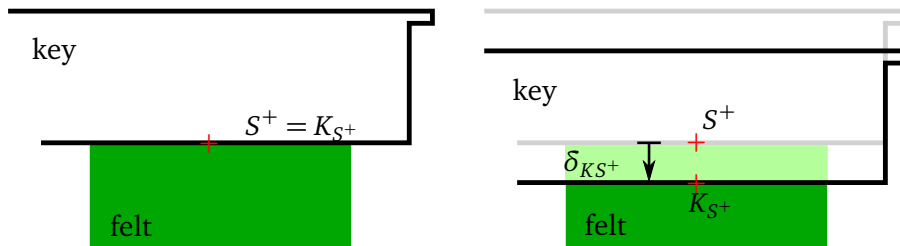


Figure C.1 – Scheme of the key compressing the front rail punching. Left: Beginning of contact. Right: Stricly positive compression of the felt.

S^+ is the centre point of the top of the front rail punching at rest (see Figure C.1), of fixed coordinates

$$S^+ = \begin{bmatrix} S_x^+ \\ S_y^+ \end{bmatrix} \quad (\text{C.4})$$

and K_{S^+} is the point of the key which is the closest to the front rail punching (see Figure C.1). Its coordinates are given by:

$$K_{S^+}(\mathbf{x}) = \begin{bmatrix} K_{S^+x}(0) \\ K_{S^+y}(0) \end{bmatrix} \cdot \begin{bmatrix} \cos(\theta_K) & -\sin(\theta_K) \\ \sin(\theta_K) & \cos(\theta_K) \end{bmatrix} \quad (\text{C.5})$$

so that finally:

$$\delta_{KS^+}(\mathbf{x}) = K_{S^+x}(0) \sin(\theta_K) + K_{S^+y}(0) \cos(\theta_K) - S^+_y \quad (\text{C.6})$$

Then,

$$\boxed{\frac{\partial \delta_{KS^+}}{\partial \theta_K}(\mathbf{x}) = K_{S^+x}(0) \cos(\theta_K) - K_{S^+y}(0) \sin(\theta_K)} \quad (\text{C.7})$$

which corresponds to the lever of the reaction force exerted by the front rail punching on the key.

The other components of $\left(\frac{\partial \delta}{\partial \mathbf{x}}(\mathbf{x})\right)^T$ can be calculated the same way.

Modèle dynamique non-régulier de la touche de piano à queue

Le mécanisme de la touche de piano à queue sert à propulser le marteau vers les cordes. Ce mécanisme permet au pianiste de contrôler avec précision la vitesse et l'instant d'impact du marteau sur la corde. Il est raisonnable de penser que c'est le comportement dynamique de la touche qui permet cette contrôlabilité. Avec pour perspective l'amélioration du rendu haptique des claviers numériques, cette thèse propose une méthode de simulation d'un modèle complet du mécanisme. Le son généré par la vibration qui suit l'impact du marteau sur les cordes n'entre pas dans le cadre de l'analyse. Des modèles du mécanisme comportant plusieurs degrés de liberté, des frottements et des contacts intermittents, ont été proposés depuis une quinzaine d'années. Notre approche se distingue de celles suivies jusqu'ici par un changement du point de vue adopté pour valider et pour simuler le modèle. En se fondant sur l'étude approfondie d'un modèle à un degré de liberté, il est en effet montré que la simulation d'un modèle dynamique complet doit se faire à l'aide d'un pilotage en déplacement, tandis que les travaux récents et anciens présentent des simulations pilotées en force.

Une analyse des problèmes numériques liés aux discontinuités de vitesses survenant au sein du mécanisme durant l'enfoncement de la touche est présentée. Ils sont résolus par des méthodes de dynamique non-régulière implémentées dans le logiciel XDE. Les résultats sont présentés sous forme de comparaison avec les mesures expérimentales. La plupart des irrégularités des forces mesurées se retrouvent dans les forces simulées, en jeu *piano* comme en jeu *forte*. Les simulations rendent également bien compte de la cinématique de chaque élément du mécanisme. Une analyse de sensibilité du comportement dynamique aux paramètres du modèle est enfin exposée.

Mots-clefs : *piano, dynamique multi-corps, dynamique non régulière, modélisation, simulation, haptique.*

Non-smooth model of the grand piano action

The grand piano action aims at propelling the hammer up to the strings. This mechanism provides the pianist with a high-controllability of the time of impact of the hammer with the strings and the hammer's velocity at the impact. This controllability is believed to be due to the dynamic behaviour of the piano action. The present thesis proposes a simulation method of a complete model of the mechanism, which opens doors to improvements of the haptic rendering of digital keyboards. The sound following the impact of the hammer on the strings is not analysed. In the last fifteen years, various models of the piano action including several degrees of freedom, friction and intermittent contacts, have been proposed. Our approach differs from existing work in that it is based on a new viewpoint for model validation and simulation. Indeed, using a in-depth study of a model with a single degree of freedom, it is shown that the simulation of a complete dynamic model must be driven with a displacement whilst, until now, only force driven simulations have been presented.

Velocity discontinuities, occurring during the descent of the key, raise numerical issues which are analysed. They are overcome by non-smooth numerical methods that have been implemented in the computer program XDE. The results of the simulation are presented and compared to experimental measurements. For both *piano* and *forte* keystrokes, most of the irregularities in the measured force are reflected in the simulated force. The kinematics of the bodies is also correctly predicted. Eventually, a sensitivity analysis of the dynamic behaviour to the model's parameters is proposed.

Keywords : *piano, multibody dynamics, non-smooth dynamics, modelling, simulation, haptic.*

Cover picture: Capture from the computer program XDE during a virtual keystroke.